
The Neural Process Family: Survey, Applications and Perspectives

Saurav Jha

University of New South Wales

saurav.jha@unsw.edu.au

Dong Gong

University of New South Wales

dong.gong@unsw.edu.au

Xuesong Wang

University of New South Wales

xuesong.wang1@unsw.edu.au

Richard E. Turner

University of Cambridge

ret26@cam.ac.uk

Lina Yao

University of New South Wales

lina.yao@unsw.edu.au

Abstract

The standard approaches to neural network implementation yield powerful function approximation capabilities but are limited in their abilities to learn meta-representations and reason probabilistic uncertainties in their predictions. Gaussian processes, on the other hand, adopt the Bayesian learning scheme to estimate such uncertainties but are constrained by their efficiency and approximation capacity. The Neural Processes Family (NPF) intends to offer the best of both worlds by leveraging neural networks for meta-learning predictive uncertainties. Such potential has brought substantial research activity to the family in recent years. Therefore, a comprehensive survey of NPF models is needed to organize and relate their motivation, methodology, and experiments. This paper intends to address this gap while digging deeper into the formulation, research themes, and applications concerning the family members. We shed light on their potential to bring several recent advances in other deep learning domains under one umbrella. We then provide a rigorous taxonomy of the family and empirically demonstrate their capabilities for modeling data generating functions operating on 1-d, 2-d, and 3-d input domains. We conclude by discussing our perspectives on the promising directions that can fuel the research advances in the field.¹

1 Introduction

Following the advent of GPU-accelerated training in the early 2010s (Cireřan et al., 2010; Masci et al., 2012; Krizhevsky et al., 2012), deep learning has enjoyed a tremendous rise in applications over the last decade. A good number of such applications include industrial and safety critical decision-making areas including but not limited to autonomous driving (Casas et al., 2020) and navigation (Abcouwer et al., 2021; Kothari et al., 2020), weather prediction² and climate modeling (Quinting & Grams, 2022), and disease (McBee et al., 2018) and workplace hazard (Wang et al., 2019a) detection. A necessary trait for models in these environments is the ability to capture the epistemic uncertainty in their predictions arising from the lack of knowledge of the physical dynamics of the world. Uncertainty awareness thus counts among the major prerequisites for practical machine learning models today (LeCun, 2022). Consequently, recent advances in deep learning have seen neural network designs that can better model the physical world (Greydanus et al.,

¹Code for our experiments will be made available at <https://github.com/srvCodes/neural-processes-survey>.

²<https://news.mit.edu/2022/using-data-and-science-forecast-climate-related-risk-grand-challenges-0407>

2019), measure uncertainties in their predictions (Louart & Couillet, 2018), and mitigate the risks attached with their tendency to be overconfident regarding a predicted confidence interval (Pereira & Thomas, 2020).

For the aforementioned objectives, the uncertainty-aware Bayesian paradigm (MacKay, 1995), with its ability to encode a prior distribution on the parameters θ of the neural network, stands among the earliest promising frameworks for risk mitigation. Upon the availability of more data, such priors can in turn be employed to periodically influence the posterior distribution. Nevertheless, Bayesian Neural Networks (BNNs) have three fundamental issues inherent to their nature. First, it is hard to specify generalization-sensitive weight priors in BNNs, *i.e.*, priors that assign higher likelihoods to better posteriors. The absence of such priors takes away the guarantee that the output distributions of BNNs reflect the true posteriors and hence, capture the uncertainties in predictions (Gelada & Buckman, 2020). Second, the inference techniques used to approximate the true posterior in BNNs are in general, not scalable in the face of high dimensional probability models and large datasets. Third and most fundamental, the motivation behind going Bayesian at the first place may not always be clear for a range of real-world problems.³

Neural Process Family. The uncertainty-aware Neural Process Family (NPF) (Garnelo et al., 2018a) aims to address the aforementioned limitations of the Bayesian paradigm by exploiting the function approximation capabilities of deep neural networks to learn a family of real-world data-generating processes, a.k.a., stochastic Gaussian processes (GPs) (Williams & Rasmussen, 2006).⁴ Neural processes (NPs) define uncertainties in predictions in terms of a conditional distribution over functions given the context (observations) C drawn from a distribution of functions. Here, each function f is parameterized using neural networks and can be thought of capturing an underlying data generating stochastic process.

To model the variability of f based on the variability of the generated data, NPs concurrently train and test their learned parameters on multiple datasets. This endows them with the capability to meta learn their predictive distributions over functions. The meta-learning setup makes NPs fundamentally distinguished from other non-Bayesian uncertainty-aware learning frameworks like stochastic GPs. NPF members thus combine the best of meta learners, GPs and neural networks. Like GPs, NPs learn a distribution of functions, quickly adapt to new observations, and provide uncertainty measures given test time observations. Like neural networks, NPs learn function approximation from data directly besides being efficient at inference.

To learn f , NPs incorporate the encoder-decoder architecture that comprises a functional encoding of each observation point followed by the learning of a decoder function whose parameters are capable of unraveling the unobserved function realizations to approximate the outputs of f (see figure 3). Despite their resemblance to NPs, the vanilla encoder-decoder networks traditionally based on CNNs, RNNs, and Transformers operate merely on pointwise inputs and clearly lack the incentive to meta learn representations for dynamically changing functions (imagine f changing over a continuum such as time) and their families.⁵ The NPF members not only improve upon these architectures to model functional input spaces and provide uncertainty-aware estimates but also offer natural benefits to a number of challenging real-world tasks. Our study brings into light the potential of NPF models for several such tasks including but not limited to the handling of missing data, handling off-the-grid data, allowing continual and active learning out-of-the-box, superior interpretation capabilities all the while leveraging a diverse range of task-specific inductive biases.

Why this survey? We conduct this survey for two main reasons. First and foremost, there exists no work detailing a comprehensive overview of the progress since the dawn of the NP family. However, the field has gathered 50+ papers over the years while incorporating a range of deep learning advances (see Figure 1 detailing the timeline of these). Therefore, a broader survey is needed to track the scope of work in the domain actively. Second, we find that although NPs were originally introduced for regression, they have so far been employed for a number of topics requiring the measure of uncertainty (see Figure 2 for a wordcloud of some most common such topics).

³<https://mlg-blog.com/2021/03/31/what-keeps-a-bayesian-awake-at-night-part-2.html>

⁴To keep our main discussion centered around deep learners, we provide a background of stochastic Gaussian processes and their limitations in Appendix A.

⁵However, as we will see in Section 3, NPs can also be enriched with the inductive biases of CNNs, RNNs, and self-attention mechanism underlying the Transformers.

details and results for modeling data generating stochastic processes with inputs lying on 1-d, 2-d and 3-d spaces. Using a number of underlying neural network architectures, we then emphasize the plug-and-play properties of uncertainty modeling with Neural Processes.

4. As an attempt to identify the limitations in the current Neural Process-based modeling frameworks and fuel further research advances, we discuss perspectives on several such directions that are plausible of bringing far-sighted impacts to the field.

The rest of the paper is organized as follows. Section 2 starts by defining the problem setup and the list of most common notations employed for Neural Processes. We then give the readers the preliminaries of NPs by detailing the groundbreaking works that established the NP family. This is followed by section 2.2 drawing connections of NPs with a range of deep learning domains including the special case of set function approximation which the NPF architectures draw heavy influence from. We begin our survey of the works extending the NP family by first presenting a comprehensive taxonomy of these in section 3. In Section 4, we outline the application-specific advances in the Neural Process family. Sections 5 and 6 then list the application areas and the nature of the tasks (based on 1-d, 2-d, and 3-d inputs) that the Neural Process family members can possibly tackle. Finally, section 7 compiles a list of our perspectives on the existing limitations of the NPF and suggest the future research directions that can help overcome these.

2 Background

Problem Setup: Adhering to the standard notations, we define our dataset D to be composed of a labeled context set $C = (X_C, Y_C) = \{(x_i, y_i)\}_{i=1}^N$ with inputs $x_i \in \mathcal{X}$ (defining function locations) and outputs $y_i \in \mathcal{Y}$ (defining function values), and an unlabeled target set $T = X_T = \{x_i\}_{i=N+1}^{N+M} \in \mathcal{X}$.⁶ We assume the location and values to be finite dimensional, *i.e.*, $x_i \in \mathbb{R}^{d_x}, y_i \in \mathbb{R}^{d_y}$. Our interest lies in predicting the outputs for T by learning the input-output mapping function $f : \mathcal{X} \rightarrow \mathcal{Y}$ that generated C . Given that f can be sampled from a distribution \mathcal{D} over such functions, it is continuous, bounded, and random by nature. Here, \mathcal{D} defines the conditional distribution $p(f(T)|C, T)$ which in turn is a joint distribution over the random variables $\{f(x_i)\}_{i=1}^{N+M}$. Training on a finite set $\mathcal{P}(\mathcal{X})$ of all observable locations of multiple such sampled functions then helps capture the ground truth stochastic process with the underlying distribution \mathcal{D} . A stochastic process thus defines the probability measure on the set of sampled functions $f : \mathcal{X} \rightarrow \mathcal{Y}$, where $f \in \mathcal{P}(\mathcal{X})$.

Given C and T , our learning objective can be formulated as finding the model with the optimal parameters that maximize the likelihood of the predictive distribution $p(f(T)|T, C) = p(Y_T|T, C)$ over the set of random functions. The statistics (mean and variance) of such a distribution provides an estimation of how uncertain the trained model is regarding its predictions being a true approximation of the ground truth values at the target locations. Accordingly, one can leverage a meta-learning setup where a neural network with parameters θ is concurrently trained and tested on multiple datasets $\{(X_{C \cup T}^i, Y_C^i)\}_{i=1}^n \sim D_i \in \mathcal{P}(\mathcal{X})$ to capture the variability of f based on the variability of the training datasets. Following this premise, Table 1 lists the most common notations used throughout this paper.

2.1 Preliminaries on the Neural Process Family

In this section, we describe the two seminal works laying the foundation for modeling stochastic processes using neural networks. These serve as the preliminaries for the field of Neural Processes given that all subsequent works build upon these. An illustration of their underlying architectures is provided in Figure 3.

Conditional Neural Processes: Garnelo et al. (2018a) first put forward the idea of conditional Neural Processes (CNPs) which model the conditional predictive distribution $p(f(T)|T, C) = p(f(T)|\rho(T, E(C)), \theta)$ defined by a real vector of all parameters θ . θ predicts the values of f by encoding the context C using the function composition $E = a \circ \phi$ where a and ϕ are the static average and learnable encoder functions, respectively. The encoding $E(C)$ together with the locations provided by T are then decoded by another learnable function ρ to predict the values for T . CNPs thus represent the observed context C with the

⁶Splitting C from T ensures that they both follow the same distribution (Le et al., 2018).

Table 1: An index of notations used throughout the paper

Function variables	
$f : \mathcal{X} \rightarrow \mathcal{Y}$	a continuous, bounded, and random function modeling the ground truth stochastic process.
ϕ	the learnable encoder neural network operating on the domain of sets.
ρ	the learnable decoder neural network.
a	the permutation-invariant average function.
E	the encoding function composed of a learnable ϕ and a fixed a , $E = a \circ \phi$.
$\Phi : X_K \rightarrow f(\mathcal{X}, \mathcal{Y})$	the permutation-invariant encoder-decoder composition $\rho \circ E$, a.k.a. Deep Set.
Φ_{conv}	an extension to Φ preserving translation equivariance on inputs, a.k.a. ConvDeepSet.
Φ_{eq}	an extension to Φ preserving equivariance over the Lie group of symmetries, a.k.a. EquivDeepSet.
$[\cdot; \cdot]$	the concatenation function acting on two vectors.
Data Variables	
\mathcal{X}	the domain of f .
\mathcal{Y}	the range of f .
x	a real-valued data point of dimension d_x , $x \in \mathcal{X}$ forming the input for f .
y	a real-valued target variable of dimension d_y , $y \in \mathcal{Y}$ forming the output for f .
C	context set comprising N labeled tuples of the form $(x_i, y_i)_{i \in \{1, \dots, N\}}$.
T	target set comprising M unlabeled tuples of the form $(x_i)_{i \in \{k, \dots, M\}}$ where $k = N + 1$ or 1 . Le et al. (2018) empirically show $k = 1$ to work best.
$\mathcal{P}(\mathcal{X})$	the finite set of all such observable locations that can be obtained by sampling f multiple times.
$I(\cdot)$	an arbitrary set index operator.
X_K	the set of all data points $\{x_i\}_{i \in I(K)}$ where $K = \{C, T\}$.
Y_K	the set of all target variables $\{y_i\}_{i \in I(K)}$ where $K = \{C, T\}$. We assume Y_T to be missing unless otherwise specified. Consequently, $C = (X_T, Y_T)$, $T = X_T$.
N	the cardinality of C .
$M + N$	the cardinality of T .
D	a dataset from which various context and target sets can be sampled.
θ	the parameter space of neural networks forming ϕ and ρ .
θ^*	the maximum likelihood estimate for θ that has the highest probability for observing the target set.
S	total number of time steps in case of problems dealing with sequential data.
t	an instant among the total time steps, $t \in S$.
\mathcal{T}	a meta-learning task given by $\{(X_{C \cup T}^i, Y_C^i)\}_{i=1}^n \sim D$.
Probability distributions	
p	the true probability distribution.
q	the variational probability distribution used to approximate p .
\mathcal{D}	the meta-learning distribution used to randomly sample f , a.k.a. the posterior predictive distribution $p(f(T) C, T)$.

encoder $\phi : C \rightarrow \mathbb{R}^e$ which is then processed by the decoder $\rho : \mathbb{R}^e \rightarrow f(\mathcal{X}, \mathcal{Y})$ to estimate the density parameters for T .⁷ In general, $\rho \circ E$ can be summarized by an encoder-decoder composition Φ :

$$\Phi(T) = \rho(E(\{x_i\}_{i=1}^N, \{y_i\}_{i=1}^N), \{x_i\}_{i=N+1}^{N+M}) \quad (1)$$

Since the input domain of Φ is the power set 2^{X_C} rather than fixed dimensional vectors and Φ relies on deep neural networks as choices for ρ and ϕ , Zaheer et al. (2017) coin it a Deep Set.⁸ The set representation for context and target data further deems the valid choices of functions for the encoder E (acting on the outputs of permutation-sensitive ϕ) to be the ones whose outputs are indifferent to the ordering of the input elements. For a supervised learning problem setup, such functions can help predict $x_i \in T$ while remaining *permutation invariant* w.r.t. the predictors. This property is a necessary condition for mimicking a stochastic process as

⁷While the encoder here represents the observed context C using a real-valued vector, we will see in Section 3.3 that such real valued representations might not always hold.

⁸As ϕ and ρ can approximate arbitrary polynomials, Deep Sets are thus capable of universal approximation.

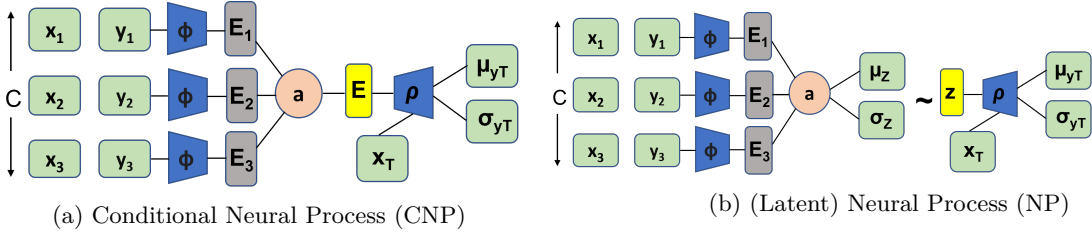


Figure 3: Illustration of Neural Process architectures adapted from Garnelo et al. (2018a): C is the context set composed of three labeled data points (x_i, y_i) . ϕ is the encoder network acting on individual data points to produce encodings E_i which are aggregated by the operator a . ρ is the decoder network conditioned on the target location x_T and the aggregated context encoding. While the CNP feeds the output of a directly to ρ , the NP first maps it to a distribution from which the latent variable z is sampled to be fed to the decoder. μ and σ denote the means and variances of the respective distributions.

it ensures *exchangeability* in the (posterior) predictive distribution $p(f(T)|T, C)$.⁹ Deep Sets thus define E to be the symmetric average over the individual contextual embeddings $\phi_{i \in N}$:

$$E(C) = a(\phi(C)) = \frac{1}{N} \sum_{(x,y) \in C} \phi_{xy}([x; y]) \quad (2)$$

where, the encoder neural network ϕ does away with the GP-styled analytical priors and instead extracts prior knowledge from the observations $[x; y]$ of f empirically. Different from other deep learning domains, the average pooling function a here is crucial for capturing set-based representation and forms a special case of a larger family of pooling functions discussed later in Section 2.2. Given the permutation invariant context encoding $E(C)$, the predictive distribution $p(f(T)|T, C)$ can now be modeled using a decoder network as a factorized Gaussian across the target set elements to satisfy the *consistency* condition of stochastic processes:

$$p(f(T)|T, C) = \prod_{x \in T} \mathcal{N}(f(x) | \mu(\rho(x, E(C))), \text{diag}[\sigma^2(\rho(x, E(C)))] \quad (3)$$

where, $\mu(\cdot)$ and $\sigma(\cdot)$ denote the mean and the standard deviation of the multivariate Gaussian distribution with diagonal covariance matrix learned by the decoder.

Note: Given that the CNP decoder derives predictions for the target points conditioned on the averaged context set encoding $E(C)$, it can be viewed as a prototypical network (Snell et al., 2017) learning the metric space where the context representation serves as a prototype to match the queried target representation. As shown in Figure 4, the classification setup of Garnelo et al. (2018a) clarifies this perspective further – the context encodings of samples from a class form the support set of the class in the embedding space and the prototype representation of each class is derived as the mean of its support set.

The optimization objective for the CNP thus boils down to finding a set of optimal parameters θ^* (out of all possible parameters θ) that maximizes the log predictive probability of observing targets given the aggregated contextual encoding:

$$\theta^* = \arg \max_{\theta} \mathbb{E}_{C, T, f(T)} [\log p(f_{\theta}(T) | T, E_{\theta}(C))] \quad (4)$$

⁹ $p(f(T)|T, C)$ models the mere predictive distribution for the CNP while measuring the posterior predictive distribution in the light of latent variable models like the NP.

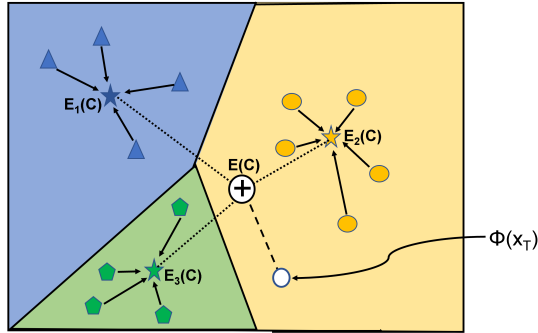


Figure 4: Depiction of the classification setup of the CNP (Garnelo et al., 2018a) from the perspective of prototypical embeddings (Snell et al., 2017): the representations of each class i are aggregated separately to form class-specific prototype $E_i(C)$. The final context encoding $E(C)$ is a result of the concatenation of the classwise prototypes $\oplus E_i(C)$ and is used to derive predictions for the queried target embedding $\phi(x_T)$.

where, $\mathbb{E}_{C,T,f(T)}$ is the expectation over distribution of datasets drawn from D , each of which contributes to the sampling of a unique C and T . Since this optimization objective is shared by all other members of the Neural Process family, these can in turn be thought to meta learn the distribution of context and target datasets while modeling the underlying stochastic process (see Section 2.2 for a meta-learning perspective to the NPF).

(Latent) Neural Processes: CNPs encode each context point independently and employ the fixed dimensional vector $E(C)$ to compute the predictive conditional distribution $p(f(T)|T,C)$, *i.e.*, they model *point-wise* uncertainties. However, we might desire our model to consider beyond point-wise uncertainties in inputs and instead exploit their correlation during prediction. In image inpainting for instance, it is desirable to assign similar pixel intensities to nearby pixel locations. There exist multiple ways to model such correlation in the deep learning domain. One could for example trade the parallelizability of predictions to instead generate predictions auto-regressively:

$$\theta^* = \arg \max_{\theta} \mathbb{E}_{C,T,f(T)} \left[\sum_{i \in |T|} \log p(f(T_i) | T_{1:i}, f(T_{1:i-1})) \right] \quad (5)$$

Equation 5 involves extending the context set for the next queried input with the current input’s prediction (Van den Oord et al., 2016). Another solution could be drawing an analogy to Gaussian processes – rather than learning the diagonal variances of the multivariate Gaussian distribution defining the input predictions, the model can be trained to learn the entire covariance among the input variables (Yoo et al., 2021). Despite their powerful expressivity, these techniques scale poorly with data.¹⁰

To achieve correlation modeling, Garnelo et al. (2018a) consider the rather intuitive possibility of a context set generating more than one function samples with different priors that can represent point-wise uncertainty on the target set equally well. In a nutshell, this hints towards the fact that the priors can be governed by a yet another uncertainty and that modeling point-wise uncertainties might not be enough to determine them. As a result, the authors propose extending CNPs with latent Gaussian variable distributions that help capture the *global uncertainty* in the overall structure of the function.¹¹ Sampling the latent distribution thus gives diverse global latent variables which are then used to condition the decoder to ensure that its predictions are diverse yet coherent as well as invariant to the individual contextual samples. It is worth noting that in the case of CNPs, the lack of such a latent space to sample from implies that any attempt at sampling multiple predictions will give us noisy averages of the observed data.

The resulting (latent) Neural Processes (NPs) incorporate a high-dimensional stochastic vector $z \sim \mathcal{Z}$ that captures all of the context information while inducing implicit randomness into the posterior of the

¹⁰More recent advances in the NP family have considered enhancing the tractability of autoregressive techniques through approximations of the full covariance matrix. For example, refer to Nguyen & Grover (2022), section 3.2.

¹¹Latent variables enable global sampling of functions, *i.e.*, one function at a time rather than one point output at a time.

functions.¹² z thus parameterizes the stochasticity of the data generating Gaussian process as $f(x) = \rho(x, z)$. Each individually sampled z thus results in a deterministic decoder function $\rho(x, z_i)$.¹³ This also offers us a Bayesian perspective to inspect z since $p(z)$ now encodes the data-specific prior learned by the model over the context set. On observing the target set, such a prior gets updated to form the posterior $p(z|C, T)$ that can better estimate the *epistemic uncertainty* due to the lack of ample context data.

$p(z|C, T)$ is, however, intractable in high-dimensional spaces due to the overtly complicated *evidence* $p(C)$.¹⁴ A well-known solution to computing $p(z|C, T)$ remains approximating it with a variational posterior $q(z|C, T)$ of z . Such a posterior is parameterized by an encoder network ϕ that is permutation invariant over C . The variational prior $q(z)$ then initializes the parameters of ϕ to follow a well-behaved distribution – often a standard multivariate Gaussian. z can thus be modeled using the factorized Gaussian which, similar to equation 3, is a function of permutation invariant mean μ and variance σ^2 guaranteeing *exchangeability* to its statistics C computed over the context set:

$$p(f(T)|T, C) = \int p(f(T)|T, z)p(z|C)dz \approx \int p(f(T)|T, z)q(z|C)dz \quad (6)$$

s.t., $q(z|C) = \mathcal{N}(z|\mu(C), \text{diag}[\sigma^2(C)])$

where, $p(f(T)|T, z)$ is the observation likelihood of z and can be parameterized by a decoder network in a fashion similar to equation 3. Given that equation 6 marginalizes over z to compute $p(f(T)|T, Y_C)$, it therefore serves as the marginal likelihood, *i.e.*, the probability of generating the values $f(T)$ based on the observations T by randomly sampling the latent prior $p(z)$. The generative model guaranteeing *consistency* to z can now be given as:¹⁵

$$p(z, f(T)|T, C) = p(z|C) \prod_{x \in T} \mathcal{N}(f(x)|\mu(\rho(x, z)), \text{diag}[\sigma^2(\rho(x, z))]) \quad (7)$$

where, $p(z|C) := \mathcal{N}(z|\mu_z, \sigma_z^2)$ is a multivariate standard normal capturing the global uncertainty of the functional sample $f \sim \mathcal{D}$. The optimization objective for training an NP can be stated in terms of maximizing the following evidence lower bound of the log probability of the predictive distribution $p(f(x)|z, x)$:

$$\begin{aligned} \log p(f(T)|T, C) &\geq \mathbb{E}_{q(z|C, T)} \left[\sum_{x \in T} \log p(f(x)|z, x) - \log \frac{q(z|C, T)}{p(z|C)} \right] \\ &\approx \mathbb{E}_{q(z|C, T)} \left[\sum_{x \in T} \log p(f(x)|z, x) - \log \frac{q(z|C, T)}{q(z|C)} \right] \quad (8) \\ &= \mathbb{E}_{q(z|C, T)} \left[\sum_{x \in T} \log p(f(x)|z, x) - D_{KL}(q(z|C, T) \| q(z|C)) \right] \end{aligned}$$

where, (C, T) is the observed dataset and D_{KL} is the reverse KL-divergence between the approximate conditional prior $q(z|C)$ and the approximate posterior $q(z|C, T)$. It is worth noting that the approximate prior $q(z|C)$ replaces the true prior $p(z|C)$ given the condition on the encoding C implies a lack of exact estimate of the prior. In order to optimize equation 8, the authors then backpropagate the gradients using the reparameterization trick (Kingma & Welling, 2014).

¹²Following the convention from a majority of works on the NPF, we use the acronym NP interchangeably for the latent as well as the generic Neural Process family models.

¹³The deterministic encoding $E(C)$ can now be thought of encoding the Gaussian variable z in a latent space which can in turn be sampled to condition the target locations. While each such sampled z will result in a distinct set of target outputs, sharing z among the target inputs ensures global consistency and coherence among the predictions.

¹⁴Computing the exact evidence requires running the inference through all possible combinations of the parameter values of the network (with the plausible range of each value being $[-\infty, \infty]$) to find the likelihood of observing the target T .

¹⁵Refer to Appendix A for a background on *exchangeability* and *consistency* conditions in stochastic processes.

2.2 Neural Process Family from the perspective of other learning areas

To model an uncertainty-aware data generating processes, the Neural Process family (NPF) exploits a range of independent deep learning research directions. In this section, we aim to connect the dots between these. We start with the most obvious set-based (permutation-invariant) representation learning capability of Neural Processes. In particular, we analyze the potential offered by different instantiations of permutation-invariant pooling operations for NPF members. We then discuss the meta-learning ability of NPF members and tie its connections to functional data analysis. We delve into the original regression-based setting that NPF members were targeted to solve. We then consider the uncertainty-based Bayesian learning paradigm and the generative modeling ability of Neural Processes. We further point out other specific instances of work along each of these directions that the NPF members resemble the most with. Figure 5 summarizes these directions from the perspective of their relationship to Neural Processes.

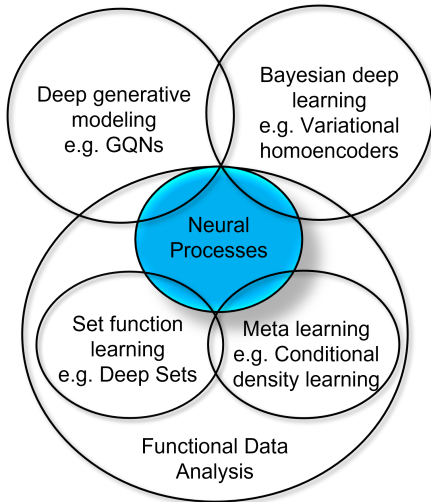


Figure 5: Illustration of Neural Processes in the light of the advances from other deep learning domains. NPs resemble closely to: deep generative models like Generative Query Networks (GQNS) (Eslami et al., 2018), Bayesian inference methods like variational homoencoders (Hewitt et al., 2018), set function approximators like Deep Sets (Zaheer et al., 2017), and model-based conditional density meta learners (Ton et al., 2021).

Set-based learning. Neural processes operate on variable length context sets by encoding them using order-sensitive neural network parameters. Subsequently, the need for an additional permutation-invariant operation (see equation 2 for instance) becomes imminent to capture the information independent of the input order. However, in contrast to their mainstream permutation-sensitive counterpart, the field of permutation-invariant deep learning has received little attention over the years. To bridge this gap, Murphy et al. (2019) first introduced the idea of Janossy pooling that stacks learning both these functions in a common framework. A naive Janossy pooling derives a permutation-invariant approximation for an input sequence $\{x_1, \dots, x_N\}$ (in our case, the context set), by considering all its possible permutations $\pi(x_{1:N})$, applying the permutation-sensitive function ϕ (the encoder) to these and averaging the outputs of ϕ (see Figure 6a). As the computational complexity of considering such exhaustive reordering of the sequence scales with $N!$, (Murphy et al., 2019) suggest using k -order permutations among other solutions for efficient approximation of the permutation invariant encoding. Building upon this restrictive setting, Wagstaff et al. (2021) show that Deep Sets and self-attention form special cases for k -ary Janossy pooling with the respective k values set to 1 and 2. We exploit this premise to highlight how some NPF members represent sets.

CNPs (Garnelo et al., 2018a) and latent NPs (Garnelo et al., 2018b) (Section 2.1) rely on feeding each context point individually to ϕ , *i.e.*, $k = 1$. While this specifies the cheapest computational instance of Janossy pooling, using $k = 1$ removes any possible inductive bias from the decoder that could have helped encoding interactions among the inputs. As a result, the decoder in these CNPs and latent NPs must learn to reason relationship among the input samples during training. Generalizing upon the argument of Wagstaff

et al. (2021) for Deep Sets, it is sound to claim that NPF members relying on these fail to induce relational reasoning into their decoders. Note that the ConvDeepSet architectures underlying the convolutional CNPs (Foong et al., 2020) also employ unitary Janossy pooling. However, convolutional CNPs induce an explicit shift equivariance bias as discussed later in Section 3.3. The Janossy pooling operations in CNPs and Convolutional CNPs are illustrated in Figures 6b and 6d, respectively.

Wagstaff et al. (2021) further show that self-attention mechanisms performing input-dependent weighted pooling of information help induce a more explicit pairwise ($k = 2$) relational reasoning of inputs into the model. This in turn allows them to map sets of points to sets of points (Lee et al., 2019). In Section 3.2, we brief the attentive Neural Processes (ANPs) (Kim et al., 2019) that leverage this inductive bias in modeling of stochastic processes. Figure 6c illustrates ANPs (and other attention-based NP derivatives) where instead of the aggregation operation Σ , the weighted pooling operations of self-attention (inducing context-context reasoning) and cross-attention (inducing context-target reasoning) now embody Janossy pooling.

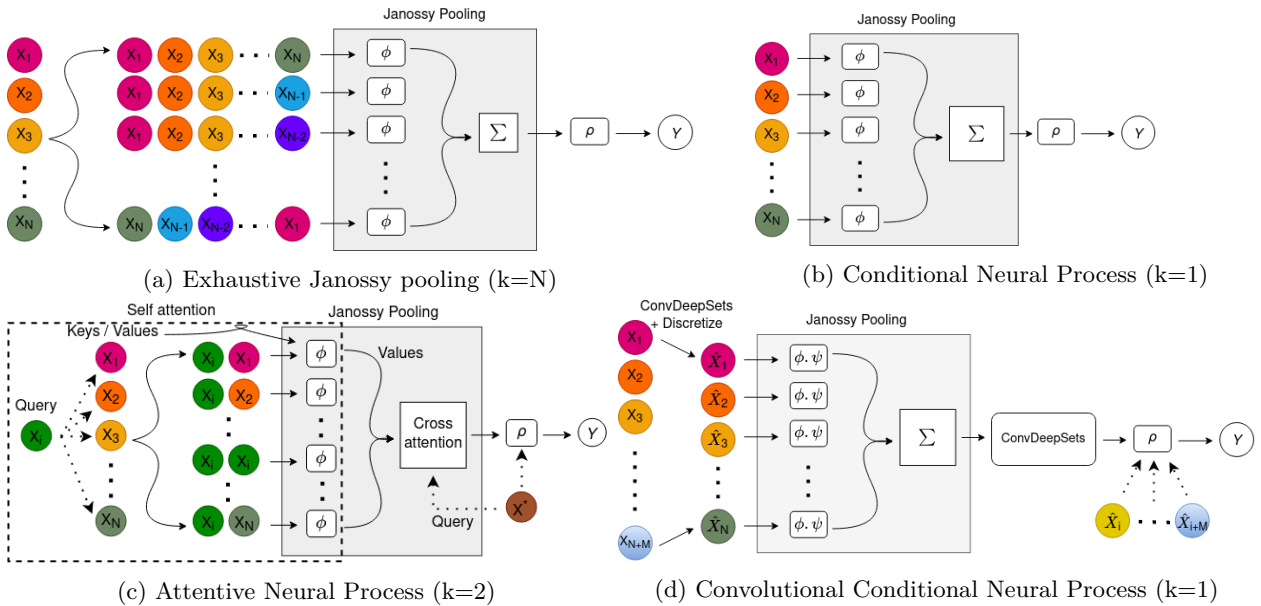


Figure 6: Neural Process Families from the eye of Janossy pooling: ϕ is the encoding function acting on inputs $\{x_1, x_2, \dots, x_N\}$ with permutation-sensitive parameters and ρ is the decoding function.

Meta-learning. A strong motivation behind CNPs (Garnelo et al., 2018a) remains mimicking the capabilities of Gaussian process to capture distribution over functions using the powerful approximation capabilities of neural networks. To do so, they leverage *meta-learning* (Finn et al., 2017) which involves training models on several learning episodes of diverse tasks so that a learner can generalize well to new unseen tasks after seeing only a few examples of the latter. In case of NPs, each such task models an underlying stochastic data generator function and comprises learning from the labelled context set C to be able to make predictions on a set of unlabelled target points T .¹⁶ Considering the supervised classification setup for instance, the fact that each learning episode gets to select (typically few and irregularly spaced) samples from arbitrarily chosen subset of total classes to form C and T accounts for the improved generalizability of the learner. Repeatedly optimizing the model on context sets labeled consistently across batches in an episode but differently across episodes helps build representations that are more transferable from previous tasks to novel tasks. The meta-learning optimization criteria thus involves maximizing the log likelihood of the conditional predictive distribution $p(Y_T|T, C)$ mentioned in equation 4.

¹⁶In the standard meta-learning literature, C and T are often synonymous to the support and the query set, respectively.

NPF models meta learn stochastic processes by employing a *model-based* approach to compute $p(Y_T|T, C)$ (Huisman et al., 2022).¹⁷ Learning over multiple tasks comprising C and T in turn helps them select inductive biases from data. For instance, training NPs for image completion with subsequent tasks consisting of images of the same object(s) captured under different conditions such as size, angle, etc. can induce group symmetry to scaling and rotation (Kawano et al., 2021). The model-based meta learner perspective thus helps compare the superior efficiency of NPs to gradient-based learners (Finn et al., 2017; Nichol & Schulman, 2018) that typically demand a significant amount of memory and computation besides suffering from training issues of model sensitivity (Antoniou et al., 2019) and affinity to local optimum (Molybog & Laveai, 2021). A meta learner rather close to NPs is that of Ton et al. (2021) meta-learning density estimation based on conditional mean embedding operators.

Functional data analysis. Given that Neural Processes meta learn distributions of (potentially discretized) data generating functions sampled irregularly along a continuum (time, space, wavelength spectra, etc.), these can be seen to perform *functional data analysis* (FDA). Analyzing functional data however involves dealing with the non-linearity of the data dimensions coupled with their intricate inter-dimensional dependencies. Subsequently, FDA is known to be a notoriously complicated task for standard machine learning algorithms (Lin & Zhu, 2019) and challenging even for deep neural networks (Rossi et al., 2005). NPs (and their variant) thus stand out in their capacity to encode the samples of infinite dimensional functional data using the finite dimensional task representation vector $E(C)$ obtained from instantiations of Janossy pooling mentioned in Section 2.2.¹⁸ To do so, they leverage an encoder-decoder pipeline where the encoder is a permutation-invariant function guaranteeing exchangeability on sets. NPF members therefore not only complement the recent advances in functional autoencoding (Hsieh et al., 2021b;a) but also open up the doors to achieve *practical* universal approximation of set functions.¹⁹ It is the latter problem formulation that has in turn put NPs as the key inspiration behind extending finite dimensional encodings (see equation 2) to infinite-dimensional functional representations (Gordon et al., 2020; Xu et al., 2020).

Regression algorithms. While NPs have been widely applied to a number of FDA tasks including classification and clustering (Pakman et al., 2020), they were originally introduced as *regression algorithms* (Garnelo et al., 2018a) that learn the ground truth stochastic process characterized by arbitrary polynomial functions f using neural network parameters. As such, a number of other tasks can be regarded as specific cases of regression. For instance, classification can be formulated as a step function regression problem (Garnelo et al., 2018a) where the global aggregation operation in equation 2 is replaced by a classwise aggregation of encodings. In section 6.3, we indeed leverage this definition of classification to implement graph-based Neural Processes for uncertainty-aware part labeling of 3-d point clouds.

Using neural networks for regression endows NPs with a range of benefits over the traditional GP-based regression approaches, namely their data-driven approach to approximate fairly complicated functions and their efficiency in inference. The regression-driven perspective to NPs further aligns well with the research direction of deep kernel learning (Wilson et al., 2016). In particular, Rudner et al. (2018) - in a different training setup - show that affine-decoder NPs are mathematically equivalent to GPs with deep kernels, *i.e.*, GPs with a covariance function parameterized by a deep neural network, while exhibiting the model behavior of non-affine-decoder NPs.

Bayesian modeling. The uncertainty-aware regression capability further offers a statistical *Bayesian* window to NPs and posits an empirical prior over the distribution of functions \mathcal{D} that jointly captures the underlying stochastic process. In particular, the KL divergence in equation 8 leverages the same network to encode the prior and the posterior distributions where the former one has seen only the context $C_i \subset D$ while the latter is informed of the targets too. Accordingly, the optimization objective of NPs becomes maximizing

¹⁷Viewing NPs in the light of prototypical networks (as noted in section 2.1) however opens up the possibility of using these for *metric-based* meta-learning.

¹⁸In practice, NPs encode only a finite dimensional spline subspace of the space of all such measurable real-valued functions.

¹⁹We emphasize on practical universal set function approximation because of the vulnerability of the NP implementations to underfit the context set (Kim et al., 2019) despite their theoretical plausibility to perform otherwise (Zaheer et al., 2017; Bloem-Reddy & Teh, 2020).

the expectation over the collection of context and target sets drawn from D (see equation 4) using several meta-learning tasks.

The meta-learning setup in turn demands hierarchy in the Bayesian model in order to infer parameters shared across tasks (Grant et al., 2018). In the particular case of latent variable NPs, optimizing such Bayesian hierarchical model further involves approximating the intractable posterior $p_\theta(z|C, T)$ with a variational posterior $q_\phi(z|C, T)$ and solving for the resulting ELBO (see equation 8).²⁰ While the Bayesian perspective puts NPs side by side with a number of popular variational inference models including partial variational autoencoders (Ma et al., 2019b), variational homoencoders (Hewitt et al., 2018) and variational implicit processes (Ma et al., 2019a), a GP-like machinery endows these a resemblance to the recent advances in efficient uncertainty-aware prediction modeling (Tsybalov et al., 2019).

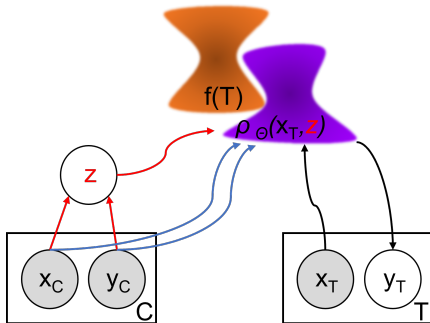


Figure 7: Graphical model depicting the CNP and latent NP as deep generative models. Gray shades stand for observed variables and arrows denote information flow. Colors differentiate model-specific setting: **red** for latent NPs, **blue** for CNPs, and **black** common to both. For latent NPs, ρ_θ is the decoder mapping the samples from the relatively simple distribution of z to the intricate distribution $\rho_\theta(z)$. Deep generative models are trained with an objective to make $\rho_\theta(x_T, z)$ resemble the true distribution $p(f(x))$ (shown in **orange**) by maximizing the likelihood $p(f(x)|z)$ of all observed $x \in C \cup T$.

Deep generative modeling. Lastly, we consider the viewpoint that NPF members are likelihood-based *deep generative models* that learn the intricate probability distribution of f based on a finite number of independently and identically distributed observations $(X_{C \cup T}, Y_C) \sim D$. Using the latent NPs as an instance, the modeling objective involves mapping samples from the tractable distribution of latent variables $z \sim \mathcal{Z}$ supported in \mathbb{R}^q to points in \mathbb{R}^{d_y} that resemble the given labels Y_C . A latent NP can then be viewed as a generator g that samples $z \sim \mathcal{Z}$ and computes $g(z)$ based on equation 7 (Ruthotto & Haber, 2021). Like other generative models, a latent NP computes the evidence $p(x)$ of a sample $x_T \in T$ using the marginalization defined in equation 6 where the observation likelihood $p(f(x_T)|x_T, z)$ accounts for the similarity of $g(z)$ to $f(x_T)$. Figure 7 illustrates this graphically for CNPs and latent NPs. On a similar note, the generative viewpoint encapsulates other recent models like the autoregressive Transformer NPs (Nguyen & Grover, 2022) – introduced in section 3.2 – that generate outputs for a target point conditioned on the context as well as the previous target predictions.

Generative modeling requires NPs to learn the true data distribution from limited observations. This then endows them a resemblance with other minimal supervision frameworks including neural statisticians (Edwards & Storkey, 2017) and generative query networks (GQNs) (Eslami et al., 2018).²¹ Subsequently, Dvijotham et al. (2018) propose placing such (probabilistic) generative models under a common verification framework by imposing the requirement that for every choice of conditioning input to the model, their outputs must satisfy a linear constraint with high probability over the sampling of latent variables.

²⁰The Bayesian training objective of maximizing the likelihood (see equation 6) endows NPs with superior efficiencies over non-Bayesian objectives like cross-validation that often suffer from curse of dimensionality (Fong & Holmes, 2020).

²¹Given their close resemblance to the NP architecture, GQNs can be thought as specific cases of NPs that also exploit meta-learning to model the distribution over functions generating scenes rather than those over the generic family of random functions.

3 Taxonomy of the Neural Process Family

In this section, we present a detailed survey of the advances in the Neural Process family. Given the broad scope of these works, we first consider establishing a common ground for structuring the various research directions. In particular, we exploit the fact that all such NPF members encode a set of assumptions as inductive biases to generalize the finite context set into a model suitable for the input domain (Wolpert, 1996). For example, the CNP model (Garnelo et al., 2018a) discussed in Section 2 relies on the average pooling operation to capture permutation-invariant context set representation. The latent NP (Garnelo et al., 2018b) improves upon this by additionally deriving a global latent distribution from the pooled encodings to induce the correlation among its outputs. By the same token, we identify a subtotal of eight major inductive biases encompassing the NPF tree. These branches along with their representatives are briefed below:

1. Task-agnostic set function approximators: These methods rely on the most basic set function approximators averaging the context encodings in order to capture permutation-invariant representations. The groundbreaking CNPs (Garnelo et al., 2018a) are a representative of this category.
2. Task-specific set function approximators: These methods employ task-specific set function approximators to overcome the limitations of their more generic task-agnostic counterparts. A representative method of this category remains attentive Neural Processes (Kim et al., 2019) leveraging attention to capture the context information relevant to the query in hand.
3. Euclidean symmetry equivariance: Methods in this NPF branch ensure that the outputs of NPs remain equivariant to the transformations applied on the inputs lying on Euclidean spaces. Depending upon the ranges of isometry targeted, such methods can guarantee shift equivariance (Gordon et al., 2020), group equivariance (Kawano et al., 2021) or full equivariance (Holderrieth et al., 2021).
4. Non-Euclidean graph connectivity: This NPF branch exploits the non-Euclidean relational information present in many real-world datasets. The dominant approach in this category remains the use of graphs for modeling dependencies among inputs. Popular methods in this branch include Graph Neural Processes (Nassar et al., 2018) modeling classes of graph-structured inputs and Functional Neural Processes (Louizos et al., 2019) building dependency graphs among the latent representation of inputs lying on regular lattices.
5. Output dependency: This NPF category addresses the fact that similar inputs might often imply correlated outputs - for instance, similar intensity values for pixels located in the neighborhood of a given pixel. As a result, the methods in this branch model *predictive correlation* by inducing the bias that not all input points are independent. The predominant approaches to capturing such predictive correlation remain using latent variables or gaussian kernel functions as such. Accordingly, (Latent) NPs (Garnelo et al., 2018b) and Gaussian NPs (Bruinsma et al., 2021) make two popular methods in this category.
6. Temporal dependency: This NPF category targets architectures that are designed to capture temporal dependencies in data. Given their ability to model temporal dynamics, these methods are more robust to distribution shifts in data and can extrapolate observed patterns into the future. Sequential Neural Processes (Singh et al., 2019) are a popular member in this branch.
7. Multi-task relatedness: Methods in this category explicitly rely on task relatedness in function spaces for enriching the transfer of useful knowledge among tasks in the meta-learning setting. Such an objective sets them apart from other NPF members that primarily optimize on a range of specialized inductive biases while leaving out multi-task learning on the premises of meta-learning. The Conditional Neural Adaptive Processes (Requeima et al., 2019) incorporating adaptation networks in (latent) NPs for learning task-specific classifier parameters remains the earliest work along this direction.
8. Domain-invariance: Methods in this NPF branch induce biases that help build representations that are distinct enough to distinguish examples belonging to the same or related domains. In other words, methods in this branch are capable of learning distance measures among the inputs belonging to the same domain. Metric-based contrastive learning approaches thus dominate this branch with a representative method being contrastive Neural Processes (Kallidromitis et al., 2021).

Figure 8 illustrates the branches together with the methods belonging to these. It is worth noting that a number of works might target encoding multiple such biases. In such cases, we break ties by categorizing them based on the primary modeling limitation they intend to overcome and subsequently, the inductive bias they rely on for this. The rest of this section details the works belonging to each NPF branch.

Note: Due to the cross-referencing among the NPF branches, some concepts might require forward lookup in the paper. These have been marked by †.

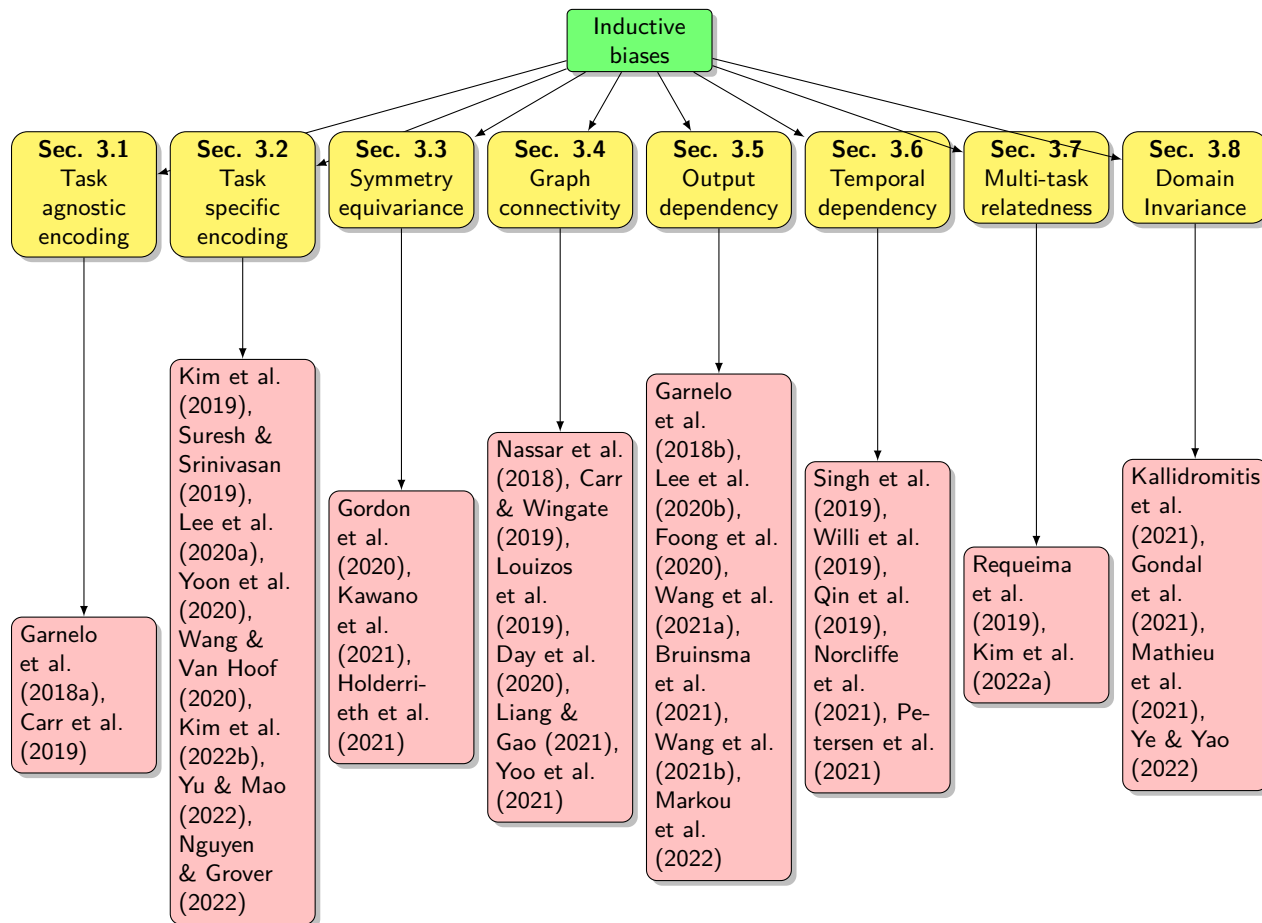


Figure 8: A taxonomy of the Neural Process family on the basis of the primary inductive biases they target.

3.1 Task agnostic set function approximation

This NPF category consists of the generic methods exploiting the set function approximation capabilities of Deep Sets for modeling stochastic processes represented by complex functions. The groundbreaking conditional Neural Processes (CNPs) (Garnelo et al., 2018a) fall into this branch (see Section 2) as such. CNPs model the parameterized distribution over functions by maximizing the data likelihood and minimizing the reverse KL divergence between the true and the approximate posterior in turn (see equation 8). For distributions supported on overlapping domains, the reverse KL divergence-based training objective helps optimize the blown up loss values (due to $\log(q(z|E(C))) = 0$) through its mode-seeking behavior.

However, there could be scenarios where a poorly specified model leads to a zero or an intractable data likelihood thus deeming the domains of the modeled and the exact distribution to be disjoint. In such a

scenario, both forward and reverse KL-divergence are prone to infinite loss values. Jensen-Shannon (JS) divergence – a function of the average of the two distributions, improves over KL by saturating the loss values to $\log(2)$ in such cases.²² Such a saturation nevertheless renders the gradients unusable (Kolouri et al., 2019). One natural solution to avoid this Achilles’ heel of distribution modeling therefore is to avoid the need for likelihood measurement. By opting to measure earth-mover’s distance between the distribution domains rather than data likelihood, generative models on Wasserstein metric have been shown to offer superior performances over their KL and JS divergence-based counterparts (Arjovsky et al., 2017).

Wasserstein Neural Processes. Inspired by the aforementioned idea, Carr et al. (2019) propose using Wasserstein distance as a proxy for KL divergence in NPs. In particular, their training objective considers minimizing the sliced Wasserstein distance (Kolouri et al., 2016) between the synthetic set of decoder predictions and the actual set of predictions instead of maximizing equation 8. To do so, they first project the high dimensional synthetic and actual predictions on to a one-dimensional distribution and then compute the regular Wasserstein distance between these. The resulting Wasserstein NPs (WNPs) are shown to quickly fit completely disjoint g -and- κ (Jorge & Boris, 1984) distributions where traditional NPs would fail due to intractable likelihood.

The most intriguing capability of WNPs remains in modeling higher dimensional distributions. To show this, Carr et al. (2019) treat image completion (see Section 6.2 for the problem definition) as a high dimensional regression task and split 32×32 images into 4×4 tiles so that f now becomes the function mapping the tile coordinates with their associated pixels while a task involves predicting the entire tiles given a set of 4-16 tiles. Using tiles as context points instead of pixels helps WNPs capture background, facial structure and color better than the likelihood-driven CNPs. At this point, it is worth noting that while such a sliced Wasserstein distance-based training objective can be used with other NP architectures, the authors only consider the CNP (Garnelo et al., 2018a) as the foundation model in their original work. We therefore classify their work as inducing task-agnostic bias.

Note: At this point, it is worth acknowledging that there is a line of work on NPF models which looks at different objective functions rather than just different models. The Wasserstein NP (Carr et al., 2019) discussed above is one example of this optimizing the Wasserstein distance between the prior and posterior distributions instead of the KL divergence. Similarly, the ConvNP (Foong et al., 2020) discussed in section 3.5 gets away with variational posterior inference and instead approximates the biased log likelihoods of observations using importance sampling.

3.2 Task specific set function approximation

While the vanilla task-agnostic functional representation allows NPs to encode sets, they remain naive when considering the context relevant to a given target query. In other words, the methods relying on task-agnostic set function approximation would assign equal weight to all the observations while predicting the value of a given function location. Task-specific set function approximators help overcoming these limitations through the use of encoding functions that are sensitive to the queried locations. For instance, self-attention (Vaswani et al., 2017) induces context-specific approximations by using these as keys, queries, and values while cross-attention leverages target set features as queries, context set features as keys, and self-attention outputs as values to assign higher weights to the relevant context.

Attentive Neural Processes: While the introduction of latent variables helped NPs to perform global sampling of functions by adapting their priors to context data at test time (see Section 2), Kim et al. (2019) show that these are still prone to underfit the observed context set they have been conditioned on. They

²²This accounts for a prominent benefit of JS distance-based generative adversarial networks (GAN) over KL-based variational autoencoders. The training objective for GANs involves approximating a dataset distribution using the generator. It is often the case that the generator’s output distribution does not overlap with the real dataset distribution.

attribute this to the finite \mathbb{R}^e -dimensional context encoding $\phi_{i \in N}$ whose computation presumes that each context point is processed individually and is assigned an equal weight by the decoder to derive prediction for a given target point. Such individual processing of data points takes away the capability of the model to perform relational reasoning (Santoro et al., 2017). Furthermore, the cardinality N of the context set has been shown to form a theoretical lower bound for \mathbb{R}^e to universally represent an arbitrary f given the relaxed constraint that the encoder and decoder set function approximators are flexible enough (Wagstaff et al., 2019).²³ Such a flexibility however, does not hold in practice and even $\mathbb{R}^e > N$ can not guarantee task-agnostic function approximators like DeepSets (Garnelo et al., 2018b) to universally represent all f .

GPs, on the other hand, avoid such underfitting through kernel functions enforcing the predictions of two points lying closer in the input space to be closer. Inspired by this, Kim et al. (2019) propose using attention as an inductive bias to model the pairwise relation among the inputs. The resulting attentive Neural Processes (ANPs) employ differentiable attention to ensure that the encoding $E(x|C)$ is locally relevant per target point $x \in T$ rather than being globally static across the target set T . The aforesaid self and cross-attention mechanisms can then be seen to refine the input features to compute the relevance. First, a similarity is computed between the context input embeddings forming the keys, and the target (in case of cross-attention) or the context (in case of self-attention) input embeddings forming the queries. The input embeddings then form the values and are aggregated with the similarities to predict the local target embedding. The two major forms of attention used in ANPs are *dot-product* and *multihead*.

Formally, if $K \in \mathbb{R}^{N \times d_\phi}$ and $V \in \mathbb{R}^{N \times d_v}$ are the matrix forms of N key-value pairs and $Q \in \mathbb{R}^{M \times d_\phi}$ be the corresponding form for the queries, then the scaled *dot-product* attention (Vaswani et al., 2017) is given as:

$$\mathbf{DotProduct}(Q, K, V) := \text{softmax} \left(\frac{QK^T}{\sqrt{d_\phi}} \right) V \quad (9)$$

where, the scaling factor $\sqrt{d_\phi}$ balances the increase in length of Q and K due to the increase in their dimensions. Using the embedding vectors of all the input sequence tokens to comprise the keys and values makes the $\mathbf{DotProduct}()$ operation to be permutation invariant. Vaswani et al. (2017) further propose a parameterized extension to equation 9 which computes head-specific values to linearly transform the keys, values and queries for each head before applying the dot-product attention. Such a multihead attention concatenates the head-specific values to learn different relations between tokens from the same input:

$$\begin{aligned} \text{head}_h &:= \mathbf{DotProduct}(QW_h^Q, KW_h^K, VW_h^V) \in \mathbb{R}^{m \times d_v} \\ \mathbf{MultiHead}(Q, K, V) &:= \text{concat}(\text{head}_1, \dots, \text{head}_H)W \in \mathbb{R}^{m \times d_v} \end{aligned} \quad (10)$$

where, h_i forms the i -th head out of H total heads and W is a linear transformation matrix ensuring consistency of dimensions among the inputs and outputs. Applying multi-head attention results in predictions that are smoother than the single-head dot product attention.

ANPs bind the potential of CNPs and latent NPs by leveraging the multi-head attention mechanism along two paths: (a) along the latent path, the mechanism computes self-attention (Vaswani et al., 2017) among the context set elements. The resulting self-attention values are then averaged to derive the context set distribution which is used to sample the global summary of contexts z ; (b) the deterministic path employs multi-head attention to compute the cross-attention (Bahdanau et al., 2015) between the context and the target set elements. The cross-attention values are then averaged to derive the deterministic encoding $r_C^* = r^*(C, T)$. The resulting predictive distribution of an ANP can thus be given as:

²³This should be read in the sense that there could be *some* such f (for example, the max operator) that require at least an N -dimensional latent space to be sum-decomposable based on the permutation invariant encoding $E(C)$.

$$\begin{aligned}
p(f(T)|T, C) &\approx \int p(f(T)|T, z, r_C^*)q(z|E_{SA}(C))dz \\
p(f(T)|T, z, r_C^*) &= \prod_{x \in T} \mathcal{N}(y_t|\mu(x, r_C^*, z), \text{diag}[\sigma(x, r_C^*, z)]^2) \\
q(z|E_{SA}(C)) &= \mathcal{N}(z|\mu(E_{SA}(C)), \text{diag}[\sigma(E_{SA}(C))]^2)
\end{aligned} \tag{11}$$

where, $E_{SA}(C)$ is computed in a way similar to equation 2 except for the encoder ϕ has now been replaced by trainable self-attention (SA) networks. Taking image completion as an example again, Kim et al. (2019) show that ANPs depict stark visual contrast in outputs compared to NPs and CNPs as the former prioritizes the context of inputs while sampling from the predictive distribution. A drawback of using attention however remains its poor scalability with high dimensional data as the complexity of **DotProduct()** evaluates to $\mathcal{O}(d_v N^2)$ owing to the multiplication QK^T . Computing the self-attention across the context-context and the cross-attention across the target-context pairs in turn implies that the computational complexity for an ANP amounts to $\mathcal{O}(N(N + M))$. In contrast, CNPs and NPs scale linearly with data.

Improved attentive neural processes: While the use of global latent variable z in ANP helps distribute the global properties of the task across all target predictions, learning some tasks could require modeling functions with varying local structures, e.g. a periodic function with input-dependent period. For better learning of such functions, Suresh & Srinivasan (2019) propose the ANP⁺⁺ model by adding two extensions to the ANP. First, ANP⁺⁺ requires each context point to have its own latent representation which is used to generate query-specific local latent representation via attention. Second, motivated by the Transformer architecture (Vaswani et al., 2017), the ANP⁺⁺ decoder extends the MLP-only ANP decoder to incorporate self-attention. The latter improvement helps adapting the decoded targets’ internal dependencies with respect to each other. The authors highlight the superior performance of ANP⁺⁺ at modeling position-specific periodic structures of a synthetic 2D non-stationary sines dataset as well on the MNIST image completion task.

Residual Neural Processes: As mentioned before, the bottleneck for expressivity in the task-agnostic NPF encoders lie in how well the finite dimensional latent summary of $\phi_{i \in N}$ approximates the random function f modeling the data generating process. While ANPs consider resolving this based on non-linear locally relevant encoding captured using self-attention networks, Lee et al. (2020a) show that despite being non-linear, self attention networks fail to approximate the optimal summary $E_{SA}^*(C)$ of an arbitrarily linear system. Addressing this, the authors propose the Residual Neural Processes (RNPs) that exploit the structural resemblance of ANPs to Bayesian Last Layers (BLLs) (Weber et al., 2018) for modeling f .

Formally, the meta-learning setup for BLL includes S learning rounds where in each round $t \in [1, S]$, a learner sees a context x_t , predicts its class label y_t , and receives a reward r_t based on whether the predicted label is the actual class c . BLLs exploit the generalized linear nature of the last layer ω_c^T of neural networks for performing closed-form model uncertainty estimation. This estimation is posed as a distribution over all possible values of the last layer weighted by their probability. In doing so, they treat the rest of the network as feature extractors $F_\theta(x)$ for the input x . The resulting network architecture $\sigma(\omega_c^T F_\theta(x))$ (where, σ is an activation function) thus reflects the posterior probability of a class label $p(c|x, \omega_c^T)$ and is optimized with the goal of minimizing a regret score $R = \sum_i^T r_i^* - \sum_i^T r_i$ with respect to the optimal reward r_i^* at step i . Such a formulation benefits BLLs in swift handling of input distribution shifts by updating F_θ in a fashion that preserves low values of R . Inspired by this, Lee et al. (2020a) consider combining BLLs with ANPs.

A limitation of BLLs is that they rely heavily on the context summary that is linear in class labels c . For the same embedding dimension d_v , BLLs thus have restricted modeling potential compared to ANPs. In contrast, RNPs bring the best of both ANPs and BLLs by first employing the former to predict the non-linear residual of $E_{SA}(t|C)$. The exact linear $E_{SA}(C)$ is then computed using BLLs before being passed to the predictive distribution $p(f(T)|T, C)$. An RNP decoder thus relies on the BLL statistics as inputs to combine the superior (non-linear) expressivity of ANPs and the faster (linear) convergence speed of BLLs.

With the goal of further enhancing uncertainty prediction in RNPs (and subsequently, in ANPs and BLLs), Lee et al. (2020a) draw their motivation from latent NPs and propose a stochastic feature extractor with a posterior conditioned on the context summary. This is specifically implemented using a stochastic context embedding z_f that defines an approximate prior $q(z_f|C)$ to infer the predictive distribution conditioned not only on the last layer ω_c^T but also on the feature extractor F_θ . This improvement endows RNPs with stochasticity in paths as well as features and in turn, helps surpass the performance of RNPs with only path-based stochasticity on 1-d function regression and 2-d image completion tasks.

Doubly stochastic Neural Processes: While introducing a latent variable z shared across all target inputs enables global sampling of functions (see Section 2) in NPs, the use of task-specific function approximators alleviates underfitting by capturing locally relevant context information. Motivated by these peculiarities, Wang & Van Hoof (2020) propose extending latent NPs by introducing an auxiliary latent variable z_* that is local to each target set point $(x^*, f(x_*))$. The authors show that this helps separate the global and sample-specific variations while increasing the expressive power of the model. The resulting Doubly Stochastic Variational Inference for Neural Processes (DSVNP) framework hosts target-specific latent encoding to capture variations of instance locality while making the inference process resemble that of ANP. In particular, DSVNP infers the global latent variable z referring to the entire observed context as well as the local latent variable z_* referring to the queried location x_* . The variational posteriors of these variables are first approximated as follows:

$$\begin{aligned} q_{\phi_{1,1}} &= q(z|C) \\ q_{\phi_{2,1}} &= \mathcal{N}(z_* | \mu(z, x_*, f(x_*)), \text{diag}[\sigma(z, x_*, f(x_*))]) \end{aligned} \tag{12}$$

where $q(z|C)$ is the posterior defined in equation 6, and $q_{\phi_{1,1}}$ and $q_{\phi_{2,1}}$ are the approximate posteriors used to sample z and z_* , respectively. Consequently, the training objective now involves maximizing the ELBO:

$$\begin{aligned} \log p(f(x_*)|x_*, x_C, y_C) &\geq \mathbb{E}_{q_{\phi_{1,1}}} \mathbb{E}_{q_{\phi_{2,1}}} \log p(f(x_*)|z, z_*, x_*) - \mathbb{E}_{q_{\phi_{1,1}}} [D_{KL}[q_{\phi_{2,1}}(z_*|z, x_*, f(x_*)) || p_{\phi_{2,2}}(z_*|z, x_*)] \\ &\quad - D_{KL}[q_{\phi_{1,1}}(z|C, T) || p_{\phi_{1,2}}(z|C)] \end{aligned} \tag{13}$$

where, (C, T) makes up the observed data points (x_C, y_C, x_T, y_T) , and $p_{\phi_{1,2}}(z|C)$ and $p_{\phi_{2,2}}(z_*|z, x_*)$ are priors parameterized with neural networks initialized using two diagonal Gaussians. For a better picture, equation 13 should be contrasted with equation 8 containing a single global posterior $q(z|C, T)$. Using global and local latent variables endows DSVNP with a hierarchical architecture which is an amalgam of latent NP and conditional variational autoencoder (Sohn et al., 2015). While DSVNPs remain suboptimal to ANPs for 1-d regression tasks involving uncertainty predictions in the interpolating regime, the authors highlight their finer potential in the extrapolating regime where vanilla NPs and ANPs often underestimate the negative log-likelihood based uncertainty measure. Moreover, using cart-pole state transition prediction and multi-output regression as examples, the authors show that DSVNPs outperform latent NPs, CNPs and ANPs on high-dimensional function modeling tasks.

Robustifying sequential Neural Processes[†]: Singh et al. (2019) introduce Sequential Neural Processes (SNPs) to induce temporal correlation in NPs modeling meta-transfer learning across sequential tasks (refer to Section 3.6 for an overview of SNPs). Following the insights brought by (Kim et al., 2019), Yoon et al. (2020) show that SNPs too are vulnerable to underfitting. They then highlight the limitation of applying attention directly to SNPs. In particular, the fact that SNPs rely on meta-transfer learning to enable temporal transfer of knowledge across tasks permits the context set at a time step t to be *sparse*, *i.e.*, only a small number of current context points provided, and *obsolete*, *i.e.*, past context coming from shifted tasks. Applying attention to such context can be delicate enough to actually hurt the model’s performance.

Towards the end goal of exploiting attention to meta learn sparse and obsolete context, the authors propose the Recurrent Memory Reconstruction and Attention (RMRA) framework. RMRA resolving the aforemen-

tioned issues in two steps: (i) it complements the sparse but original context by augmenting it with a generated *imaginary* context that acts as a proxy for applying attention, and (ii) it addresses obsolete context through a Recurrent Memory Reconstruction (RMR) method that recurrently reforms the imaginary context for obsolete past tasks by transforming them into meaningful representations at each time step.

Formally, for a time step $t \in S$, RMR generates a new imaginary context \bar{C}_t with K imagined key-value pairs forming memory cells where the key and the value sets are given by $\bar{X}_t = \{\bar{x}_t^k\}$ and $\bar{V}_t = \{\bar{v}_t^k\}$ for $k \in [1, K]$. The imagined context generation process can be seen as a function of the real context C_t of the current task \mathcal{T}_t , the real and imagined past context \bar{C}_{t-1} , and the past hidden states $\bar{\mathcal{H}}_{t-1}$:

$$\bar{C}_t, \bar{\mathcal{H}}_t = \text{RMR}(C_t, \bar{C}_{t-1}, \bar{\mathcal{H}}_{t-1}) \quad (14)$$

where, the set of hidden states $\bar{\mathcal{H}}_t = \bar{\mathcal{H}}_t^{\text{key}} \cup \bar{\mathcal{H}}_t^{\text{val}}$ is comprised of the key and value-generating hidden states. Equation 14 works in two steps. First, the imaginary keys are generated by feeding a concatenated set of previous imaginary keys \bar{X}_{t-1} and a permutation-invariant encoding $E(C_t)$ of the real context C_t to a key-tracker Recurrent Neural Network (RNN). The RNN’s updated hidden state \bar{h}_t^{key} then generates the new imaginary keys \bar{X}_t . Second, using the new imaginary keys \bar{X}_t , the new real context C_t , the previous values \bar{V}_{t-1} and their corresponding hidden states $\bar{H}_{t-1}^{\text{val}}$ as inputs, RMR generates a new value set \bar{V}_t :

$$\begin{aligned} \bar{X}_t, \bar{h}_t^{\text{key}} &= \text{GenerateKey}(C_t, \bar{X}_{t-1}, \bar{h}_{t-1}^{\text{key}}) \\ \bar{V}_t, \bar{H}_t^{\text{val}} &= \text{GenerateValue}(\bar{X}_t, C_t, \bar{V}_{t-1}, \bar{H}_{t-1}^{\text{val}}) \end{aligned} \quad (15)$$

The first value generation step is accordingly named as *value-flow tracking* in the sense that the value proposals across tasks are captured by assigning an RNN for each memory cell so that the cell tracks the flow of a value. This is followed by the *value-flow interaction* step given that the proposed values of each memory cell are interactively updated using self-attention across other values in the proposal set and the real context set. Finally, the imaginary context \bar{C}_t from equation 14 is incorporated into the observation model in SNP to form the observation likelihood $p(f(T_t)|T_t, z_t, \bar{C}_t)$. The resulting combination of RMR with SNP forms the Attentive SNP with RMR (ASNP-RMR) model whose generative process is given as:

$$p(f(T), Z, C|T, C) = \prod_{t \in S} p(f(T_t)|T_t, z_t, \bar{C}_t) p(z_t|z_{<t}, \bar{C}_t) p(\bar{C}_t|\bar{C}_{<t}, C_{\leq t}) \quad (16)$$

For a comparison of ASNP-RMR’s modifications over SNP, equation 16 can be compared against 31 that lacks an imaginary context. Similar to the autoregressive variational approximation in SNPs (see equation 32), the training objective for ASNP-RMRs is given by:

$$p(Z|\bar{C}, D) \approx \prod_{t \in S} q(z_t|z_{<t}, \bar{C}_{\leq t}, O) \quad (17)$$

where, $O = (C, T, f(T))$ is the observed dataset. In contrast to equation 33, the optimization now involves maximizing the following ELBO including the imagined context set over all time steps:

$$\begin{aligned} \log p(f(T)|T, C) &\geq \sum_{t \in S} \mathbb{E}_{q(z_t|O)} [\log p(f(T_t)|T_t, z_t, \bar{C}_t, C_t)] - \\ &\mathbb{E}_{q(z_{<t}|O)} [D_{KL}(q(z_t|z_{<t}, \bar{C}_{\leq t}, O) \| p(z_t|z_{<t}, \bar{C}_{\leq t}, C_{\leq t}))] \end{aligned} \quad (18)$$

The resulting ASNPs converge faster than ANPs (Kim et al., 2019) and SNPs (Singh et al., 2019). Similar to SNP, the authors further employ ASNP-RMR to generative query networks (GQNs) forming the attentive GQN-RMR (ATGQN-RMR) model. They report that ATGQN-RMR with unlimited attention window can outperform temporal GQNs as well as the ATGQNs with attention limited to a well-defined window size.

Neural processes with stochastic attention: Highlighting the underfitting in CNPs and NPs, Kim et al. (2022b) further show that the noise sensitivity of these vanilla models makes them fall short in capturing contextual embeddings under noisy situations and restrictive task distributions.²⁴ As a better approach to capture context encoding that remains well differentiated from the target encoding, the authors build upon ANPs and information theory to consider inducing stochasticity into the attention. In doing so, they preserve the decoder architecture of ANPs (Kim et al., 2019) while modifying the encoder. Moreover, they claim the independence between the critical conditions for contextual embeddings in NPs and the target features.

Formally, stochastic attention (with a key-based contextual prior) helps capture predictive distributions of the form $p_\theta(f(T)|T, z, r_C^*)$ (see equation 11) that correlate more with the context information (z, r_C^*) under noisy conditions. Similar to the ANP, such an attention works by building a global representation z over entire context points and a local representation r_i for each target point $x \in T$ to model their individual predictive distributions. Unlike the ANP, stochastic attention however leverages the Bayesian attention module (Fan et al., 2020) for capturing local representation r_i weighed by the stochastic attention values w_i . Furthermore, backpropagating the gradient values in such a framework involves reparameterization by drawing random noise samples $\epsilon_1 \sim \text{Unif}(0,1)$, $\epsilon_2 \sim \mathcal{N}(0,1)$ where, ϵ_1 is used for deriving $\{w_i\}_{i=1}^N$ and ϵ_2 for deriving z . The resulting model is then trained using amortized variational inference.

Through a number of tasks including 1-d and 2-d regression, and predator-prey modeling, Kim et al. (2022b) show that stochastic attention-based NPs surpass the performance of CNPs (Garnelo et al., 2018a), NPs (Garnelo et al., 2018b) and ANPs (Kim et al., 2019). To further simulate a noisy 1-d regression task, their evaluation setup includes generating a periodic noise in the training step. An intriguing application of stochastic attention in their work is recommending movies for a new user based on the real-world MoveLens-100K dataset.²⁵ Here, the authors show that the proposed method achieves lower mean squared error than the ANP alongside a number of other established methods (Rashed et al., 2019; Berg et al., 2017).

Patch attentive Neural Processes: Attention-based task-specific set function encoders helps avoid underfitting in the works mentioned so far. However, as mentioned previously, its application (see Figure 6) involves two computationally intensive steps: (a) self-attention requires computing how each context point attends to all other context points, (b) cross-attention requires computing the attention weights of all context points for each target query. These computations render the efficiency of attention-based NPs heavily dependent on length of the input sequence. For higher dimensional tasks such as 2-d image completion (where each image pixel forms an input element), a number of works, such as that of Gordon et al. (2020), find it infeasible to compute attention on images of resolution higher than 32×32 .²⁶ Inspired by the success of Vision Transformers (ViTs) (Dosovitskiy et al., 2021), Yu & Mao (2022) sketch an outline for using these as NP encoders by replacing the finer pixel inputs for linear mapping of image patches.

The authors first consider splitting an image into equal-sized context P_C and target P_T patches such that shared convolutional kernels compute patch representation vectors. The vectors representing the context patches along with the positional encoding for the patch are then employed in the latent and deterministic paths for feature extraction. Following ANPs (Kim et al., 2019), the authors average the encoder’s representations r_i of individual context points to compute the deterministic global vector and the latent global vector. The deterministic path then serves for cross-attention computation based on the individual context representations r_i as keys, and the target patch representation r^* together with its positional encoding as values. On the other hand, the latent path samples the global latent variable z from the distribution of latent global vectors (see equation 11). The decoder is a standard multi-layer perceptron (MLP) which feeds on z along with the representation r^* and the positional encoding pos^* of the target patch to compute predictions.

Note: At the time of writing, Yu & Mao (2022) merely sketch the above architecture without an empirical verification of its performance. Nevertheless, we mention the work in this

²⁴A preliminary version of this work appeared in the workshop paper of Kim et al. (2021).

²⁵<https://grouplens.org/datasets/movielens/100k/>

²⁶Using global attention on higher resolution images has been a long-standing issue in the domain of computer vision. For instance, a 256×256 ImageNet (Deng et al., 2009) input can involve computing global attention weights in the order of 256^4 , *i.e.*, each of the 256×256 pixels attending to all the 256×256 pixels.

survey given that an efficient attention application carries a huge potential to advance the expressivity of the NPF family for visual data.

Transformer Neural Processes: The latent variable NPs seen so far share the common limitation of intractable marginal likelihoods. While maximizing the ELBO serves to be a well-established get around for training such models, the resulting latent representation learned by these may not always be meaningful (Chen et al., 2017). To address this, Nguyen & Grover (2022) consider replacing the latent variables with fully attentive Transformer architectures. The resulting Transformer Neural Processes (TNPs) treat uncertainty-aware meta-learning as a sequence-modeling task and incorporate the Transformers into the NP framework in three major steps. First, the sequence-modeling formulation involves considering all input points $\{x_i, y_i\}_{i=1}^{N+M}$ as an ordered sequence such that the predictive likelihood of the M target points are modeled autoregressively (see equation 5).

Second, to achieve context invariance and target equivariance while modeling the sequence, the positional embeddings of Transformers are traded for a concatenation of the features x_i and labels y_i of context and targets. To generalize this strategy for the predictive target locations depending on the previous pairs $(x_j, y_j)_{j=1}^{i-1}$ and the current input x_i , these are padded with dummy 0 labels. The autoregressive ordering of the resulting sequence of $N + M$ real and M padded points is then preserved by manipulating the attention among these. In particular, the context points $(x_i, y_i)_{i=1}^N$ only attend to themselves while the real target points $(x_i, y_i)_{i=N+1}^{N+M}$ and the padded target points $(x_i, 0)_{i=N+1}^{N+M}$ attend to all context points as well as the previous target points $(x_j, y_j)_{j=N+1}^{i-1}$. Labeling this model as the Autogressive TNP (TNP-A), the authors highlight its superior expressivity and low tractability.

Third, to tune the expressivity and tractability of TNP-A, the authors propose two variants of it. The former of these, namely the Diagonal TNP (TNP-D) remains computationally cheaper through its assumption of conditional independence among the target outputs $y_{N+1:N+M}$ given the context points and the target inputs $x_{N+1:N+M}$. Such an independence is reflected by removing the real targets from the ordered input sequence and computing a diagonal covariance matrix. The latter variant, namely the Non-Diagonal TNP (TNP-ND) strikes a balance between the TNP-A and the TNP-D by parameterizing the decoding distribution using a multivariate Gaussian with an expressive non-diagonal covariance matrix Σ . To enhance the tractability of TNP-ND, the authors replace Σ using the lower triangular matrix L obtained from its Cholesky factorization.

Following the standard NP experimental protocols, the authors discuss the superior performance of TNPs over the state-of-the-art NPs (Lee et al., 2020b; Kim et al., 2019) on 1-d and 2-d regression tasks, with the TNP-A surpassing its less expressive and more tractable variants. On the contextual wheel bandit problem (Riquelme et al., 2018) however, the TNP-D and the TNP-ND occasionally outperform the TNP-A based on the choices for the sizes of the low-reward regions while the TNPs still outperforming other NP variants.

3.3 Euclidean symmetry equivariance

To ensure that the predictions are equivariant to the transformations applied on the inputs, a category of NPF exploits the symmetry of the data lying on Euclidean spaces. If an input-output mapping $\xi(\cdot)$ is equivariant to a family of transformations, *i.e.*, a group G , a transformation t applied on the input of $\xi(\cdot)$ should result in an output also transformed by t . It is worth noting that this category targets equivariance and not merely invariance to transformations; and the latter restricts the expressive power of neural networks by dropping relevant information. Based on the type of equivariance targeted, we further divide this category of the NPF into two major sub-branches: the specific shift equivariant and the more generic group equivariant Neural Processes. The division reflects the particular importance the former sub-branch carries for visual signals.

Shift-equivariant Neural Processes. Perhaps the most influential factor behind the success of CNNs have been their weight sharing feature endowing them with the ability to output predictions that mirror the input shifts.²⁷Incorporating this as an inductive bias with convolution helps CNNs optimize massively

²⁷We refer to convolution operations being shift-equivariant rather than translation-equivariant. This is in light of recent studies showing the potential limitations of the discrete nature of shifts at inheriting the equivariances dealing with the continuous nature of translations (McGreivy & Hakim, 2022).

on efficiency by expending their parameter space in learning other useful input patterns. However, using CNNs to achieve translation equivariance within NPF architectures is not straightforward. As mentioned in section 2.1, set-based encoders in Neural Processes map the context set C to finite \mathbb{R}^e -dimensional vector embedding $E(C)$. Given that NPs learn a function $f : \mathcal{X} \rightarrow \mathcal{Y}$ over C , the notion of mirroring a shift on f makes sense only if $E(C)$ were to reside in a functional space rather than a vector space. Taking this into account, Gordon et al. (2020) extend Deep Sets Φ to Convolutional Deep Sets (ConvDeepSets) Φ_{conv} that are capable of producing functional input embeddings.

Unlike MLP-based Deep Sets operating on continuous input-output spaces, the use of CNNs in ConvDeepSets restricts input-output mapping to be discrete. While continuous visual signals like images can be easily discretized in to on-the-grid data, *i.e.*, reckoning the pixel locations, discretizing (the functional embeddings of) continuous data belonging to other modalities such as irregularly sampled time series is difficult. This deems them unsuitable for CNN filters. Gordon et al. (2020) propose a three-step getaway for such modalities: discretizing the embeddings of continuous off-the-grid inputs, feeding these to CNNs, and mapping the discrete CNN outputs back to a continuous functional space. For the latter mapping, a radial basis function (RBF) kernels with weights equal to that of the outputs are used. Undoing the discretization on outputs can in turn be seen as approximating the vanilla decoder ρ .

Formally, let $\hat{x} \in \hat{X}_C$ be the context locations obtained by discretizing the input space $x \in X_C$. The ConvDeepSet Φ_{conv} can be seen to bear the architecture of equation 1 except for the fact that the encoding $E(C)$ lying on the infinite-dimensional functional space is now computed as:

$$E(C)(\hat{x}) = \sum_{(x,y) \in C} \phi_y(y)\psi(x - \hat{x}) \quad (19)$$

where, ϕ, ψ makes up the encoding operation. The choice for the decoder ρ , now operating in the function space, remains a shift-equivariant CNN for both on-the-grid and off-the-grid cases. However, the choices of ϕ and ψ might vary for these. For the on-the-grid case, ϕ is a power series of order 1 reflecting the output cardinality per input location while ψ is an RBF kernel with a learnable lengthscale parameter checking the extrapolation range of the model. For the off-the-grid case, ϕ is the context mask tensor appended with the context points while ψ is the filter of the convolution operation.

From the perspective of target-specific function approximation, the encoder ϕ in ConvDeepSet can be viewed as an attention mechanism that projects the label y_i of a context sample on to a discrete space \mathcal{S} based on the similarity between a discretized query x_S and a context key $x \in X_C$. The resulting deterministic ConvDeepSet representation Φ_{conv}^S is then passed through the filter ψ . Similarly, the decoder constitutes another ConvDeepSet whose discretized keys and values comprise x_S and Φ_{conv}^S while queries being $x \in X_T$. Gordon et al. (2020) show that the resulting Convolutional CNP (ConvCNP) model surpasses the CNP as well as the ANP on a range of regression tasks while its complexity still growing linearly with the number of inputs.

Group equivariant Neural Processes. Despite their shift equivariant inductive biases, CNNs have been shown to spend a considerable amount of their precious weight-sharing capacity in learning redundant symmetries of the same feature templates (Olah et al., 2020). Such a structural phenomenon further gets distributed unevenly across the network layers thus ruling out the point of layerwise resolution. Instead, going beyond shift and inducing equivariances to a group of symmetries such as rotation, scale, reflection, hue, etc. can help optimize further on the network capacity of CNNs. Such inductive biases help provide geometric guarantees that the learned representations remain stable to groups of local and global transformations while also avoiding the potential loss of information.

Kawano et al. (2021) first put forward the idea of inducing group equivariance into the NPF by extending ConvCNP to include further symmetries in scalar fields. Termed as EquivCNP, their extended model targets equivariance over the classical Lie Group by leveraging LieConv (Finzi et al., 2020) as the choice of convolutional layer.²⁸ To do so, they first derive a continuous and group-equivariant extension of DeepSet which

²⁸Lie group G is known for its smooth manifold with the mapping $L_g : G \rightarrow g, g \in G$ defined by $x \rightarrow gx$. Consequently, the derivative of the tangent space of G at the identity is isomorphic to that of the tangent space at g , and encompasses a vector

they term as EquivDeepSet Φ_{eq} . Φ_{eq} bears structural resemblance to DeepSet Φ and ConvDeepSet Φ_{conv} in that Φ_{eq} adheres to the form of equation 1. This means that like Φ_{conv} , Φ_{eq} is comprised of a well-defined encoder of the form $\phi.\psi$ and a decoder ρ , where ϕ is a power series of order 1. However, unlike Φ and Φ_{conv} operating on vector and functional spaces, Φ_{eq} now acts upon the homogenous space of G .

The key to achieving group equivariance in Φ_{eq} lies in the choice of: (a) the encoding kernel $\psi : \mathcal{X}^2 \rightarrow \mathbb{R}$ which offers continuous G -invariant interpolation and can be either an RBF kernel or a LieConv layer depending on whether the input data is continuous (1-d regression) or discrete (images), and (b) the decoder ρ , which is a G -equivariant function mapping a function space \mathcal{H} to $f : \mathcal{X} \rightarrow \mathcal{Y}$ and is a LieConv layer. While the ability to change its kernel size based on the specified group equivariance endows EquivCNP with performances suboptimal to ConvCNP on 1-d regression tasks, it has its edge on the 2-d image completion task where the equivariance to scaling provides EquivCNPs with superior zero-shot generalization capability.

Holderrieth et al. (2021) further extend the scope of equivariance in the NPF to stochastic vector-valued fields. In particular, the authors formalize the necessity of equivariance in the predictive posterior defined over the observed points in a stochastic field by showing that the prior over such a field is inherently invariant. Given their objective of learning steerable feature maps F with inputs $x \in \mathcal{X}$ as n -dimensional space coordinates and outputs $y \in \mathcal{Y}$ as d -dimensional feature vectors, they name their model as Steerable CNPs (SteerCNPs). Following Weiler & Cesa (2019), SteerCNPs employ linear fiber representations of *fiber bundles* (Cohen et al., 2019), *i.e.*, the parameterization of a set of isomorphic spaces called fibers by a base space to define the laws of transformations for F .

Similar to EquivCNP Kawano et al. (2021), SteerCNPs leverage EquivDeepSet Φ_{eq} and a G -equivariant decoder ρ over fiber input-output pairs. However, the choice of decoder is now a steerable CNN (Cohen et al., 2019) and the target group of equivariances is now limited to rotations and reflections instead of the entire Lie Group symmetries. SteerCNPs work analogously to ConvCNP and EquivCNP in that the encoder produces a functional representation $E(C)$ of the context set C which is discretized and fed to the decoder ρ . ρ , however, outputs general fiber representation vectors which are passed through a quadratic covariance activation function to ensure positive definite covariance matrices.

Holderrieth et al. (2021) show that SteerCNPs outperform ConvCNPs in terms of mean log-likelihood scores on 2-d image in-painting tasks. This, when contrasted with the sub-optimal performance of EquivCNPs (Kawano et al., 2021) even on 1-d regression tasks, calls for a notable improvement. Their ablation on augmented image in-painting further demonstrates the benefit of imposed equivariant constraints in the NPF members at overcoming the natural limitations of learning complex distributions from fewer data. However, SteerCNPs remain sensitive to the fiber group sizes. In particular, the authors show that increased fiber group sizes on 1-d regression lead to larger marginal asymmetries thus hurting the model’s performance.

3.4 Non-Euclidean graph connectivity

The NPF branches we saw so far produce latent/deterministic encodings without taking neighborhood connectivity into account. For instance, task-agnostic and transformation equivariant set encoders aggregate independently processed encoding of the context points while attention-based set encoders capture relational reasoning in data through fully-connected relational graphs of all possible input pairs. Such encodings fail to exploit the graph connectivity inductive bias ingrained in the topology of a number of real-world problems including but not limited to traffic networks (Małecki, 2017), social networks (Hunt et al., 2011), and cell dynamics (Bock et al., 2010). These problems are known to be governed by neighborhood rules – for instance, Conway’s game of life (Conway et al., 1970) governs cellular automata. Subsequently, we dedicate this NPF branch to methods that explicitly induce non-linear connectivity biases of datasets into the models. Given the natural tendency of graphs to represent such connections, these make a popular choice of data structures for the methods in this branch. To survey these, we first mention an explicit notation on graphs.

Note: When viewed together, Euclidean symmetry equivariance (section 3.3) and non-Euclidean

space whose components can be readily used for closed form matrix operations involving logarithms and exponentials – the two operations employed by LieConv for mapping elements to the Lie Group. See Finzi et al. (2020) for further details.

graph connectivity (section 3.4) inducing biases can be thought of exploiting the geometries underlying the data. Including these as sub-categories to a geometry-inducing bias branch could thus make an alternative to the NPF taxonomy. However, based on the fact that geometric deep learning usually concerns the non-Euclidean domains of graphs and manifolds, we consider listing these as independent NPF branches.

Notation: Graph-based representations assume the input context and target sets to span beyond regular lattices. It is therefore desirable that we extend our notations to non-Euclidean spaces. Formally, a graph \mathcal{G} is defined by the tuple (V, E) where $V = \{v_i, y_i\}_{i=1:N^v}$ is the set of nodes with attribute v_i and an optional label y_i , and $E = \{e_{ij}\}$ is the set of edges with attribute e_{ij} defining the edge connecting the node v_i with v_j . Alternately, if we denote the adjacency matrix of the graph by \mathcal{A} , then e_{ij} exists iff $A_{ij} = 1$. Graph neural networks (GNNs) rely on these matrices to represent each node by recursively aggregating and transforming the representation vectors of the neighboring nodes (Xu et al., 2019).

Among the most widely used GNNs are the ones relying on message-passing (Scarselli et al., 2008). Such networks model local layer-wise updating of node representations on arbitrary sized graphs by the operation: $h_i^{l+1} = f(h_i^l, \square_{j \in \mathcal{NB}(i)}, g(h_j^l, h_i^l, e_{ij}))$, where \square is a permutation-invariant aggregation function acting on the neighborhood \mathcal{NB}_i of a node v_i , and f and g are learnable functions.²⁹ In case the update operation for a central node assigns the same weight value to each of its neighbor, then the GNN is said to be *isotropic*.³⁰ Furthermore, Spectral GNNs are subclasses of GNNs that make use of spectral operators such as the normalized symmetric Graph Laplacian (L) to encode the local structural information of graphs:

$$L = I_n - \mathcal{DM}^{-1/2} \mathcal{ADM}^{-1/2} \quad (20)$$

where, \mathcal{DM} is the degree matrix of the graph. Intuitively, L measures the smoothness of a function over its domain which in terms of a node is the difference between its value and the averaged value of its neighbors. One popular instance of spectral GNNs are Graph Convolutional Networks (GCNs) (Kipf & Welling, 2019) that rely on localized first-order approximation of spectral graph convolution operations.

Conditional graph Neural Processes: Nassar et al. (2018) incorporate GCNs as encoders for the Neural Process architecture (see equation 1) to improve the learning of functions representing classes of graphs. Similar to CNPs, the proposed conditional graph Neural Processes (CGNPs) feed on N context and M target points. However, the context C and target T sets now also include their respective $N - n$ and $m - M$ neighborhood points: $C = \{(v_i, y_i)\}_{i=1}^{n \geq N}$; $T = \{v_i\}_{i=n+1}^{n+m}$ where, v_i and y_i carry the aforesaid meanings. While processing a node $v_i \in C \cup T$, CGNP therefore encodes its k -hop neighborhood using message-passing isotropic bipartite GCNs (Nassar, 2018). As a result, the encoder ϕ gets to observe the set $C \cup T \cup \{x_j | j \in \cup_{i \in C \cup T} \mathcal{NB}(i)\}$. The extent of locality used in the convolutions is governed by the neighborhood radius $r = \mathcal{NB}/10$. A graph reduction operation `red` reduces the $(n + m)$ -dimensional latent output of the encoder which is then decoded by another bipartite GCN to output an approximation of the underlying data-generating function f .

Nassar et al. (2018) further view CNPs as a special case of CGNPs with an unstructured (edgeless) graph where each node only connects to itself. In other words, CGNPs reduce to CNPs for $r = 0$. Put this way, CNPs can be seen to be capturing local structure of f at a global level while CGNPs interpolate f in local neighbourhoods. The authors empirically validate this based on a toy 1-d regression task example with $n + m = 8$. Using $r = 0.7$ here significantly improves the performance of CGNPs while at $r = 0$, CGNPs perform similar to CNPs.

Graph Neural Processes: Among the widely known issues surrounding graph structured data remains missing edge variable information arising from noisy data acquisition processes (Burt, 1987). While impu-

²⁹A common choice for g is the sum of all messages M_t obtained from neighbors where M_t depends on neighboring hidden states h_j^l and edges e_{ij} . Similarly, f is usually an average between the previous hidden state h_i^l and the message g .

³⁰Message-passing thus helps GNNs use the local structural information, *i.e.*, features aggregated from the neighbors as an input feature while encoding the context set.

tation of such edges can be performed classically using mean filling, Huisman (2009) show that replacing the missing values with draws from a conditional distribution can greatly reduce bias in variances and covariances. Inspired by this, Carr & Wingate (2019) employ Neural Processes (with neutral conditional estimation) to impute the value distribution on edges. The proposed graph Neural Processes (GNPs) describe each edge using the local structural eigenfeatures alongside the tuple $(v_i, u_j, \mathcal{DM}_{ii}, \mathcal{DM}_{jj})$. The local structural eigenfeatures are obtained using eigenvector matrix Λ of the spectra of L such that the columns of the matrix define eigenvectors of L .

The training setup for GNPs include $p.n$ context points where p is drawn from a uniform distribution with pre-specified lower and upper bounds, and $n = |E|$. The context and target points are drawn from a single graph. GNPs thus learn a representation over a family of graphs to impute edge values on new members of the family. The choice of encoder and decoder in GNPs is a four-layer MLP with ReLU non-linearities. The workflow of GNPs is similar to that of NPs for encoder ϕ (with graph structured inputs) and aggregation a . However, the input to the decoder ρ for a given edge e_k is a concatenation of the aggregated encodings of its nodes with a list of their attributes. ρ then predicts a distribution of size equivalent to the number of unique attributes $|\cup e_k : e_k \in E|$ defined for an edge. Given the need for such categorical outputs per edge, GNPs minimize multi-class cross entropy loss as their training objective. Using a collection of 16 graph benchmark datasets, Carr & Wingate (2019) demonstrate the superior performance of GNPs over classical (random and most-common edge label imputation) as well as statistical (random forest and simple GNN) methods.

Message-passing Neural Processes: Day et al. (2020) propose the Message-Passing Neural Processes (MPNPs) for the semi-supervised node classification problem. Here, we are given a partially-labeled set of nodes with attributes $X \in \mathcal{X}$ and their neighbors $A \in \mathcal{A}$ sampled from a continuous bounded function $f : \mathcal{X}, \mathcal{A} \rightarrow \mathcal{Y}$. We desire to predict the labels for the subset $X' \subseteq X$ with missing labels. While the context set still constitutes N labeled nodes and their k -hop neighbors, the target set for MPNP includes all $N + M$ samples and their neighbors without labels, *i.e.*, $T = \{v_i\}_{i=1}^{n+m}$. Similar to CGNPs, MPNPs maintain rich encoding of the context nodes by exploiting the relational structure between the context set and its neighborhood. However, the encoder and decoder now are composed of MLP layers rather than GCNs. Motivated by latent NPs, MPNPs make use of the aggregated context encoding $E(C)$ to parameterize a global latent variable z which is then used to condition the decoder for predicting labels $f(x)$ s.t. $x \in T$. The inclusion of neighborhood information in the context encoding thus helps z to capture relational structure underlying the stochastic processes that generate the input. Following equation 6, z can be modeled as a function of permutation invariant mean μ and variance σ^2 . The optimization objective for training an MPNP decoder ρ first involves estimating the epistemic uncertainty $p(z|C, T, f(T))$ with a variational posterior $q(z|C, T, f(T))$ and then maximizing the resulting ELBO.

Day et al. (2020) apply MPNPs to two sets of node labeling tasks: (i) fixed labeling where the same set of classes appear in every example, (ii) arbitrary labeling where models are required to adapt to arbitrary node labels assigned on a per-dataset basis. Examples of (i) include protein-protein interaction site prediction and state evolution prediction for cellular automata. On the other hand, for setting (ii), they introduce a Cora-Branched task where academic papers from 11 computer science disciplines are represented by bag-of-words vectors with edges indicating that one of the papers cited the other (McCallum et al., 2000). The authors show that on all these tasks, MPNPs outperform the non-message passing NPs limited by their ability to leverage relational information between points.

Neural processes for graph neural networks: Liang & Gao (2021) propose Neural Processes for graph neural networks (NPGNNs) for transductive and few/many-shot inductive link predictions. Graph link prediction involves predicting the unknown links in the entire graph given the information about all the nodes (transductive) or only a subset of the latter (inductive). Few-shot link prediction (Chen et al., 2019) marks a further challenging task by exposing only limited information about the graph and leaving a large proportion of the links to be predicted. To reflect these, the context and target sets are now given as $C = \{(v_i, \mathcal{A}_i)\}_{i=1}^N$ and $T = \{v_i\}_{i=1}^{N+M}$, respectively. Adhering to the aforesaid notation, we assume that the underlying function mapping the nodes and links is given by $f : \mathcal{X} \rightarrow \mathcal{A}$.

With the goal of predicting \mathcal{A}_T , NPGNNs can be thought of combining CGNPs with MPNPs. Similar to CGNPs, NPGNNs employ message-passing GCNs (Kipf & Welling, 2019) in their encoder. Similar to MPNPs, the context set encodings are aggregated to parameterize a global latent representation z which is then concatenated separately with the features of target nodes as well as their neighbors. Using the concatenated representations, the MLP-based decoder produces a latent embedding vector u_i for each node $v_i \in C$. Finally, a sigmoid operation on the inner product of each u_i with all other $u_{j \neq i}$ gives the probability of the existence of an edge between the nodes v_i and v_j .

Given that NPGNN decoder outputs the probability of the existence of edges between nodes, the training objective thus involves modeling the adjacency matrix \mathcal{A} using a variational posterior and maximizing the resulting ELBO in a way similar to that of equation 8. On transductive link prediction, Liang & Gao (2021) compare NPGNNs with a number of strong baselines which they outperform. These include the Spectral Clustering (Tang & Liu, 2011), DeepWalk (Perozzi et al., 2014), and Variational Graph Autoencoders (VGAEs) (Kipf & Welling, 2016). On many-shot inductive link prediction, the authors show that NPGNNs outperform VGAEs. Finally, on the few-shot link prediction task, NPGNNs are shown to be more robust since they can retain reasonable performances with only 30% of the nodes and 10% of the links given.

Functional Neural Process: (Louizos et al., 2019) propose the Functional Neural Processes (FNPs) as a new family of exchangeable stochastic processes that adopt priors over the relational structure of the local latent variables instead of explicitly specifying a prior distribution over latent global variables (like that of NPs). The former property helps FNPs model dependencies among the points of dataset $D = \{(x_1, y_1), \dots, (x_N, y_N)\}$ by well-preserving the exchangeability and consistency conditions discussed in equations 2 and 3, respectively. While other methods belonging to this NPF branch assume D to be graph-structured, FNPs (Louizos et al., 2019) accept D lying on regular lattices and instead build a graph of dependencies among the local latent variables that encode D . The latter property also endows FNPs with a resemblance to the autoencoder-based generative models (Kingma & Welling, 2014).

FNPs work on five sets of inputs. Resembling the context and target sets, FNPs split D into two input sets: the reference set R consisting only the input covariates $x \in \mathcal{X}$ and the other set $O = \mathcal{X} \setminus R$ consisting the remaining points. Note that while the reference set might resemble the context sets we have been using so far, it excludes the label information $y \in \mathcal{Y}$. Further, $D_x = \{x_1, \dots, x_N\}$ is a finite random set from \mathcal{X} that marks the observed inputs and $M = D_x \setminus R$ is a subset of D_x containing the points common with O . Finally, $B = R \cup M$ contains all the reference set points along with the points of D_x . Using these five, FNPs model $f : \mathcal{X} \rightarrow \mathcal{Y}$ in the following three steps.

The first step involves embedding each point in B independently to a latent representation u_i using a factor of distributions $p_\theta(u_i|x_i)$ whose mean and variance are modeled using a neural network with inputs $x_i \in B$. The resulting set of latent representations for B is denoted by \mathbf{U}_B . The second step draws inspiration from the kernel-based covariance matrices of Gaussian processes and constructs two random binary adjacency matrices to model the correlations among the points in B . One of the matrices models a bipartite graph \mathbf{A} from R to M while the other gives a directed acyclic graph \mathbf{G} among the points in R . To reflect directed acyclic graphs, the binary adjacency matrices are re-arranged into a triangular structure with zeros along the diagonal.

The distribution $p(\mathbf{A}|U_R, U_M)$ of \mathbf{A} is simply defined by a factor of Bernoulli distributions conditioned on the probability $g(u_i, u_j)$ that a point $i \in M$ depends on another point $j \in R$. On the other hand, \mathbf{G} first guarantees acyclicity by leveraging a parameter-free scalar projection $t(\cdot)$ to define a topological ordering of the vectors in U_R , *i.e.*, $u_i > u_j$ when $t(u_i) > t(u_j)$. Based on the rearrangement trick, such an ordering is then used to model the distribution $p(\mathbf{G}|U_R)$ of \mathbf{G} conditioned on the probability $g(u_i, u_j)$ that a point $i \in R$ depends on the rest of the points $j \in R$. Specifying \mathbf{A} and \mathbf{G} in terms of $g(\cdot, \cdot)$ thus helps inducing relational bias of a point with respect to its neighbors.

The third step involves specifying a predictive model that induces the dependency graphs \mathbf{A} and \mathbf{G} . To achieve this, FNP models predictive distribution $p(y_B, Z_B|R, \mathbf{G}, \mathbf{A})$ for each target variable y_i that depends on R according to the dependency graphs and employs a local latent variable z_i to summarize the context

conditioned on the selected parent points x_R and their targets y_R in R . Parameterizing the predictive distribution thus helps defining the following two variations of the FNP models:

$$\begin{aligned}\mathcal{FNP}(D) &:= \sum_{G,A} \int p(U_B|X_B)p(G,A|U_B)p(y_B, Z_B|R, G, A)dU_B dZ_B dy_{i \in R \setminus D_x} \\ \mathcal{FNP}^+(D) &:= \sum_{G,A} \int p(U_B, G, A|X_B)p(y_B, Z_B|R, U_B, G, A)dU_B dZ_B dy_{i \in R \setminus D_x}\end{aligned}\tag{21}$$

where, $\mathcal{FNP}^+(D)$ further conditions on the latent variables u . The marginalization over the reference set points in equation 21 can be particularly handy when using extra unlabelled data to learn a better embedding u . However, (Louizos et al., 2019) avoid such marginalization by choosing $R \subseteq D_x$. Given the intractability of the marginals, the training of these models thus relies on variational inference using the approximate posterior $q(U_D, G, A, Z_D|X_D)$ to define the ELBO for the marginal likelihood of D . On the challenging task of detecting whether an input point is in or out-of-distribution (OOD), (Louizos et al., 2019) show that the proposed FNPs achieve accuracy comparable to NPs (Garnelo et al., 2018b) while surpassing the latter on robust uncertainty metrics such as entropy and the area under receiver operating characteristics curves. In other words, the two variants of FNPs reliably produce low entropy values on in-distribution test sets and high entropy values on OOD test sets with \mathcal{FNP}^+ performing the best.

Note: The attentive neural process (Kim et al., 2019) discussed in section 3.2 can thus be seen to make a special case of the FNP with deterministic versions of the context graph \mathbf{G} and the context-target graph \mathbf{A} (Tang & Matteson, 2021). In this case, \mathbf{G} models the self-attention among the context set elements while \mathbf{A} models the cross-attention between the target and the context set elements.

Conditional temporal Neural Processes: Yoo et al. (2021) propose incorporating a CNP-inspired covariance loss function into the total loss of the model for finding the basis function spaces $\Phi(\mathcal{X}_l)$ that can learn the input-output mappings $f : \mathcal{X} \rightarrow \mathcal{Y}$ for dataset $D = \{\mathcal{X}_l, \mathcal{Y}_l | l = 1, \dots, n\}$ by taking the dependencies of output variables into account. Since such a basis function reflects the feature space, for a given $\mathcal{X}_l \in \mathbb{R}^{S \times N \times F}$, $\mathcal{Y}_l \in \mathbb{R}^{S \times N \times G}$ where, S, N, F, G are the time stamp window, the context set size, and the number of input and target variable features, respectively, $\Phi(\mathcal{X}_l) \in \mathbb{R}^{1 \times N \times F'}$ where, F' is the dimension of the basis function. The motivation for modeling Φ comes from the fact that CNPs predict the mean and variance of each target point by implicitly finding the feature space in which target points and their covariance matrix have linear relations. Learning such a feature space explicitly could thus help modeling the missing dependencies in the prior information. Given the covariance $\Sigma_{i,j}$ between the two variables \mathcal{Y}_i and \mathcal{Y}_j , the total loss of the regression model is given by:

$$\begin{aligned}\mathcal{L} &= \mathcal{L}_{\text{mse}} + \lambda \mathcal{L}_{\Sigma} \\ \text{s.t., } \mathcal{L}_{\text{mse}} &= \frac{1}{n} (\mathcal{Y} - \hat{\mathcal{Y}})^2, \quad \mathcal{L}_{\Sigma} = \frac{1}{n^2} \sum_{i=1}^n \sum_{j=1}^n (\Sigma_{i,j} - \sigma^2 \Phi(\mathcal{X}_i) \Phi(\mathcal{X}_j)^\top)^2\end{aligned}\tag{22}$$

where, \mathcal{L}_{mse} and \mathcal{L}_{Σ} are the mean squared error and the covariance loss of the model with predictions $\hat{\mathcal{Y}}$. The authors show that optimizing with covariance loss helps finding function spaces where, only the basis functions belonging to the same class have high covariance while the others have low covariance. They further show the advantage of complementing the training loss of state-of-the-art models (Qu et al., 2019; Izadi et al., 2020) for classifying images on a number of datasets including MNIST and CIFAR-10. For evaluation of regression performances, the authors extend the work of Yu et al. (2018) by employing the spatio-temporal GCN (ST-GCN) with and without the covariance loss. In particular, they compare the

velocities of cars on the PeMSD7(M) dataset based on the diagonal (variance) and non-diagonal (covariance) elements of $\Phi(X)\Phi(X)^\top$ with that of $\mathcal{Y}\mathcal{Y}^\top$. Their results indicate that ST-GCN with covariance loss can better reflect the variance and covariance of the target variables in the basis functions.

3.5 Output dependency

The members of this NPF branch operate with inductive biases that ensure correlation among the inputs is reflected in the outputs. Such a property is suited for real-world tasks such as climate and brain signals modeling that demand capturing dependencies among a number of input variables over temporal and spatial dimensions. The latent NP (Garnelo et al., 2018b) discussed in Section 2.1 falls into this branch.

Convolutional Neural Processes: Foong et al. (2020) combine the potential of ConvCNP (Gordon et al., 2020) (see Section 3.3) and latent NP by adding a global latent variable to ConvCNP. The proposed Convolutional NP (ConvNP) thus draws coherent samples from the predictive distribution (instead of independent samples per data point) while maintaining shift equivariance. Similar to NPs, ConvNPs can be trained by stochastic gradient maximization of the log likelihoods averaged over a sequence of meta-learning tasks represented by the context set C and target set T :

$$\mathcal{L}_{ML}(\theta, \phi; \xi) := \log \left[\frac{1}{L} \sum_{l=1}^L \exp \left(\sum_{x \in T} \log p_\theta(f(x)|x, z_l) \right) \right]; \quad z_l \sim E(C) \quad (23)$$

where, L is a hyperparameter in the range [16, 32], the latent variable z_l is drawn from the encoding $E(C)$ computed by a ConvCNP encoder (see equation 19). The choice of ConvNP decoder ρ (conditioned on z) is an arbitrary shift equivariant map between function spaces. In particular, ρ is a CNN allowing $f = \rho(z)$ to model the value of z at multiple locations to induce dependency among the outputs. Similar to ConvCNPs, the domain of z is discretized on a grid $(x_i)_{k=1}^K$ with $z := (z(x_i))_{k=1}^K$ which limits the equivariance of ConvNPs up to shifts on it.

It is worth noting that ConvNPs are trained by approximating the biased likelihood objective \mathcal{L}_{ML} using importance sampling rather than the amortized variational inference technique used to train latent NPs. This endows them with practical advantages over ELBO maximization used for variational inference in latent NPs (see equation 8). While the latter objective guarantees better performance in the *infinite* data/model capacity limit by allowing the model to recover the exact inference for z based on Bayesian consistency, enforcing such consistency for z in the more common *limited* data/model capacity scenarios impels resource inefficiency. \mathcal{L}_{ML} , without a variational posterior term, not only avoids this but is further easy to be specified for any map modeling a predictive process.

Foong et al. (2020) show that maximizing \mathcal{L}_{ML} leads to better results than maximizing ELBO not only for ConvNPs but also for ANPs (Kim et al., 2019). Besides demonstrating the superior performance of ConvNPs over ConvCNPs and ANPs on the more common 1-d regression and 2-d image completion tasks, the authors present its advantages on tasks concerning modeling of real-world environmental data (Buontempo et al., 2020).

Neural Processes with Position-Relevant-Only Variances: A setting common to most of the latent variable NPs Garnelo et al. (2018b); Kim et al. (2019); Singh et al. (2019) is that they decode the predictive distribution using a single latent variable and thus correlate the distribution with not only the function’s positions \mathcal{X} but also the function’s values \mathcal{Y} . A consequence of the correlation is that any distribution shifts in the random functions modeling future target sets can greatly increase the model’s uncertainty. Wang et al. (2021a) propose handling such out-of-distribution (OOD) data by decoupling the inference of the predictive distribution’s variance from the function values. Their model, Neural Processes with Position-Relevant-Only Variances (NP-PROV), thus derives its predictive mean and variances from two distinct latent spaces while still modeling the correlation among the predictions.

While the mean values of an NP-PROV decoder are conditioned on the context values Y_C as well as on self/cross-correlations among the context-context and context-target locations, its variances are conditioned

only on the latter cross correlations. The authors achieve this by extending ConvCNPs using kernels resembling Gaussian processes. They put forward separate approaches to derive position-relevant-only variances for off/on-the-grid data using context-context and target-target self-correlations $\mathbf{K} = \mathcal{K}(X_C, X_C^\top)$ and $\mathbf{K}_{**} = \mathcal{K}(X_T, X_T^\top)$, and context-target cross-correlation $\mathbf{K}_* = \mathcal{K}(X_C, X_T^\top)$, where \mathcal{K} is the covariance function. Predicting variance involves replacing the function values Y with the covariance \mathbf{K}_* for the off-the-grid scenario and employing a context mask for the on-the-grid scenario. The authors show that such a formulation allows NP-PROV to surpass the log-likelihood scores of ConvCNPs on SVHN (Netzer et al., 2011) and mini-Imagenet (Vinyals et al., 2016) datasets while delivering competitive scores on MNIST (Deng, 2012) and CelebA 32×32 (Liu et al., 2015).

Gaussian Neural Processes: While the use of latent variables enable NPs to produce coherent samples, they inevitably give rise to intractable likelihood and complicated variational inference-based learning objectives. To bypass these intricacies, Bruinsma et al. (2021) propose replacing latent variables by instead extending ConvCNPs (Gordon et al., 2020) to achieve coherence in predictions. In doing so, they propose the subfamily of Gaussian NPs that exhibit the following key characteristics: (i) Gaussian NPs incorporate shift equivariance in modeling the predictive distributions with Gaussian processes (Williams & Rasmussen, 2006), (ii) Gaussian NPs host a closed-form likelihood while modeling correlations in the predictive distribution, (iii) Gaussian NPs guarantee universal approximation similar to ConvCNPs. Moreover, the authors interpret the standard maximum likelihood objective used for training CNPs as a well-behaved relaxation of the KL-divergence between stochastic processes (Matthews et al., 2016).

Building upon section 2, NPs can be seen to meta learn a Gaussian approximation $\tilde{\pi} : \mathcal{O} \rightarrow \mathcal{D}_G$ of the *posterior prediction map* $\pi_f : \mathcal{O} \rightarrow \mathcal{D}$ where, \mathcal{O} is the collection of observed datasets $O_{i=1}^{N+M} = \{(C, T)\}_{i=1}^{N+M} \sim f$ and \mathcal{D} is the family of posteriors over f . CNPs learn the approximation $\tilde{\pi}$ by assuming the posteriors \mathcal{D}_G to be obtained from a fixed prior and hence, fail to model the predictive correlations. In contrast, Gaussian NPs relax the aforementioned constraint and allow $\tilde{\pi}$ to be more flexible in modeling \mathcal{D}_G . Formally, Gaussian NPs approximate $\tilde{\pi}$ by finding a minimizer $\tilde{\pi}(O)$ for the KL-divergence D_{KL} between the predictive map π_f and a Gaussian process μ for every $O \in \mathcal{O}$. Such a minimization objective however comes with two major hindrances. First, the *existence* of such minimizers might be undefined for very high dimensional observations since D_{KL} no longer remains finite for all the values around $\tilde{\pi}(O)$. By instead relaxing the objective to include only finite-dimensional indices $|x|$ of f , Bruinsma et al. (2021) ensure that there exists an $|x|$ -dimensional Gaussian distribution μ_G^x such that $D_{KL}(P_x \pi_f(O), \mu_G^x) < \infty$:

$$\tilde{\pi}^x(D) = \arg \min_{\mu^x \in \mathcal{D}_G^{|x|}} D_{KL}(P_x \pi_f(D), \mu^x) \quad (24)$$

where, $P_x f = (f(x_1), \dots, f(x_{|x|}))$ projects f onto the index set x . While equation 24 solves the problem of *existence* of minimizers by uniquely defining an approximating process $\tilde{\pi}(D)$ satisfying $P_x \tilde{\pi}_f(D) = \tilde{\pi}^x(D)$, there still remains the problem of *approximability* that seeks to minimize $D_{KL}(\pi_f(D), \mu)$ to approximate the minimizer whenever one exists. In order to address this, the authors define another objective that approximates the solution to equation 24 by averaging over all index sets of a finite size $n \geq 2$ size defined by the prior $p(x)$. The latter objective can be restated in terms of likelihood maximization as:

$$\tilde{\pi} \approx \arg \max_{\pi \in \mathcal{M}_G^{\text{f.d.d.}}} \frac{1}{N+M} \sum_{i=1}^{N+M} \log \mathcal{N}(f(x_i^{(t)}) | \mathbf{m}_i, \mathbf{K}_i) \text{ with } P_{x_i^{(t)}} \pi(O_i^{(c)}) = \mathcal{N}(\mathbf{m}_i, \mathbf{K}_i) \quad (25)$$

where, $\tilde{\mathcal{M}}_G$ denotes a noisy Gaussian prediction map π that is continuous along its finite dimensional distributions (f.d.d.), and $\mathbf{m} : \mathcal{O} \rightarrow C(\mathcal{X}, \mathcal{Y})$ and $\mathbf{K} : \mathcal{O} \rightarrow C^{\text{p.s.d.}}(\mathcal{X}^2, \mathcal{Y})$ denote the continuous mean and continuous positive semi-definite (p.s.d.) covariance kernel functions of μ , respectively. With a slight abuse of notation, we now refer to context $c \in C$ and target $t \in T$ points using their respective superscripts.

While specifying a mapping from datasets to continuous mean functions for \mathbf{m} becomes straight forward with a ConvDeepSet (Gordon et al., 2020), doing so for kernel functions \mathbf{K} is not feasible given that \mathbf{K} accepts set of duplicate inputs \mathcal{X}^2 . The authors thus propose extending \mathbf{K} for the input space \mathcal{X}^2 by first viewing

it as a continuous function that is equivariant to diagonal translations and then continuously extending it to be equivariant with respect to all translations. The extended kernel mapping $\hat{\mathbf{K}} : \mathcal{O}_2 \rightarrow C(\mathcal{X}^2, \mathcal{Y})$ is thus permutation and shift equivariant. The resulting ConvDeepSet architecture for \mathbf{K} can now be given as:

$$\mathbf{H} = \phi(O^{(c)}, Z) \xrightarrow{(1)} \mathbf{K} = \prod^{p.s.d.} \text{CNN}_{2d}(H) \xrightarrow{(2)} \mathbf{K}^{(t)} = \sum_{l=1}^L \psi(x_i^{(t)} - \tilde{x}_l) \mathbf{K}_l \psi(\tilde{x}_l - x_j^{(t)}) \quad (26)$$

where, $\mathbf{H} \in \mathbb{R}^{M \times M \times 3}$ is the context encoding mapped to a 2-d grid at locations $\tilde{x} = \{\tilde{x}_1, \dots, \tilde{x}_L\}$, $\tilde{x}_l \in \mathbb{R}^{2d}$ and is passed through the covariance kernel \mathbf{K} parameterized by a CNN producing an $\mathbb{R}^{M \times M}$ output matrix. The $\prod^{p.s.d.}$ operation projects the CNN outputs onto the nearest positive semi-definite matrix to ensure that \mathbf{K} is positive-definite prior to being interpolated by the decoder kernel $\mathbf{K}^{(t)}$ for the desired target locations $x^{(t)}$. The interpolation then involves aggregating \mathbf{K} over the grid locations $l \in L$ using an RBF kernel ψ . Adhering to the convention used by the follow up works in the Gaussian NP subfamily, we coin the model characterized by equation 26 as FullConvGNP. (Bruinsma et al., 2021) show that FullConvGNPs surpass the 1-d regression performances of a number of preceding NP variants that model predictive correlations including ConvNPs (Foong et al., 2020), and ANPs (Kim et al., 2019). Furthermore, they outperform the baseline ConvCNPs (Gordon et al., 2020) which do not model output dependencies.

Convolutional Gaussian Neural Processes: FullConvGNPs model output dependencies by directly parameterizing the predictive covariance of the outputs using mean \mathbf{m} and covariance \mathbf{K} . However, their specification for covariance \mathbf{K} (step 2 in equation 26) relies on costly 2^*d convolution operations for d -dimensional data. This limits their applications to 1-d data since convolutions of $D > 3$ are rarely implemented by popular deep learning libraries. Markou et al. (2022) overcome this inefficiency by allowing \mathbf{m} and \mathbf{K} to be convolution-free:

$$\mathbf{m}_i = \phi(x_{t,i}, r), \quad \mathbf{K}_{ij} = k(g(x_{t,i}, r), g(x_{t,j}, r)) \quad (27)$$

where, $r = E(C)$ is the aggregated encoding, k is a positive-definite function, and ϕ and g represent neural networks with output dimensions \mathbb{R} and \mathbb{R}^{D_g} , respectively. Training the proposed modification to FullConvGNPs using the maximum likelihood objective stated in equation 25 now involves optimizing over the collection of parameters of ϕ , g , and r . Consequently, the proposed model still overcomes the problem of independent predictions of inputs (a phenomena which the authors refer to as *mean field* predictions).³¹

Markou et al. (2022) further experiment two specifications for \mathbf{K} . The first involves a cost-efficient linear covariance kernel which is linear in the parameters and in the query locations. Its expressive capacity is however limited by the finite number of basis functions supported by the kernel. The second choice for \mathbf{K} involves a kvv covariance kernel where k is the Exponentiated Quadratic (EQ) function while v is a neural network with real-valued outputs. While the unbounded number of basis functions endows kvv kernel with an enhanced expressivity, the cost of drawing samples from it scales cubically with the number of query locations. Choosing ϕ , g , and r to be convolutional, Markou et al. (2022) propose the ConvGNP as a cost-efficient alternative to FullConvGNP.

By applying ConvGNPs to model synthetic datasets alongside a range of other NP variants, the authors draw several interesting observations. First, they observe *mean-field* NPs such as CNPs (Garnelo et al., 2018a) (relying only on the averaged encoding) to be sub-optimal compared to FullConvGNPs and ConvGNPs. This is due to the fact that the latter models facilitate drawing coherent function samples. Furthermore, they find that the kvv kernel (without limits on the number of basis functions) does not only outperform the linear kernel but also delivers performances on par with that of the computationally heavier FullConvGNP.

Bootstrapping Neural Processes: Similar to Louizos et al. (2019), Lee et al. (2020b) also point out the limited flexibility of latent NPs at modeling *data-driven* uncertainty in stochastic processes based on a

³¹A preliminary version of this work appeared in the workshop paper of Markou et al. (2021).

single latent variable.³² While Louizos et al. (2019) address this by establishing a relation structure over the local latent variables (see Section 3.4), Lee et al. (2020b) consider extending NPs with classic bootstrapping (Efron, 1992), a yet another *data-driven* technique. Classic bootstrapping methods model uncertainty on a variety of estimation problems based on sampling a population with replacement for the simulation of its distribution. In the context of NPs, this is synonymous to estimating the parameter θ modeling $f(\hat{C})$ given our dummy context set $\hat{C} = \{x_i\}_{i=1}^N$:

$$\tilde{C}^{(j)} \stackrel{s.w.r.}{\sim} \hat{C}, \quad \tilde{\theta}^{(j)} = f(\tilde{C}^{(j)}) \forall j \mid j \in [1, J] \quad (28)$$

where, $\stackrel{s.w.r.}{\sim}$ denotes sampling with replacement and J is the total number of bootstrap samples. The resulting Bootstrapping Neural Processes (BNPs) thus model functional uncertainty of a given dataset by inducing it through the uncertainties observed in the combined predictions computed on multiple resampled datasets $\tilde{C}^{(j)}$. The combination of individual predictors $\phi(\theta)$ given by bootstrap estimates $\{\tilde{\theta}^{(j)}\}_{j=1}^J$ thus allows BNPs to exploit **Bootstrap aggregating** (bagging) wherein a bagging predictor is computed as $\frac{1}{J} \sum_{j=1}^J \phi(\tilde{\theta}^{(j)})$. Moreover, BNPs are robust to out-of-distribution (OOD) test data given that bagging helps ensemble Bayesian posteriors from multiple bootstrap samples (Huggins & Miller, 2019).

The authors further adapt Equation 28 to estimate the conditional predictive distribution $p(f(T)|T, E(C))$ of a labeled dataset D composed of a context set $C = \{(x_i, y_i)\}_{i=1}^N$ and a target set $T = \{x_i\}_{i=N+1}^{N+M}$. In particular, they employ *residual bootstrapping* which fixes $x_i \in \mathcal{X}$ while resampling the residuals of predictions. This involves fitting a model on C to obtain the distribution parameters $\{(\mu_i, \sigma_i)\}_{i=1}^N$ and then computing the residual $\epsilon_i = \frac{y_i - \mu_i}{\sigma_i}$ with resampling to obtain $\tilde{\epsilon}_1^{(j)}, \dots, \tilde{\epsilon}_n^{(j)} \stackrel{s.w.r.}{\sim} \epsilon$ where, $\epsilon = \{\epsilon_i\}_{i=1}^N$ and $j \in [1, J]$. The resampled residuals are thus used to construct bootstrap datasets $\tilde{x}_i^{(j)} = x_i, \tilde{y}_i^{(j)} = \mu_i + \sigma_i \tilde{\epsilon}_i^{(j)} \forall i \mid i \in [1, N]$.

Lee et al. (2020b) first put forward an application of residual bootstrapping to NPs that performs bagging of predictions by passing the bootstrapped contexts as inputs. However, they point out that such a naive plugging of residual bootstrapping to NPs result in poor predictive accuracy with large residuals either because of possible accumulation of errors from fitting multiple bootstrap datasets or the distribution mismatch arising from predictions on bootstrapped contexts that the model does not get to see during training. BNPs then improve over such naive residual bootstrapping by first employing paired bootstrapping to compute residuals from multiple resampled contexts rather than the full context C :

$$\hat{C}^{(j)} := (\hat{X}^{(j)}, \hat{Y}^{(j)}) := \{(\tilde{x}_i^{(j)}, \tilde{y}_i^{(j)})\}_{i=1}^N \stackrel{s.w.r.}{\sim} \{(x_i, y_i)\}_{i \in N} \quad (29)$$

Leveraging \hat{C} for the residual computation helps expose the model to residuals with diverse patterns during training and hence, enhancing its robustness to OOD target sets. For inference on the full context C , the resampled contexts $\hat{C}^{(j)}$ are passed through the encoder ϕ and decoder ρ which gives their distribution $\{\hat{\mu}_i, \hat{\sigma}_i\}_{i \in N}$ as the output of the residual bootstrapping. The resulting distribution is then used to compute and resample residual $\epsilon_i^{(j)}$. The overall model can be formulated as:

$$\begin{aligned} \hat{E}(\hat{C}) &= \phi(\hat{C}^{(j)}), & (\hat{\mu}_i^{(j)}, \hat{\sigma}_i^{(j)}) &= \rho(x_i, \hat{\phi}^{(j)}) \forall i \mid i \in N \\ \epsilon_i^{(j)} &= \frac{y_i - \hat{\mu}_i^{(j)}}{\hat{\sigma}_i^{(j)}} \forall i \mid i \in N, & \tilde{\epsilon}_1^{(j)}, \dots, \tilde{\epsilon}_N^{(j)} &\stackrel{s.w.r.}{\sim} \{\epsilon_i^{(j)}\}_{i \in N} \end{aligned} \quad (30)$$

Similar to naive residual bootstrapping, the resampled residuals and the output distribution parameters $(\hat{\mu}_i^{(j)}, \hat{\sigma}_i^{(j)})$ are used in constructing bootstrap contexts $\{\tilde{x}_i^{(j)}, \tilde{y}_i^{(j)}\}_{i \in N}$ which in turn are used for the final prediction. Unlike NPs feeding the decoder with the deterministic representation $E(C)$ (see equation 2) and the latent variable z (see equation 7), BNPs provide the decoder with $E(C)$ and the bootstrapped

³²The authors call NPs to be *data-driven* based on the fact that these *learn* priors from the data rather than from pre-specified kernels.

representation $\tilde{E}(C) = \phi(\{\tilde{x}_i^{(j)}, \tilde{y}_i^{(j)}\}_{i \in N})$. For the decoder to process the combined representation of these, a linear *adaptation layer* $g(E, \tilde{E}^{(j)})$ is prepended. BNPs thus form plug-and-play tools for increasing the robustness of a base NP variant with a minimum overhead of adding an adaptation layer to the base model.

Lee et al. (2020b) further provide an intuitive explanation of how BNPs maintain robustness in the face of data distribution shift. Under such situation, the base model computes larger residuals which get reflected in the bootstrapped contexts and propagate on to the bootstrapped representations. The bootstrapped representations in turn drive the model to produce high variance approximations of the data distribution and hence counter the increased uncertainty due to OOD inputs. Through an extensive set experiments on a range of tasks including 1D regression, 2D image completion, and bayesian optimization (Brochu et al., 2010), the authors demonstrate that BNPs and BANPs, *i.e.*, BNP plugged to a base attentive NP (ANP) (Kim et al., 2019) can outperform the deep ensemble (Lakshminarayanan et al., 2017) of the CNP (Garnelo et al., 2018a) and a conditional version of ANP (without the latent variable).

Global convolutional Neural Processes: Wang et al. (2021b) propose the Global Convolutional Neural Processes (GB-CoNPs) to study the causality (model-driven and data-driven) behind global uncertainty in latent NPs (Garnelo et al., 2018b). While latent NPs draw the encoder function E_θ from a distribution $p(E_\theta)$, these fail to consider the fact that the same context set can encode more than one descent function samples – say, with differing periodicity $E_{\theta_1}, \dots, E_{\theta_n}$. Here, each function sample captures the local uncertainties equally well. However, their periodic differences points towards a distinct prior encoded by each of them. This in turn suggests the existence of another *global uncertainty* modeling the latent prior.

GB-CoNPs work by replacing the deterministic space \mathcal{S} used to project the deterministic ConvDeepSet representation $\Phi_{conv}^{\mathcal{S}}$ in ConvCNP with a latent space \mathcal{L} shared between the context and the target set. The out-of-range inputs are then generalized through a shared global prior and the discretized \mathcal{L} which embeds the global uncertainty $p(z)$ (see equation 7) in the random function f . Incorporating a latent space in Φ_{conv} helps sample different z values reflecting diverse priors over the functions.

The authors show that GB-CoNPs outperform the log-likelihood of NPs (Garnelo et al., 2018b), attentive NPs (Kim et al., 2019) and ConvCNP (Gordon et al., 2020) on 1-d and 2-d regression tasks with the latter involving standard image classification datasets such as MNIST, SVHN, and CelebA32. Only on CelebA32 do GB-CoNPs lag behind ConvCNP. As a more intriguing application, they discuss the superior performance of GB-CoNPs at modeling the spatio-temporal COVID-19 dataset.³³

3.6 Temporal dependency

This NPF branch takes into account the temporal dynamics underlying a sequence of stochastic processes. Some representatives of such tasks include modeling time-series data, rendering dynamic 3D scenes with objects interacting over time, and learning reinforcement learning (RL) agents with increasingly more challenging tasks. Capturing such temporal correlation thus amounts to modeling a sequential stochastic process of stochastic processes.

Sequential Neural Processes: Sequential Neural Processes (SNPs) (Singh et al., 2019) perform meta-transfer learning by modeling stochastic processes that change dynamically with time. In doing so, the knowledge from a task’s context is transferred across temporal transitions of latent state-spaces. To achieve this, SNPs employ the Recurrent State-Space Model (RSSM) (Hafner et al., 2019) for better generalization to non-Markovian non-Gaussian sequences of stochastic processes. With slight abuse of notations, we now formalize such a sequential learning setting.

Let $C_t = \{(x_i^t, y_i^t)\}_{i=1}^{N(C_t)}$ be the set of observed context points drawn from the true stochastic process f_t at a time step $t \in [1, S]$ and $T_t = \{(x_i^t)\}_{i=1}^{M(T_t)}$ be the corresponding unlabeled target set. In contrast to their definitions seen so far, C and T now reflect the context and target sets over all time steps $t \in [1, S]$. Furthermore, unlike the fixed context set size N that we have been dealing with, the size $N(C_t)$ of context sets are now variable over time and can be zero for a given t as such. Similar to latent NPs, SNPs model

³³<https://www.kaggle.com/datasets/fireballbyedimyrnmom/us-counties-covid-19-dataset>

f_t as the standard distribution over latent variables z_t conditioned on the given context set C_t . However, they additionally condition the distribution over the latents of the past stochastic processes $z_{<t}$. The latent z_t sampled from the resulting distribution $p(z_t|z_{<t}, C_t)$ is then used to model T_t through the posterior $p(f(T_t)|T_t, z_t)$. Generalizing over all time steps $[1, S]$, SNPs generate the output predictions $f(T)$ of targets $T = \cup_{t=1}^S T_t$ and their corresponding latents $Z = \cup_{t=1}^S z_t$ conditioned on T as well as the context $C = \cup_{t=1}^S C_t$:

$$p(f(T), Z|T, C) = \prod_{t \in S} p(f_t(T_t)|T_t, z_t)p(z_t|z_{<t}, C_t) \quad (31)$$

where, the observational likelihood $p(f(T_t)|T_t, z_t)$ is modeled in a fashion similar to equation 3 while $z_0 = \text{null}$. The proposed modeling of z using RSSM thus accounts for the fact that for a spatio-temporal f_t , the latent variable z_t models a spatial stochastic process. In other words, z_t captures only the spatial relationship among the data points $\{x_t^i\}_{i=1}^{N(C_t)}$ at time step t without modeling the temporal relationships $x_{t-1}^i \rightarrow x_t^i$ between these. Modeling Z and C over time endow SNPs with the following two special properties. First, C helps SNPs to be a *generalization of NPs* when considering either a unitary set of sequences, or multiple sequences with $T_{t < T} = \text{null}$ and $T_t \neq \text{null}$. However, unlike the permutation invariant sum aggregators used in the standard NPF set approximators, SNPs leverage permutation-sensitive state transitions as the stochastic context aggregators. Second, Z enables SNPs to *meta-learn* distributions over task sequences by transferring knowledge encoded in the past latents $z_{<t}$. Similar to other latent variable models, the training objective of SNPs deals approximating the intractable posterior $P(Z|C, T)$ but in a temporal auto-regressive fashion:

$$p(Z|O) \approx \prod_{t \in S} q(z_t|z_{<t}, C, T) \quad (32)$$

where, the observed dataset, $O = (C, T, f(T))$. A naive training objective for SNPs then involves maximizing the following ELBO over all time steps using the reparameterization trick (Kingma & Welling, 2014):

$$\log p(f(T)|T, C) \geq \sum_{t \in S} \mathbb{E}_{q(z_t|O)} [\log p(f_t(T_t)|T_t, z_t)] - \mathbb{E}_{q(z_{<t}|O)} [D_{KL}(q(z_t|z_{<t}, O) || p(z_t|z_{<t}, C_t))] \quad (33)$$

where, $\log p(f_t(T_t)|T_t, z_t) = \sum_{x_t \in T, y_t \in f(T)} \log p(y_t^t | x_t^t, z_t)$. The authors however report that optimizing equation 33 can lead to *transition collapse* of KL divergence D_{KL} – a prior-induced variant of the posterior collapse problem (Bowman et al., 2016). Here, the rich conditional prior $p(z_t|z_{<t}, C_t)$ already provides the decoder with low uncertainty information about the task sequences from the path of past latents $z_{<t}$ and thus ignores the path of context C_t . To address this, Singh et al. (2019) propose the *posterior-dropout* ELBO that encourages the prior to use C_t path while reducing D_{KL} by enforcing a restriction on the information carried by the $z_{<t}$ path. To do so, they randomly select timesteps $\mathcal{S} \subseteq [1, S]$ where, z_t is sampled based on the prior transition p . For the remaining time steps $\bar{\mathcal{S}}$, z_t is sampled using the posterior transition q . The approximate posterior $q(\bar{Z})$ is now given as a factor of the two independently sampled latents:

$$q(\bar{Z}) = \prod_{t \in \mathcal{S}} p(z_t|z_{<t}, C_t) \prod_{t \in \bar{\mathcal{S}}} q(z_t|z_{<t}, O) \quad (34)$$

For the specific case of 2-d image completion task, only the timesteps $t \in \bar{\mathcal{S}}$ contribute to the reconstruction locations. Unlike \mathcal{S} , such locations constitute the posterior transitions that the encoder has observed. The posterior-dropout ELBO is then given as:

$$\mathbb{E}_{\bar{\mathcal{S}}} \log p(f_t(\bar{\mathcal{S}})|T, C) \geq \mathbb{E}_{\bar{\mathcal{S}}} \left[\mathbb{E}_{Z \sim q} \left[\sum_{t \in \bar{\mathcal{S}}} [\log p(f(T_t)|T_t, z_t) - D_{KL}(q(z_t|z_{<t}, O) || p(z_t|z_{<t}, C_t))] \right] \right] \quad (35)$$

The entire maximization objective for training is thus a weighted sum of equations 33 and 35 where the contribution of the posterior dropout ELBO is zero at the start of the training and increases with the saturation of the reconstruction loss. The authors apply SNPs with posterior dropout to extend generative query networks (GQNs) at handling temporally progressing scenes with dynamic viewpoint-to-image mappings.³⁴ On both 2d and 3d dynamic scene inference, such temporal GQNs outperform their predecessors at estimating the uncertainty of future time-step predictions irrespective of the assistance from the context. While the authors discuss posterior dropout improving the generation quality of temporal GQNs, they also mention the cost of increased uncertainty arising from it. This is mainly due to the enforced consideration of information from the context path even when the past scene modeling in the latent path $z_{<t}$ is incorrect.

Recurrent Neural Processes: While SNPs learn stochastic processes responsive to time scales, this might not be enough to model most real-world phenomena which incorporate hierarchies of such scales. For example, the electricity usage patterns for households often peak during daytime and remain relatively low at night. Further, the electricity consumption (in cold areas) can be highest during winter and milder during summer. When modeled together, such patterns lead to faster latent time scales (daily usage) often superimposed by slower time scales (seasonal usage). Addressing this limitation, Willi et al. (2019) propose the Recurrent Neural Processes (RNPs) that extend NPs with hierarchies of state space models. Owing to these state spaces, RNPs can be extended to model multiple layers of stacking among stochastic processes.

SNPs namely add a recurrent state to the prior on z_t to model temporal relationships among the data points (see equation 31). Willi et al. (2019) suggest that such a recurrent hidden state not only lacks a principled way of propagating forward temporally varying uncertainty but also fails to incorporate the expressivity of NPs by rather treating the modeling of temporal dynamics and stochastic process as two different tasks. RNPs address these flaws by reformulating equation 31 to incorporate an additional temporal stochastic process $v : \{z_t\}_{t \in S}$ that models the temporal dynamics among all of the spatial stochastic processes z_t :

$$P(f(T), V, Z|T, C, S, L) = \prod_{t \in S} \left(\prod_{i \in I(T_t)} P(f_t(x_t^i) | x_t^i, z_t) \right) P(z_t | C_t, v, t) P(v | L) \quad (36)$$

where, $I(\cdot)$ is the indexing operator and v has its context defined over $L = (S_L, Z_L) = (t, z_t)_{t \in I(L)}$. Equation 36 now no longer models the recurrence over the spatial process z_t given that v is sufficient to capture the temporal dynamics. The temporal indexing S however remains shared between the temporal stochastic processes v and the observed data sequence $\{(y_t^i, x_t^i)\}_{i=1}^{N(C_t)}$ thus resulting in an often unrealistic one-to-one mapping between the latent and the observed time steps. To address the one-to-many mapping between these, a new time line S_{obs} is introduced as the temporal indexing of the observed data $\{(y_{t_{obs}}^i, x_{t_{obs}}^i)\}_{i=1}^{N(C_t)}\}_{t \in S_{obs}}$. The connection between S – the timeline of the temporal stochastic process v , and S_{obs} – the timeline of the observed data is then learned by arranging their indices in a bipartite graph. The resulting model thus forms a hierarchical generalization to NPs seen in section 2.

Recurrent attentive Neural Processes: Moving beyond recurrent state-space models, Qin et al. (2019) propose a parallel path to capture uncertainty in predictions of temporally changing stochastic processes. In particular, they extend ANPs (Kim et al., 2019) with Recurrent Neural Networks (RNNs) by exploiting the fact that ANPs construct multiple observations of a stochastic process and are thus capable of uncovering the order underlying a sequential data. The resulting Attentive Neural Process RNN (ANP-RNN) leverages these observations to learn the uncertainty propagating through temporally progressive stochastic process in data-efficient scenarios.

To formally define ANP-RNN, the authors first consider sequences of inputs leading up to a time step t as vectors $\{\bar{x}_1 = [x^1], \dots, \bar{x}_n = [x^1, \dots, x^n]\}, x^t \in \mathcal{X}$ with the corresponding real-valued labels $y = \{y_i\}_{i=1}^n$. They then assume that only the most recent L steps of such sequences are relevant for the prediction. Consequently, the objective of ANP-RNNs is to learn the distribution of random functions $f : \mathcal{X}^L \rightarrow \mathbb{R}^d$ considering $\bar{x}_i = \{x^{i-L+1}, \dots, x^i\}_{i=1}^n, x^t \in \mathcal{X}$. RNN-ANP uses a recurrent encoder $\phi : \mathcal{X} \rightarrow \mathcal{H}$ to extract the

³⁴Refer to the role of NPs as deep generative models in section 2.2 for a discussion on their resemblances to GQNs.

latent encoding $H \in \mathcal{H}$ of the input sequences. The ANP exploits these encodings to learn the information of the future transformed targets $(H_T(X_T), \hat{f}(\phi(X_T))) := (\phi(X_T), \hat{f}(\phi(X_T)))$ conditioned on that of the past observed contexts $(H_C(X_C), Y_C) := (\phi(X_C), Y_C)$. The overall ANP-RNN model is thus defined as:

$$p(f(X_T)|X_T, C) \approx \int p(f(X_T)|X_T, z, r_C^*, H_T, H_C, Y_C)q(z|H_C, Y_C)dz \quad (37)$$

where, $r_C^* := r^*(C, T)$; $C = (X_C, Y_C)$, $T = X_T$ are the query-specific representations used to define the attentive context for a target query X_T . In contrast to naive ANPs (see equation 11), ANP-RNNs can be seen to be exploiting the deterministic transferred space H to model the distribution of stochastic processes. Except for the 1-d regression task, the authors show that such an exploitation helps ANP-RNNs perform better than NPs and ANPs on real-world sequential data. A toy real-world example they cover is predicting the lane-changing behavior for autonomous vehicles on the NGSIM dataset.³⁵

Neural ODE processes: While sequential models help capture a dynamically changing process over time, such processes in real-world systems are often governed by the infinitesimal changes in a number of intricate physical variables. It is therefore desirable to view the optimization of the training objective in terms of infinitesimal changes in parameters of the network. Modeling such changes in turn amounts to solving ordinary differential equations (ODEs) for the predictions of the network. Inspired by this, neural ODEs (Chen et al., 2018) rely on parameterizing the derivatives of ODEs using neural networks. Neural ODEs thus offer an explicit treatment of time – a property lacking from Neural Processes that treat time as an unordered set and thus fail to measure the time-delay between real-world observations unless otherwise forced by the training objective. However, neural ODEs are limited in their capacity to estimate uncertainties and adapting quickly to the changes in the observed data – two properties inherent to NPs. Norcliffe et al. (2021) thus propose to combine the benefits of both these by leveraging NPs to parameterize the ODE derivatives.

The proposed Neural Ordinary Differential Equations Processes (NDPs) extend NPs to model the time-delays between different observations in low and high-dimensional time series by maintaining an adaptive data-dependent distribution over the underlying ODE. Their problem definition thus consists of modeling samples drawn irregularly from an underlying family of random functions $f : \mathcal{S} \rightarrow \mathcal{Y}$ where, $\mathcal{S} = [t_0, \infty]$ and $\mathcal{Y} \subset \mathbb{R}^d$ are the time stamps and state values of a dynamically adapting stochastic process, respectively. Following the convention of NPs (Garnelo et al., 2018b) and considering $I(\cdot)$ to be the indexing operator, they split each instantiation $\mathcal{F} \in f$ into a context set $C = \{(t_i^C, y_i^C)\}_{i \in I(C)}$ and a target set $T = \{t_i^T\}_{j \in I(T)}$ where the values $\hat{y}_i^T \approx f(T)$ are to be predicted. In order to learn the distribution over ODEs, NDPs employ NPs to model the context set distributed over the initial time t_0 and use this knowledge to predict the ODE trajectories at a time stamp t_i^S as:

$$\hat{y}_i^T = h_2(z(t_i^T)) \quad \text{s.t.}, \quad z(t_i^T) = z(t_0) + \int_{t_0}^{t_i^T} \phi_\theta(z(t), t)dt, \quad z(t_0) = h_1(y_0) \quad (38)$$

where, h_k is a neural network, and $\phi_\theta(z, t)$ denotes the velocity of a state z learned by the encoder network ϕ with parameters θ . NDPs thus rely on the NP setting to encode a context set into two latent variables: an *initial state* $L(t_0) \sim q_L(l(t_0)|C)$ derived from the initial time stamp t_0 and a permutation-invariant *global control* $D \sim q_D(d|C)$ derived from the mean of the context set encoding computed by a neural network. These variables ensure that the latent context evolves according to a neural ODE (Chen et al., 2018) with an initial position $L(t_0)$ and controlled by D . The NDP decoder then feeds on the random state $L(t_i^T)$ of the ODE at time t_i^T to predict its corresponding state value. NPs thus define a lower bound for the expressivity of NDPs in the case where the latent neural ODE learns a trivial velocity $\phi_\theta(z(t), t) = 0$ with a constant random state $L(t) = L(t_0)$. In this case, the latent variable z of a regular NP is substituted by a distribution over the state values \mathcal{Y}_i^T defined by $p(l(t_0)|C)$ and parameterized by the decoder outputs.

GP-ConvCNPs: Petersen et al. (2021) point out the limitation of ConvCNPs for modeling temporally changing data distribution and incorporate a Gaussian Process (GP) into the model as a solution. The

³⁵<https://ops.fhwa.dot.gov/trafficanalysistools/ngsim.htm>

resulting GP-ConvCNP model preserves the ConvCNP architecture (see equation 19) except for using a GP posterior in place of the deterministic kernel density estimate E' . Such a posterior encodes a normal distribution for the target set $T = \{x_t\}_{t=1}^{N+M}$ with a mean $m(x_t) = k_{tc}^T(k_{cc} + \sigma^2\mathbb{I})^{-1}y_c$ conditioned on the context $C = \{(x_c, y_c)\}_{c=1}^N$ and a covariance $K(x_t) = k_{tt} + \sigma^2 - k_{tc}^T(k_{cc} + \sigma^2\mathbb{I})^{-1}k_{tc}$ based on a kernel $k_{ij} = k(i, j)$ and a learnable noise parameter σ controlling the proximity of the predictions to that of the context points. In terms of implementation, GP-ConvCNPs employ GPs with a learnable length scale Gaussian kernel (same as that of ConvCNP).

The above reformulation of encoding E' from equation 19 bridges the gap between ConvCNPs and NPs by offering GP-ConvCNPs the best of both worlds: similar to NPs, it enables sampling from the GP posterior distribution while similar to ConvCNPs, it enhances extrapolation to out-of-distribution target ranges through smoothing of the data distribution. Through a comparison of GP-ConvCNP performances with that of the NP, the ANP and the ConvCNP, Petersen et al. (2021) show that the former performs the best on modeling a range of tasks including 1-d synthetic data regression, real-world temperature time series, and predator-pray population dynamics. While GP-ConvCNPs surpass ConvCNPs in terms of log-likelihood on 2-d image completion tasks, the authors also point out its added cost ($\sim 1.5x$) in terms of convergence time.

3.7 Multi-task relatedness

Given their capability to encode multiple datasets as distributions over functions, NPF members make a sound choice for transferring the contextual knowledge among related meta-learning tasks. The transfer learning thus enriches the performance of individual tasks in the limited training data regime. A common application of NPs to multi-task learning involves drawing multiple tasks from the same distribution. This is practically achieved by sampling the context and target sets from the same dataset, and in most cases, limiting the context to be a subset of the target. Doing so ensures smooth optimization of the prior-matching KL term in the ELBO (see equation 8) given that the context-based prior and the target-based posterior now follow the same distribution.

Sampling datasets from the same i.i.d. distribution however reflects little on robust real-world scenarios where a learning agent (e.g., an autonomous driving engine) can be presented with multiple tasks (e.g., driving straight, driving with one or more turns, full navigation with or without dynamic obstacles, etc.) where the context data of different tasks are sampled from distinct distributions (e.g., different weather conditions). The methods in this NPF branch thus target enriching multi-task learning in the face of tasks derived from such heterogeneous distributions.

Notation: Borrowing the notation from Section 2, we define a multi-task learning setup as having a number L of training tasks such that the data for each task $l \in [1, L]$ is divided into a context set $C^l = \{(x_i^l, y_i^l)\}_{i=1}^{N_l}$ and a target set $T^l = \{x_i^l\}_{i=N_l+1}^{N_l+M_l}$ where $\{x_i^l\}_{i=1}^{N_l+M_l} \in \mathcal{X}_l$ and $\{y_i^l\}_{i=1}^{N_l} \in \mathcal{Y}_l$. To reflect the heterogeneity in distributions, each task l can be seen to be generated by a distinct continuous and random function $f^l : \mathcal{X}_l \rightarrow \mathcal{Y}_l$.

Conditional neural adaptive processes: Requeima et al. (2019) point out the trade-off faced by few-shot multi-task classifiers while adapting to new tasks – they need to strike a balance between model capacity and reliability of adaptation based on the number of parameters adapted to each task while still being resource efficient during adaptation. To balance this, the authors propose the Conditional Neural Adaptive Process (CNAP) as a CNP-based approach. Considering our definition for multi-task setup, CNAPs model CNPs as a combination of a task-specific adaptation model $\psi^l = \psi_\phi(\cdot)$ with global parameters ϕ shared across tasks and a classification model with another set of global parameters θ . Keeping this in mind, equations equation 2 and equation 4 can be put together as:

$$p(f^l(T^l)|T^l, \theta, C^l) = p(f^l(T^l)|T^l, \theta, \psi^l = \psi_\phi(C^l)) \quad (39)$$

where, ψ^l is a fixed dimensional vector input to the model parameterized by θ , and θ and ϕ are learned by maximizing the likelihood of observations. Using the above formulation, CNAPs learn θ in an offline fashion to capture abstract features enabling transfer learning across multiples tasks. However, unlike CNPs, CNAPs

allow ψ^l to be learnable model parameters so that the classifier can capture broader ranges of data distributions. In particular, θ is modeled by a ResNet (He et al., 2016) whose feature representation $F_\theta(\cdot)$ when adapted for a task l using a set of local feature extractor parameters ψ_f^l leads to the representation $\psi_\theta(\cdot; \psi_f^l)$. To enable such task-specific adaptation of $\psi_\theta(\cdot)$ using a smaller number of task-specific parameters, CNAPs employ a ResNet18 with feature-wise linear modulation (Perez et al., 2018) layers after every convolutional layer. At the same time, the last layer of θ is made task-specific using the weights $\psi_\omega^l \in \mathbb{R}^{d_f \times n^l}$ where d_f is the dimension of the feature extractor’s output $\psi_\theta(\cdot)$ and n^l is the cardinality of classes in task l .

The global classifier parameters θ are trained in a two-step process. In the first step, θ are pre-trained on a large dataset using all available classes. The second step follows by freezing θ and training ϕ in an episodic manner to output ψ_f^l over a meta-training dataset of each task l in the multi-task setting. Freezing the pre-trained high-capacity θ after first step leads to decreased training times besides enhancing the generalization of ϕ as it now has more room for learning ψ_f^l . For training the task-specific adaptation model parameters ϕ , CNAPs adapt the maximum-likelihood objective of CNPs based on context-target splits. The loss value for the adaptation network is given as:

$$\mathcal{L}(\hat{\phi}) = \frac{1}{M.L} \sum_{l=1}^L \sum_{i=N_l+1}^{N_l+M_l} \log p(f(T_i^l)|T_i^l, \psi_\phi(C^l), \theta) \quad (40)$$

CNAPs establish a new state-of-the-art performance on the challenging Meta-Dataset (Triantafillou et al., 2020) consisting of large-scale heterogenous train and test time tasks resembling real-world scenarios. As an intriguing application of CNAP’s generalization capability, (Requeima et al., 2019) further evaluate it on task-incremental learning as well as active learning setups. On the demanding exemplar-free task incremental setup (Pelosin et al., 2022), CNAPs achieve performances comparable to robust continual learning models (Chaudhry et al., 2018) despite having trained for few-shot classification on orders of magnitude fewer examples. On the active learning setup (Cohn et al., 1996), CNAPs outperform the widely-used distance-based prototypical networks (Snell et al., 2017). In essence, these results demonstrate the benefits of CNAPs in leveraging task transfer for quicker and robust calibration to new domains and learning scenarios.

Multi-task Neural Processes: In order to improve the context representation for a given task by exploiting complex relationships with related tasks, (Kim et al., 2022a) propose the multi-task Neural Processes (MTNPs) that derive the priors of prediction functions in a hierarchical Bayesian inference framework. Unlike CNAPs targetting only classification, MTNPs also leverage task-transfer for regression.

Following our defined notation for multi-task setup, latent variables for a task l can be given as $Z^l = f^l(\{x_i^l\}_{i=1}^{N_l}) \in \mathbb{R}^{N_l \times d_y}$. Denoting the entire collection of context sets $\{C^l\}_{l=1}^L$ in the dataset as $\{C^l\}$, (Kim et al., 2019) model the joint predictive distribution with respect to the latent random function set $\{f^l\}$ as:

$$p(\{f^l(T^l)\}|\{T^l\}, \{C^l\}) = \prod_{l \in L} \int p(f^l(T^l)|T^l, f^l) p(f^l|\mathcal{M}) df^l \quad (41)$$

where, \mathcal{M} is a global variable introduced to collect useful information from context $\{C^l\}_{l=1}^L$ of all tasks and provide it to each individual task. In order to model the Gaussian distribution underlying each stochastic process, $p(f^l|\mathcal{M})$ is defined as a task-specific deep neural network (classifier or regressor) parameterized by a random variable ψ_l , *i.e.*, $f^l(X) = X\psi_l^\top$. Conditioning ψ_l on the global variable \mathcal{M} gives a data dependent prior thus resulting in the following predictive distribution for the l -th task over its target set:

$$p(f^l(T^l)|T^l, \{C^l\}) = \int p(f^l(T^l)|T^l, \psi_l) p_\theta(\psi_l|\mathcal{M}) d\psi_l \quad (42)$$

With the goal of aggregating \mathcal{M} in the face of distribution shift between tasks, a higher-level latent variable α_l is introduced. α extracts the shared knowledge from \mathcal{M} thus controlling its access for each task. The

resulting hierarchical Bayesian modeling of functions is given as:

$$p_{\theta}(\psi_l|\mathcal{M}) = \int p_{\theta_1}(\psi_l|\alpha_l, \mathcal{M})p_{\theta_2}(\alpha_l|C_l)d\alpha_l \quad (43)$$

where, $p_{\theta_1}(\psi_l|\alpha_l, \mathcal{M})$ and $p_{\theta_2}(\alpha_l|C_l)$ are prior distributions of the latent variables ψ_l and α_l , respectively. Substituting equation 43 into equation 42 gives the hierarchical context model of MTNPs:

$$p(\{f^l(T^l)\}|\{T^l\}, \{C^l\}) = \prod_{l \in L} \int \int p(f^l(T^l)|T^l, \psi_l)p_{\theta_1}(\psi_l|\alpha_l, \mathcal{M})p_{\theta_2}(\alpha_l|C_l)d\psi_l d\alpha_l \quad (44)$$

We refer the reader to Kim et al. (2022a) for the optimization and inference details of MTNPs. Besides providing a range of multitask classification and regression experiments to demonstrate the advantage of MTNPs over NPs, the authors also discuss its capacity for exploring spatial context information. On the latter note, they formulate brain image segmentation as a pixel-wise regression task where a probability value for each pixel belonging to a (tumor) region is to be predicted. The segmented area obtained from MTNP predictions are shown to outperform the robust U-Net segmentation baseline (Ronneberger et al., 2015) in terms of dice similarity coefficients.

3.8 Domain Invariance

This NPF branch targets learning more general representation of inputs with an immediate downstream application being distinguishing the inputs belonging to similar domains. Given the implications of the no free lunch theorem for generalizability of predictive models trained using specific learning objectives, it is important that such domain invariance is induced in a self-supervised manner. The learned task-agnostic representations can then be employed to a wide range of downstream unlabeled applications. A popular choice for self-supervised learning objectives in the Neural Process family are contrastive losses (Chopra et al., 2005) that compare the similarity across the representation of inputs. Neural processes with the ability to approximate distributions over functions, can further enable contrastive learning of domain invariant function representations by bringing the representations from the same function closer and that from other functions further apart.³⁶ This forms the key motivation for the works described in this branch.

Contrastive Neural Processes: While it is easy to employ geometric transformations for building robust augmentation pipelines in vision-based domains (Oord et al., 2018), time series domains such as audio processing, financial forecasting, etc. demand for tailored augmentation pipelines. Towards the end goal of self-supervised learning of representations using augmentations that are generalizable across application domains, Kallidromitis et al. (2021) propose the contrastive Neural Processes (ContrNPs). Their framework exploits the fact that the aggregated observation embedding constructed by NPs is shared across the target set while modeling a distribution over functions. Using regression forecasting in NPs as a supervised signal for unsupervised learning can therefore help generate multiple observations of the same data point if the sampling functions are distinct. Each set of observation here corresponds to an augmentation as such. While such a framework is generalizable across any type of data, ContrNP primarily target time series in the lack of established augmentations for these.

ContrNP consists of two major components: a forecasting component based on Neural Processes and a learning component based on a choice of self-supervised contrastive loss. Building upon the notations of section 3.6, ContrNP models a dataset \mathcal{S} defined over S time segments: $\mathcal{S} = \{D_s\}_{s=1}^S = \{(x_s, y_s)\}_{s=1}^S$. The objective of ContrNPs can be summarized as learning a rich time-dependent representation $\mathbf{R}_s = \psi_{\theta}(D_s)$ for the underlying random function $f : \mathcal{X} \times \mathcal{Y}$ in the latent space. To represent an input time series changing over time, \mathcal{S} is split into K segments $\{\mathcal{S}_1, \dots, \mathcal{S}_k, \dots, \mathcal{S}_K\}$ where each segment encodes a function f_k and can be further randomly split into $M \in \mathbb{Z}^+$ groups $\{\mathcal{S}_{k,m}\}_{m=1}^M$. The division into groups reflect the view that

³⁶While the first proof of this concept was put forward by Gondal et al. (2021), they do not consider using efficient regression techniques provided by Neural Processes for richer representation learning. On a similar note, (Mathieu et al., 2021) also exploit self-supervised contrastive learning for NPs but they do away with exact reconstruction of posterior samples. We thus consider discussing these works from the perspective of future research directions (see Section 7).

two different subsets $\mathcal{S}_{k,m}$ and $\mathcal{S}_{k',m'}$ represent the same underlying function provided $k = k'$ and different functions if $k \neq k'$. Each such group is then divided into a context set $C_{k,m}$ and a target set $T_{k,m}$.

Given the ability of off-the-grid ConvDeepSets to achieve shift equivariance by mapping the inputs x_s to a functional space corresponding to the difference between the inputs (see equation 19), ConvCNPs make a natural choice to predict out-of-context time series representations. Consequently, ContrNPs rely on ConvCNPs for feature extraction. To model the intra-group relatedness among samples, $\mathcal{S}_{k,m}$ is divided into three parts: the left range $\mathcal{S}_{k,m}^L$, the center range $\mathcal{S}_{k,m}^C$, and the right range $\mathcal{S}_{k,m}^R$ based on $x_{i'} \leq a$, $a < x_{i'} < b$, and $b \leq x_{i'}$ with carefully chosen thresholds a and b . Using only the center range as the context set and the entire $\mathcal{S}_{k,m}^L$ as the target set enforces ContrNPs to generalize on a much larger proportion of the dataset. This in turn mimics heavier data-agnostic augmentations driven by sampling.

The specification of M groups is used while extracting the encoder representations $R_{k,m}$ and $R_{k,m'}$ of the function f_k using the context sets $\mathcal{S}_{k,m}^c$ and $\mathcal{S}_{k,m'}^c$, respectively. Such representations then serve as examples for the classic anchor and positive samples of the contrastive loss function while the rest of the representations $R_{k'}(k \neq k')$ of the batch are treated as negative examples. The total training loss for ContrNPs can thus be given as a sum of the negative log likelihood loss and the the contrastive loss function $\mathcal{L}_C(\theta, \mathcal{S}_{1:K})$ (Chen et al., 2020). However, these losses are now adapted to sampled functions instead of representations:

$$\begin{aligned} \mathcal{L}(\theta) &= -\lambda \sum_{k \in K} \sum_{m \in M} \log P(y_{k,m} | \phi_\theta(R_{k,m}), x_{k,m}) + \mathcal{L}_C(\theta, \mathcal{S}_{1:K}) \\ \text{s.t., } \mathcal{L}_C(\theta, \mathcal{S}_{1:K}) &= \sum_{k \in K} \sum_{m \in M} \sum_{m' \in M} \mathbb{I}_{[m \neq m']} \log \left[\frac{\text{sim}(R_{k,m}, R_{k,m'}) / \tau}{\sum_{k'=1}^K \sum_{m''=1}^M \mathbb{I}_{[k' \neq k]} \text{Sim}(R_{k,m}, R_{k',m''}) / \tau} \right] \end{aligned} \quad (45)$$

where, $\text{sim}(\cdot, \cdot)$ is the cosine similarity operator, τ is the annealing factor, $\mathbb{I}_{[\cdot]}$ is an indicator function, and $R_{k,m} = \psi_\theta(\mathcal{D}_{k,m})$ is the anchor representation extracted by the ConvCNP encoder ψ_θ with $R_{k,m'}$ and $R_{k'}$ being its positive and negative counterparts. λ determines the tradeoff between the log likelihood objective interpolating within the function and the contrastive learning objective distinguishing functions from one another. The latter among these objectives helps achieve domain invariance in the functional space by minimizing the distances of anchors with the positive examples and maximizing those with the negative examples. Through a range of classification and clustering experiments designed to reflect the suitability of representations on real-world tasks, the authors demonstrate the advantage of ContrNPs over a number of strong contrastive learning baselines (Chen et al., 2020; Oord et al., 2018).

Contrastive Conditional Neural Processes: Ye & Yao (2022) further leverage contrastive learning to address the limitations of CNPs at jointly optimizing *in-instantiation* observation prediction, *i.e.*, generalization among the samples of a function and *cross-instantiation* meta-representation adaptation, *i.e.*, generalizing across a family of functions in the face of high-dimensional and noisy time series data. In particular, they highlight three major drawbacks arising from the CNP’s optimization objective: (i) lack of predictive correlations (see Section 3.5), (ii) limitations of generative models in forming abstractions for high-dimensional observations (Kipf et al., 2019), and (iii) supervision collapse in meta-learning (Doersch et al., 2020) due to entangled prediction and transfer tasks. To address these, they propose extending CNPs using an in-instantiation temporal contrastive learning (TCL) loss to align predictions with encoded ground-truth observations and a cross-instantiation function contrastive learning (FCL) loss to decouple meta-representation adaptation from generative reconstruction.

Using the convention for ContrNPs, the framework for the proposed Contrastive CNP (ContrCNP) treats a dataset \mathcal{S}_k at a segment $k \leq K$ to be composed of context $C = \{(x_c^f, y_c^f)\}_{c \in I_C^f}$ and target sets $T = \{x_t^f\}_{t \in I_T^f}$ which have been uniformly drawn from an underlying data-generating continuous bounded function f . The workflow of ContrCNP then improves upon the vanilla CNPs in the following ways. Firstly, instead of feeding the concatenated context features $x_{c=1:|C|}$ and their corresponding labels y_c to the encoder $h_c(\cdot, \cdot)$, ContrCNP first pre-processes these using distinct domain-specific feature extraction networks ψ and ϕ . The pre-processed encodings are then used by the encoder to output the local representation $r_c^f = h_c(\psi(x_c^f), \phi(y_c^f))$.

Second, rather than a direct averaging over the local representations r_c^f , ContrCNP passes these through a multi-head self-attention module (Vaswani et al., 2017) to capture the correlation among the context examples using a position-aware importance matrix. The encoded representations r_c are then averaged to obtain a permutation-invariant summary of all the time-observation pairs from C . By concatenating the query index $\psi(x_c^f)$ with contextual representation r^f , the decoder g estimates the observation $\hat{y}_T^f = f(x_T)$ which, similar to equation 3, is a joint Gaussian distribution.

In order to enforce temporal local alignment between the encoding of the predicted and the ground truth observation, the in-instantiation TCL loss is optimized to maximize the likelihood of the predictive embedding conditioned on sets of context set C^f sampled from $f \in \mathcal{D}$ different instantiations. Prior to applying TCL, the concatenated target index and contextual representation is transformed with predictive head φ which is further passed through a non-linear head $\rho_p : \mathbb{R}^{\phi, \varphi} \rightarrow \mathbb{R}^z$ that maps these to a low dimensional space suitable for similarity $\text{sim}(\cdot, \cdot)$ computation, *i.e.*, $\hat{z}_k^f = \rho_p(\hat{\varphi}_k^f)$, $z_k^f = \rho_p(\varphi(y_k^f))$ with $\hat{\varphi}_k^f = \varphi(x_k^f, r_c^f)$. Inspired by SimCLR (Chen et al., 2020), TCL treats z_k and \hat{z}_k as positive pairs and constructs negative samples from the remaining batch indices:

$$\mathcal{L}_{\text{TCL}} = \sum_{f \in \mathcal{D}} \sum_{k \in K} \log \frac{\exp^{\text{sim}(\hat{z}_k^f, z_k^f)/\tau}}{\exp^{\text{sim}(\hat{z}_k^f, z_k^f)/\tau} + \sum_{f' \in \mathcal{D}} \sum_{i=1}^{|T|+|C|} \mathbb{I}_{[i \neq k]} \exp^{\text{sim}(\hat{z}_k^f, z_i^{f'})/\tau}} \quad (46)$$

Following (Gondal et al., 2021) and (Kallidromitis et al., 2021), ContrCNPs generalize contextual representations across functional spaces by allowing the representations of the same function to be mapped together and those from different functions to be mapped further. Preserving this optimization objective, the cross-instantiation FCL loss involves randomly splitting the context set C^f into two disjoint subsets C_1^f and C_2^f . Each subset can thus be thought to capture a partial view of the context set and is processed by multi-head attention modules (similar to TCL) to obtain representations r_i^f, r_j^f across $f \in \mathcal{D}$ context sets. These representations are then projected by a head $\rho_P : \mathbb{R}^r \rightarrow \mathbb{R}^z$ to obtain the low-dimensional representation $q_i^f = \rho_P(r_i^f)$ and $q_j^f = \rho_P(r_j^f)$:

$$\mathcal{L}_{\text{FCL}} = \sum_{f \in \mathcal{D}} \sum_{1 \leq i < j \leq 2} \log \frac{\exp^{\text{sim}(q_i^f, q_j^f)/\tau}}{\exp^{(q_i^f, q_j^f)/\tau} + \sum_{f' \in \mathcal{D}} \sum_{1 \leq i \leq j \leq 2} \mathbb{I}_{[f \neq f']} \exp^{\text{sim}(q_i^f, q_j^{f'})/\tau}} \quad (47)$$

The overall training loss of Contrastive CNPs is thus a sum of the observation reconstruction objective (similar to equation 4), \mathcal{L}_{TCL} , and \mathcal{L}_{FCL} with a calibrated contribution of the latter two losses. (Ye & Yao, 2022) show that such a training objective helps Contrastive CNPs surpass the performance of CNPs (Garnelo et al., 2018a), ANPs (Kim et al., 2019), and ConvCNPs (Gordon et al., 2020) on a number of tasks including 1d function regression, 2d population dynamics prediction, and higher dimensional image completion on Rotating MNIST³⁷ and synthetic bouncing ball datasets.

4 Other Domain-specific advances

In Section 3, we covered the major branches of the NPF that target inducing bias(es) into the models to generalize well on unseen data. While these make up the mainstream theoretical advances in the Neural Process family, a detailed look into the literature sheds light on a yet another track of research advances in the family. This track namely leverages the previously introduced models to deal with domain-specific problems. In what follows, we identify five such major domains of applications where members of the NPF have been successfully employed to solve problems from multiple perspectives: recommender systems, hyperparameter optimization, neuroscience, space science, and physics-informed modeling of dynamic systems. We then point out a few more such application areas which have seen sparse applications of the NPF members (from only one perspective) so far. We categorize the latter as miscellaneous.

³⁷<https://github.com/cagatayildiz/ODE2VAE>

Recommender systems. With the objective of addressing cold-start problem in recommender engines, (Lin et al., 2021) employ Neural Processes as model-based alternatives to the often used gradient-based meta learners (Finn et al., 2017) that perform gradient updates for parameter initialization without taking into account the relevance of different tasks, *i.e.*, the recommendations of different users. The proposed task adaptive Neural Process (TaNP) assumes each such task to be an instantiation of a stochastic process and adapts to these based on a latent variable structure, a customized module and an adaptive decoder. The customization module learns the relevance of different tasks using a task identity network which for each context set, first produces a temporary task embedding and then applies a global pooling on these to globally learn a final task embedding capturing the relevance of different tasks. The final task embedding is then leveraged by the adaptive decoder to generate its parameters using feature modulation (Perez et al., 2018). Using real-world recommendation datasets such as the MovieLens-1M,³⁸ the authors show that TaNPs surpass the performance of state-of-the-art meta-learning recommenders on a diverse range of metrics including Precision@N and Mean Average Precision@N. More recently, Wang et al. (2022a) adapt an encoder-decoder architecture based on conditional Neural Processes (Garnelo et al., 2018a) for collaborative filtering. Similar to TaNP, their framework, the conditional collaborative filtering process (CCFP) predicts recommendations for partial user-item interaction data, *i.e.*, the target set. However, they treat the permutation invariant encoding $E(C)$ (see equation 2) as the global representation of a typically large context set.

Hyperparameter optimization. Hyperparameter optimization (HPO) concerns selection of the optimal combination of hyperparameters for maximizing a machine learning model’s performance.³⁹ A naive way to decide such hyperparameters is to carry an exhaustive trial of the whole training process using the evaluated values (obtained from an acquisition function such as the expected improvement EI measure) of the chosen hyperparameters. However, given that each such trial can bear enormous costs (consider calibrating a power grid system each time a generator is added (Shangguan et al., 2021)), the widely-used sequential model-based optimization (SMBO) branch of HPO considers leveraging cheap-to-evaluate surrogate models which are learned by iterating between fitting these on hyperparameter performances observed in historical datasets and using these to decide what further configurations need to be investigated to improve the surrogate. A Bayesian approach to SMBO further deals with querying the distribution (over functions) defined by the surrogate model, with the chosen hyperparameters.

Given the success of GPs (Swersky et al., 2013) and neural networks (Snoek et al., 2015) as choices for surrogate models in Bayesian SMBO, Neural Processes with the benefits of both thus stand as potential candidates for stochastic modeling of HPO. Motivated by this, Luo et al. (2020) propose the multitask CNP (MTCNP) where GPs are replaced by CNPs as the choice of surrogate models for multi-task learning of a set of related optimization problems. The MTCNP model namely incorporates a correlation learning layer allowing the sharing of information among multiple task-specific CNPs. In essence, the correlation layer models the nonlinear correlation among several optimization tasks. The authors then propose two variants of MTCNP: (a) the one-to-many MTCNP where each task samples the same variate X and the fitness of X is evaluated for all tasks, (b) the many-to-many MTCNP where an individual task l samples its corresponding variate X_l independent of the other tasks and the fitness of X_l is evaluated only on the l -th task.

On a similar note, Shangguan et al. (2021) propose the Neural Process for Bayesian Optimization (NPBO) framework to automate HPO of black-box power systems whose knowledge of internal workings is assumed to be unknown. Optimizing such power systems can be crucial to reduce the time and costs of machine calibration while ensuring their real-time functioning. To do so, NPBO uses the EI measure as acquisition function and replaces GPs with NPs for better scalability and accuracy in higher dimensional spaces. In particular, the authors evaluate the mean squared error of NPBO on an IEEE 14-bus system (Bharath, 2020) simulated using the power system simulation tool PSS@E (Weber, 2015) and show that it surpasses the classical Random search and GP-based Bayesian optimization besides other state-of-the-art benchmarks.

Wei et al. (2021) study HPO in the context of SMBO based on transfer learning of hyperparameter configurations. While such a transfer of knowledge is known to offer promising results for SMBO (Feurer et al., 2015), the authors highlight the inaptness of the existing GP-based surrogate models in transferring HPO

³⁸<https://grouplens.org/datasets/movielens/1m/>

³⁹In real-world scenarios, such machine learning models often represent physical systems that are to be optimized.

knowledge given their scaling and fitting limitations. To overcome these challenges, they propose adapting Neural Processes to meta-learn the joint transfer of observations, the parameters of historical surrogates and the initial configuration of other datasets. The resulting encoder-decoder HPO surrogate is thus named as transfer Neural Process (TNP) and incorporates a dataset-aware multihead attention mechanism that implicitly learns a kernel function measuring the similarity between a target data point and all observed datasets. To further scale such a kernel to accommodate wider range of datasets, TNPs exploit meta-learning (Finn et al., 2017) for its resemblance to a hierarchical Bayesian model providing a global kernel that models the dependency of dataset-specific kernels.

Neuroscience. Cotton et al. (2020) leverage the meta-learning ability of Neural Processes to predict the responses of the visual cortex neurons to novel stimuli based on few observed stimulus-response pairs mapped by the neural tuning function. Using such K -shot regression formulation of stimulus-response samples, they first point out the limitation of NPs at learning a neuron’s tuning function space. Inspired by the success of CNNs incorporating a factorized readout between the tuning function’s location and properties on the aforementioned task (Klindt et al., 2017), the authors then put forward the idea of factorized Neural Process. Factorized NPs host a factorized latent space that is obtained by stacking multiple NPs and passing the latent variable computed by earlier layers to deeper layers. This in turn enables the latent space of factorized NPs to represent tuning functions that are partitioned into their location and properties. Choosing the real visual cortex responses of mice, the authors empirically show that factorized NPs perform on-par with state-of-the-art predictive models (Klindt et al., 2017) while reducing the readout time by $\frac{1}{80}$. The latter improvement particularly enables factorized NPs to perform real-time inference of tuning functions.

Pakman et al. (2020) study Neural Processes in the context of neural spike sorting – the grouping of spikes into clusters such that each cluster reflects the activity of different putative neurons. To do so, they propose the neural clustering processes (NCPs) that are trained using context set points $\{x_i\}_{i=1}^N \in \mathcal{X}$ and their $K < N$ distinct cluster labels $c_i \in \mathcal{Y}$ (obtained from a generative model). At test time, NCPs are capable of generating approximate posterior samples of cluster labels given the target points $x_i \in T$. Besides computing fixed-dimensional encoding $H_k, 1 \leq k \leq K$ that induces permutation invariance for samples within the same cluster, NCPs additionally leverage the aggregations G and U that ensure invariance under the permutation of the cluster labels and the unlabeled data points, respectively. While the base NCP variant uses $\mathcal{O}(N)$ forward passes per dataset, the authors also put forward a scaled variant of NCP that can achieve the same in $\mathcal{O}(K)$ forward passes. For the task of spike sorting, NCPs leverage a spike waveforms encoded with a CNN, a variable-input softmax function, and an amortized training objective based on factorized posterior to approximate $p(c_n | c_{1:n-1}, x)$.

Space science. Extraterrestrial data is usually captured (by earthly telescopes or space probes) under challenging and uncertain environments – for example, consider capturing snaps of planets during a briefly scheduled flyby (Hammel, 2020). As such, these are typical of voids and irregularities. While interpolating (Reuter et al., 2007) can offer a possible solution to filling such voids, interpolation relies on spatial continuity and thus produces values that often mirror the local information while ignoring the global topological patterns. On the other hand, a simple application of deep generative models like GANs (Goodfellow et al., 2014) might fill the void smoothly but fails to provide uncertainty estimates. Considering the capability of Neural Processes to overcome these challenges by stochastic modeling of data, applying these to fill in the voids in data offers a promising direction in space science applications.

Park & Choi (2021) employ attentive Neural Processes (ANPs) (Kim et al., 2019) for the probabilistic reconstruction of no-data gaps in the digital elevation maps (DEMs) of the moon’s surface captured by narrow-angle cameras (NACs). The authors further propose a sparse variant of ANP that relies on randomly sampling K points from the original attention window containing $S_i \gg K$ context samples which contribute to the computation of attention weights for a given context point x_i . The proposed sparse ANP thus reduces the computational complexity of ANPs from linear to a constant multiple of the squared dataset size. Evaluating on the NAC-DEM data of the Apollo 17 landing site, the authors demonstrate the superiority of SANPs over ANPs, NPs and GPs in terms of negative log likelihood, mean absolute and root mean squared errors.

Čvorović-Hajdinjak et al. (2022) consider Neural Processes for the modeling of stochasticity in the optically variable light curves (characterized by irregular, gapped and sparse luminosity over a brief time) of active galactic nuclei (AGN) resulting from the complex disturbed environments created by the gravitational forces of a nearby supermassive black hole. Using CNPs (Garnelo et al., 2018a) to model the Flux of 153 AGNs surveyed by the Swift Burst Alert Telescope (Tueller et al., 2008), the authors detail their experimental results on a range of performance metrics for CNPs such as efficiency at modeling GP generated data, execution time, iteration vs. speedup, iteration vs. loss values, etc.

Pondaven et al. (2022) employ ConvCNPs (Gordon et al., 2020) and ConvLNPs (Foong et al., 2020) to study the problem of inpainting missing pixel values in satellite images. In particular, they consider correcting the scanlines of the LANDSAT 7 images downloaded using the Google Earth Engine API. A peculiarity of their implementation lies in using the Multi Scale Structural Similarity metric (Wang et al., 2003) as a choice of log-likelihood function for generating sharper mean predictions of images. The authors report evaluations on two experimental scenarios: (a) the in-distribution setting where the models are trained and tested on the satellite images of the same country, (b) the out-of-distribution setting where the models trained on images of one country are deployed to inpaint the images of other countries. It is the latter scenario where meta-learning enables the Neural Processes to perform zero shot generalization.

Physics-informed dynamic systems. Inclusion of a priori physics-informed knowledge into the design of systems modeling real-world dynamic entities helps improve data efficiency, generalization as well as interpretability (Karniadakis et al., 2021). For instance, Jacobian matrix in a robot manipulator provides the relation between joint velocities and end-effector velocities. In the particular case of neural networks, incorporating such knowledge can further take away their black-box nature and make them interpret the laws of experts and/or nature. Inspired by this, Chakrabarty et al. (2021) study Neural Processes to model climate-related impact of energy consumption in buildings by calibrating the digital twins of their grid-interactive simulations. Such twins incorporate the physics of heating, ventilation, and cooling (HVAC) and therefore, host interpretable outputs and parameters. To this end, the authors employ ANPs that are trained with the objective of finding optimal parameters (see equation 4) that minimize the calibration cost between the outputs collected from a real system and a simulated model reflecting the digital twin.

In contrast to HVAC physics, another widely used method for inducing the knowledge of physical world while modeling dynamical systems is by including the corresponding Ordinary Differential Equations (ODEs) into the learning problem’s cost function. An ODE of degree n describes a physical system with a function F of an independent variable x and a dependent variable y along with its n -th order derivatives y^n : $F(x, y, y', \dots, y^n) = 0$. While (Norcliffe et al., 2021) (see Section 3.6) apply neural ODEs (Chen et al., 2018) to model the time-delays between observations in time series data, ODEs further host a multitude of applications in modeling continuous-time real-world phenomena ranging from thermodynamics (for example, Newton’s law of cooling) to epidemiology (Ahmed et al., 2021). As such, we dedicate a separate mention for uncertainty-aware ODE modeling applications rather than including them in Section 3. Given that the complex dynamical behavior of a system can be modeled as a stochastic process, Gaussian processes applied to non-parametric stochastic differential equation (SDE) modeling have been shown to successfully forecast the behavior of such continuous-time systems (Garcia et al., 2017).

Wang & Yao (2021) consider Neural Processes to model SDEs defining forward passes in DNNs as state transformations of a dynamical system. The resulting problem setup is thus capable of estimating epistemic uncertainty in DNNs using real valued continuous-time stochastic processes like the Wiener process (Øksendal, 2003). To achieve this, the authors first emphasize the limitation of existing neural SDE models like the SDE-Net (Kong et al., 2020) in detecting out-of-distribution data when presented with noisy in-distribution data. They then consider improving the accuracy of SDE-Net (Kong et al., 2020) on noisy in-distribution data by extending it with Neural Process variants (CNPs, ANPs and ConvCNPs). In particular, their framework considers fixing the missing rates for in-distribution 1-d regression and 2-d image completion tasks by exploiting the shift equivariance of ConvCNPs, and for in-distribution multidimensional regression tasks by leveraging the permutation invariance of CNPs and ANPs.

More recently, Wang et al. (2022c) proposed using Neural Processes as stochastic surrogates for modeling ODEs defining the simulation of complex nonlinear systems through finite element analysis (FEA)

(Zienkiewicz et al., 2005). The resulting FEA-informed model, the Neural Process-ODE (NP-ODE) incorporates two types of encoders: an deterministic encoder based on ANPs performing cross-attention between a target encoding and the deterministic context encodings, and a stochastic encoder based on latent NP. The encoder thus generates output distributions for uncertainty quantification which is passed to a neural-ODE (Chen et al., 2018) acting as decoder for endowing improved generalizability when solving systems modeled by ODEs.

Robotics. With the ubiquitous spread of automation in machines, uncertainty-aware predictions in these are crucial for their real-world deployment. In what follows, we identify the budding applications of Neural Processes to the domain of uncertainty-aware robotic task modeling. Chen et al. (2022) employ Conditional Neural Processes for robotic grasp detection of unseen objects. Their framework involves a CNP implementation on top of DexNet-2.0 (Mahler et al., 2017) to meta learn physical embeddings of objects from a few observations – namely their cropped depth images, the grasping heights between the gripper and estimated grasping point, and the binary grasping results.

Similarly, Li et al. (2022) leverage CNPs on the upstream task of 6D pose estimation that can enable a robotic arm to be aware of the position and orientation of objects in its vicinity. They formulate the estimation problem in terms of calculating the rigid transformation $[R; t]$ from the object coordinates to the camera coordinates, where R and t denote the rotation matrix and the translation vector, respectively. The calculation proceeds in three stages. First, a FFB6D fusion network (He et al., 2021) extracts per-point features of sampled seed points from the input depth images. Second, a CNP predicts the translation offsets between seed point features selected from context images and predefined keypoints. The keypoint candidates are finally leveraged to obtain the keypoint prediction in the camera coordinates based on the mean shift procedure (Comaniciu & Meer, 2002).

Miscellaneous. While the aforementioned domains comprised works from multiple research directions, we found some further budding NPF application domains that still contain work done in isolation. A summary of few such works together with their target domains is detailed in table 2. As the NPF members enjoy increasing popularity across a range of real-world application domains, we expect the entries in this table to grow with a number of such related entries eventually forming their own application domain. The latter claim is evident by the fact that we found two such works (Xue et al., 2022; Chen et al., 2022) to appear in the NPF literature during the course of work on this paper.

5 Datasets

Given the diversity of the fields that members of the Neural Process family have been successfully applied to, we consider compiling the list of datasets along with their nature and their key area of focus to be timely. Table 3 lists some of such most representative datasets used for evaluating Neural Process architectures over the years. The powerful approximation and faster inference capability of neural networks have allowed the NPF members to be adapted to datasets spanning higher dimensions as well as continuum.

It is worth noting that the key to modeling the stochastic processes generating these datasets lies in the appropriate problem formulation. For instance, the MNIST digits (LeCun et al., 1998) can be employed in the context of regression as well as classification based on whether we choose to model the stochastic process generating the distribution of pixel intensities or the distribution of digit labels (Garnelo et al., 2018a). Similarly, the Omniglot dataset (Lake et al., 2015) with fairly large number of classes and few instances per class suits well for one-shot classification but can also be used in the regression setting of image in-painting. On the other hand, 3-d point cloud datasets such as ShapeNet (Chang et al., 2015) host large combination of possible coordinate locations. Naively regressing the (binary) existence of points based on their 3-d coordinate locations can be expensive as such. In fact, in section 6.3, this forms our motivation to instead opt for part labeling – with labeled input points serving as locations rather than all possible 3-d coordinates – as the toy depiction of NPs modeling functions on 3-d input domains.

Author	Target domain	Remark
Kia & Marquand (2019)	Detecting psychiatric disorder biomarkers in clinical fMRI scans	Leverages a tensor Gaussian predictive process (Kia et al., 2018) framework to formulate the spatially structured mixed-effects in functional magnetic resonance imaging (fMRI) data as stochastic processes. Latent variable NPs are then applied to achieve the normative modeling (Marquand et al., 2016) of these.
Heo et al. (2020)	Interactive Attention Learning (IAL) for improving interpretability of neural networks	Proposes the IAL framework for generating cost-effective attention guided by an active human-in-the-loop correction of a neural network’s attention interpretations. Exploits latent variable NPs that learn a latent summary of the context set whose human-generated attention annotations are given and feeds the summary to an attention generating network in addition to the time and feature-wise attentive encodings.
Sinitisin et al. (2020)	Editable training of neural networks to correct mistakes	Propose adding condition vectors to intermediate activations of CNPs to reduce the effect of catastrophic forgetting in editable training by minimizing the KL divergence between the predictions of original and edited models.
Vaughan et al. (2021)	Statistical downscaling of climate model outputs	Exploits ConvCNPs to address the limitations of existing statistical multi-site downscaling methods, namely training on off-the-grid climate data, predicting on arbitrary locations including the ones unseen during training, and using sub-grid-scale topographic information for final predictions.
Wichern et al. (2021)	Unsupervised detection of anomalous machine sounds	Uses ANPs to define priors over log mel spectrograms of normal sounds thus bypassing the need for pre-specified masked regions (Suefusa et al., 2020) over these. The anomaly scores of frames and frequencies are proportional to the model’s difficulty of reconstructing them.
Wang et al. (2021c)	Fake news detection for emergent events with few verified posts	Points out the limitation of ANPs using soft-attention-based weighted averaging of context for trimming irrelevant data in class imbalanced fake news context sets. Proposes employing a hard-attention mechanism (Jang et al., 2017) that can instead select the context point most related to a query.
Xue et al. (2022)	Predictive autoscaling of computing resources in the cloud	Employs ANPs to meta learn the unit workload to CPU utilization mapping in a model-based reinforcement learning setting that seeks the optimal numbers of virtual machines in the cloud to maintain the CPU utilization is at a target level.
Wu et al. (2022)	Multi-fidelity surrogate modeling of epidemiology and climate modeling tasks	Leverages latent NPs to build Multi-fidelity Hierarchical Neural Processes (MF-HNP) that learns the joint distribution of high and low-fidelity outputs. MF-HNP fuses data with varying input and output dimensions at different fidelity levels. Training involves inferring two latent variables, one for each fidelity level instead of the global z .
Wang et al. (2022b)	Semi-supervised image classification of unlabeled points conditioned on labeled ones	Uses a combination of conditional and latent neural processes for incrementally obtaining noise-free predictions on unlabeled target points. A highlight of the work is its realistic test setup – the NPs store training examples in memory banks and use these as context while testing.

Table 2: A summary of budding application domains of the NPF research that host relatively sparse research.

6 Experiments: Modeling functions with NPs

In this section, we discuss the range of tasks that can be targeted using the Neural Process family. In particular, we categorize the tasks where the continuous bounded function $f : \mathcal{X} \times \mathcal{Y}$ modeling the ground truth stochastic process can be a function of one ($\mathcal{X} \in \mathbb{R}$), two ($\mathcal{X} \in \mathbb{R}^2$), or three ($\mathcal{X} \in \mathbb{R}^3$) dimensional inputs. For empirical affirmation, we conduct experiments on a representative task of each such category

Application	Dataset	First usage	Dimensions	Size	Continuum
Image completion	MNIST (LeCun et al., 1998)	Garnelo et al. (2018a)	2-d		Spatial
	CelebA (Liu et al., 2015)		2-d		Spatial
	EMNIST (Cohen et al., 2017)	Lee et al. (2020b)	2-d		Spatial
Higher dimensional image completion	SVHN (Netzer et al., 2011)	Gordon et al. (2020)	2-d		Spatial
	Zero Shot Multi MNIST		2-d		Spatial
	Rotating MNIST (Casale et al., 2018)	Norcliffe et al. (2021)	3-d		Spatio-temporal
One-shot classification	Synthetic bouncing ball (Sutskever et al., 2008)	Ye & Yao (2022)	3-d		Spatio-temporal
	Omniglot (Lake et al., 2015)		2-d	32,460	Spatial
Bandit formulation of paraphrase identification	Quora Question Pairs ⁴⁰	Weber et al. (2018)		400,000	Text
	MSR corpus (Dolan et al., 2004)			5,800	Text
Predator-Prey population modeling	Hudson’s Bay hare-lynx data (Goel et al., 1971)	Gordon et al. (2020)			
Photometric time series modeling	PLAsTiCC (Allam Jr et al., 2018)	Gordon et al. (2020)	2-d	3,500,734	Temporal
User cold-start recommendation	MovieLens-1M ⁴¹				
	Last.FM ⁴²	Lin et al. (2021)			Text
Traffic speed modeling	Gowalla (Cho et al., 2011)			16,937,179	
	PEMS-BAY (Wu et al., 2019)	Yoo et al. (2021)		7,245,000	
Noisy time series modeling	METR-LA (Jagadish et al., 2014)				
	AFDB (Moody, 1983)		2-d		Temporal
	IMS Bearing (Qiu et al., 2006)	Kallidromitis et al. (2021)	2-d		Temporal
Geographical precipitation modeling	Urban8K (Salamon et al., 2014)		2-d	8,732	Temporal
	ERA5-Land (Muñoz-Sabater et al., 2021)	Foong et al. (2020)	3-d		Spatio-temporal
Physics-informed modeling	Cart-Pole simulator (Gal et al., 2016)	Wang & Van Hoof (2020)		Variable	
Graph data modeling	Graph benchmark datasets (Kersting et al., 2016)	Carr & Wingate (2019)		Variable	Graphs
	Cora (McCallum et al., 2000)			2,708 nodes	Graphs
Graph link prediction	Citeseer (Giles et al., 1998)	Liang & Gao (2021)		3,327 nodes	Graphs
	PubMed (Sen et al., 2008)			19,717 nodes	Graphs
Point cloud part labeling	ShapeNet (Chang et al., 2015)	Day et al. (2020)	3-d		Spatial
Continual Learning	Split-MNIST (Zenke et al., 2017), Split-CIFAR100 (Chaudhry et al., 2018)	Requeima et al. (2019)	2-d		Spatial
	Flowers (Nilsback & Zisserman, 2008), Omniglot (Lake et al., 2015)	Requeima et al. (2019)	2-d		Spatial

Table 3: Table showing the diversity of applications, their associated datasets, and their first usage in the context of Neural Processes.

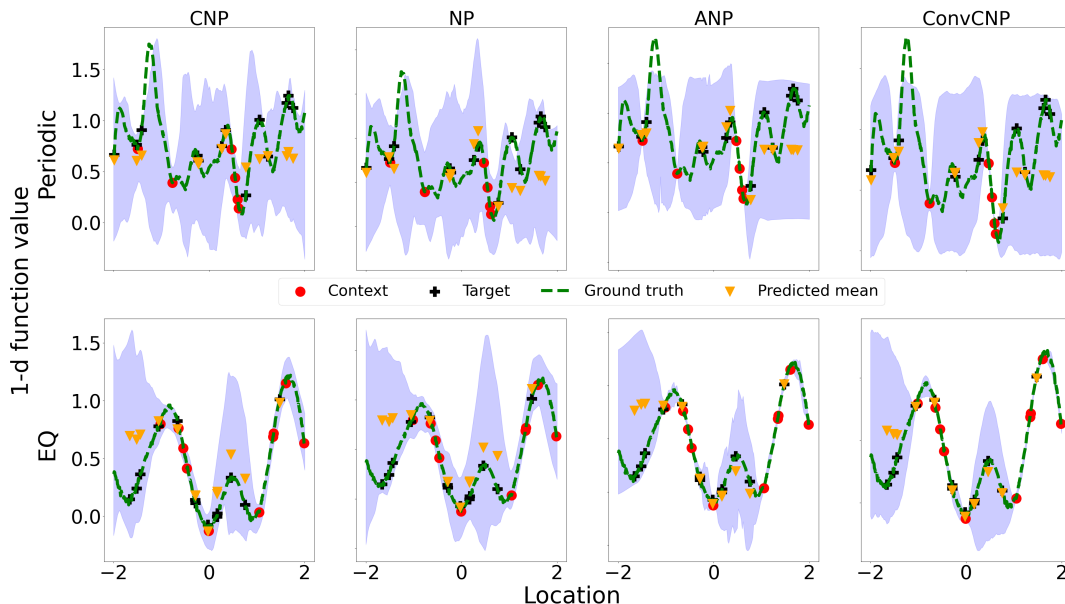


Figure 9: The mean and variance of the CNP, the NP, the ANP, and the ConvCNP on the 1-d regression task of predicting the values at the target locations of a ground truth Gaussian process (dashed green lines) based on periodic (top row) and EQ (bottom row) kernels.

using baseline Neural Process variants and discuss the implications of the results. On 1d and 2d inputs, we leverage the previously established regression frameworks for our experiments. On 3d inputs, our work marks the first step to show the results of ShapeNet part labeling using Neural Processes. Our experiments further demonstrate the plug-and-play characteristic of the Neural Process framework using a variety of deep learning architectures. Finally, it is worth highlighting the fact that our motivation behind the experiments in this section remains pointing out the nature of tasks that NPs can address rather than benchmarking their performances.

6.1 1-d function modeling

To show a 1-d input modeling task, we first generate two datasets using GPs with a static exponential quadratic (EQ) and a periodic kernel. We then employ Neural Processes to regress the value of these kernel functions at the locations provided. To do so, we train our models by sampling a curve from the GP with a variable number of context and target points. Each model is trained for $2e^5$ iterations. For evaluation, we interpolate the models by randomly choosing the number of context points in the range $[5, 20]$ while fixing the number of target points at 13. Following the standard evaluation protocol for regression tasks, we use the negative log likelihood (NLL) loss to report the predictive log-likelihood and mean squared error (MSE) to report the reconstruction error of the models.

Table 4 shows the mean and standard deviation of the NLL and MSE of the four most commonly used Neural Process variants: the CNP (Garnelo et al., 2018a), the NP (Garnelo et al., 2018b), the ANP (Kim et al., 2019), and the ConvCNP (Gordon et al., 2020) on the in-domain target set of data generated by the EQ and periodic kernels. A noteworthy point is the suboptimal performances of the NP compared to the CNP given that the former learns to estimate the variance in the latent space instead of the output space. Furthermore, inducing shift equivariance bias can be seen to favor ConvCNP even on the in-domain target points.

Model	EQ		Periodic	
	NLL	MSE	NLL	MSE
CNP	1.11 ± 0.47	0.0204 ± 0.021	0.199 ± 0.248	0.052 ± 0.022
NP	1.087 ± 0.426	0.02 ± 0.019	0.172 ± 0.214	0.052 ± 0.02
ANP	1.108 ± 0.44	0.0195 ± 0.021	1.047 ± 0.585	0.032 ± 0.023
ConvCNP	2.44 ± 0.867	0.01 ± 0.018	1.41 ± 0.77	0.027 ± 0.024

Table 4: Mean and standard deviation (over 5 runs) of log likelihood and reconstruction error on the 1-d regression tasks for exponential and periodic function families.

A visualization of the predicted mean and variances in Figure 9 shows that while all the models fit the periodic data with higher variances, the EQ kernel in particular favors ConvCNP and ANP with smoother predictive curves implying enhanced predictive correlation modeling, *i.e.*, proximity in the input space in such case is reflected in the output space. Both attention as well as shift equivariance biases are thus helpful at improving the predictive correlation of the models. More detailed experiments with 1-d input data can include evaluating the models on out-of-domain target set as well as on the datasets generated by other kernel functions (Gordon et al., 2020).

Model	MNIST	CelebA-32
CNP	2062.849	2559.732
NP	-2175.749	1508.08
ANP	2507.989	5238.15
GBCoNP	2743.51	5315.59

Table 5: Test set log likelihood scores for image completion on MNIST and CelebA-32 datasets after 50 training epochs: we use the pretrained weights of Dubois et al. (2020) for the CNP, the NP, and the ANP, and that of Wang et al. (2021b) for GBCoNP, *i.e.*, the latent variant of ConvCNP.

6.2 2-d function modeling

For inputs location in 2-d space, we consider using Neural Process variants to model the visually intelligible outputs of continuous bounded functions f guiding the process of RGB and grayscale image pixel generation. Following the notion of Garnelo et al. (2018a), modeling image completion amounts to learning the mapping f between the 2-d input coordinates and their respective output intensities I , *i.e.*, $I = [0, 1]$ for grayscale and $I = [0, 1]^3$ for RGB images.⁴³ We subsequently employ the MNIST handwritten digit (LeCun et al., 1998) and the CelebA dataset (Liu et al., 2015) to cover our cases for grayscale and RGB ranges. We use the same four Neural Process variants as in 1-d regression task except for ConvCNPs which we replace with its latent variable counterpart GBCoNP (Wang et al., 2021b) for crisper visualizations. We leverage the pretrained weights of Dubois et al. (2020) for the CNP, the NP, and the ANP, and that of Wang et al. (2021b) for the GBCoNP.⁴⁴ Table 5 reports the test set log likelihood scores for each model after 50 training epochs.

We visualize the predictive mean and variances of each model by randomly selecting 5%, 10%, and 50% of the total image pixels as the observed context points and providing the locations of the entire image pixels (including the context) as targets. As shown in Figure 10, the mean predictions of each model on both the datasets become less blurry with an increase in the context sizes. In the particular case of Celeb-A dataset with a majority of female faces, the CNP with a lack of latent sampling has its mean predictions resemble closely to the average of all the faces, *i.e.*, more feminine attributes. In terms of variances, an increase in context leads to smoothing of the edges and boundaries that the model is initially more uncertain of.

⁴³For intuition, imagine an image lying on a 2-d surface. Image completion involves learning a function whose domain consists of all the pixel coordinates and the range involves all of pixel intensities. Once the NP has learned such a function, it can be queried with a given subset or all of the pixel locations of the image to predict their respective intensities.

⁴⁴<https://github.com/xuesongwang/global-convolutional-neural-processes>

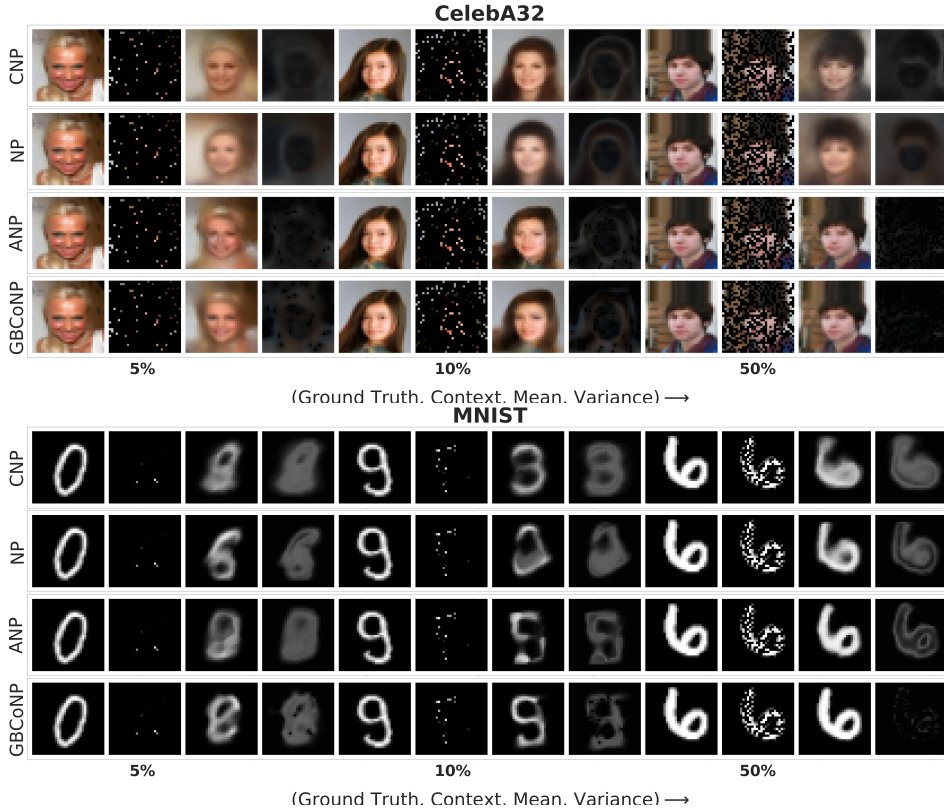


Figure 10: Predictive mean, and variances of CelebA 32×32 (top) and MNIST 28×28 (bottom) images with three different context settings amounting to 5, 10, and 50% of the total image pixels. Increasing the number of context locations can be seen to decrease the predictive variance.

The variances are more pronounced on MNIST where a context of 5% implies insufficient information and hence, all the models have higher variances throughout the plausible digit surface area. GBCoNP, with more smoothed boundaries on larger context sizes, can be seen to be the most efficient in terms of utilizing the amount of available observation.

To emphasize the role of latent distribution in capturing global uncertainty, we experiment with drawing samples that are coherent with the observations. To do so, we fix the number of context points and show how latent variable models, namely the NP and the ANP can exploit the covariance between these as well as the target points to generate a range of predictions that are equally justifiable to the context. Figure 11 shows a few such coherent samples for the models on the CelebA and MNIST datasets. It is worth noting that the deterministic nature of the CNP limits it from generating such coherent possibilities. In the lack of a latent distribution, sampling from the CNP will amount to mere noises added on top of the model’s mean predictions. Lastly, for a list of further possible 2d modeling tasks and datasets, we refer the reader to Table 3.

6.3 3-d function modeling

To demonstrate an application of NPs for modeling processes involving 3d inputs, we tackle the problem of part segmentation on ShapeNet part dataset (Yi et al., 2016). By opting for part labeling, we also intend to show the application of the NPF for classification tasks. The ShapeNet part dataset hosts 50 such part labels on 16,881 3d point clouds belonging to 16 categories of objects. Each label is semantically consistent across the shapes of a category. We adhere to the official train-validation-test split (Chang et al., 2015). Our architecture for Neural Process involves incorporating a graph neural network, namely the dynamic graph CNN (DGCNN) (Wang et al., 2019b). The input setting follows the segmentation task convention: a

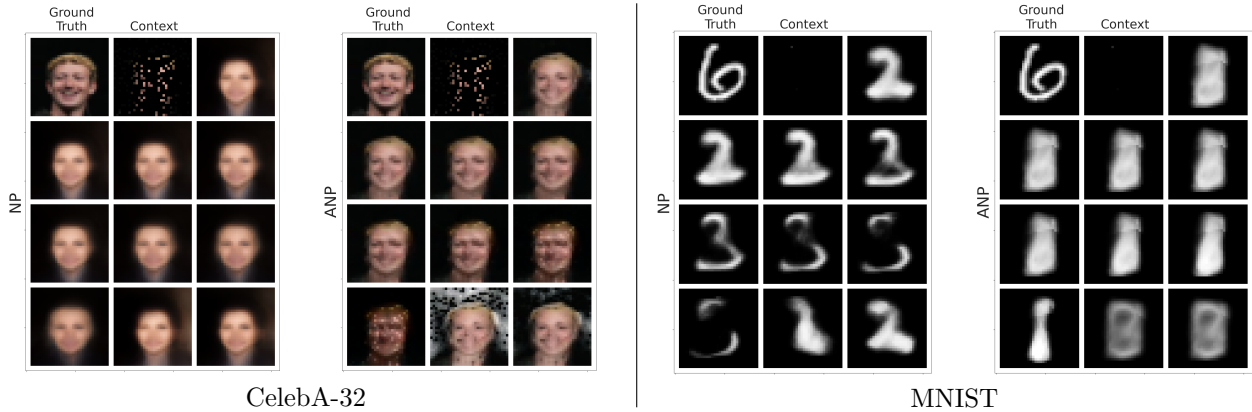


Figure 11: 4×3 grids depicting the variation in predictive means of the NP and the ANP over 10 distinct priors on CelebA-32 (left) and MNIST (right) context points, each prior is a sampled latent variable. For reference, the first two images of each grid represent the ground truth and the context, respectively.

list of coordinate locations/features (x, y, z) capturing the local geometry of a object and an 1d categorical descriptor of the object for the cloud’s global representation. Given the part labels of the context set, the goal is to predict the target set labels as well as uncertainties within the same cloud.

We tailor the original architecture of DGCNN into the encoder and decoder modules to adhere to the NPF tradition. The encoder extracts the coordinate features of the context set with edge convolutions. The resulting vector after max-pooling becomes the global representation of the cloud object. In the CNP scenario, we can utilize this representation as the functional prior to decode labels for the target set, whereas such functional prior becomes a distribution in the case of latent models. By minimizing the distributional discrepancies between the context set and the target sets, we enable the tractability of the latent representations. Our decoder incorporates three inputs to present the final prediction: the global representation from the encoder, the intermediate features extracted from the target set through edge convolutions and the categorical descriptor. We modify the final deterministic layer into a Bayesian linear layer (BLL) with the weights and biases having their corresponding means and variances. The prediction is then obtained by sampling the weights and biases from the BLL and calculating the standard cross-entropy loss using these. According to the reparameterization trick (Kingma et al., 2015), the uncertainty can be formalized by passing the last hidden layer with the variance of the BLL weights and biases.

Extending NPs to classification setting amounts to equation 6 defining a categorical distribution instead of a Gaussian distribution (Lukasiewicz & Wang, 2022). Our training objective thus involves minimizing the loss function \mathcal{L} being a linear combination of three components: the categorical cross entropy loss \mathcal{L}_{CE} with label smoothing (Wang et al., 2019b), the normalization of the Bayesian linear layer (\mathcal{L}_{BKLL}) and in the case of the latent models, the KL divergence between the prior and posterior distributions (\mathcal{L}_{KL}):

$$\mathcal{L} = \mathcal{L}_{CE} + \mathcal{L}_{KL} + 0.01 * \mathcal{L}_{BKLL} \quad (48)$$

Considering the memory requirements, we fix the number k of nearest neighbors for dynamic edge convolutions to be 40 during training. We randomly select 30% of point locations as the context set from a total of 512 points in a cloud during training. The remaining points in the same cloud form the target set for prediction. For testing, we sample 1024 points and split these into various context sizes while keeping the entire samples for prediction. Additionally, we ensure that the test-time context set spans all possible labels in the cloud by selecting these through label-wise stratified random sampling. This accounts for the scenarios involving possible forgetting of non-dominant classes by the network due to the categorical imbalances among the 3d points (He et al., 2020). Following Wang et al. (2019b), we use a batch size of 32 for training and 16 for testing.

The mean and variance of the DGCNN-based CNP and NP models based on 1% context, *i.e.*, 10 observed points across 5 different categories, namely chair, table, airplane, guitar, and lamp are shown in Figure

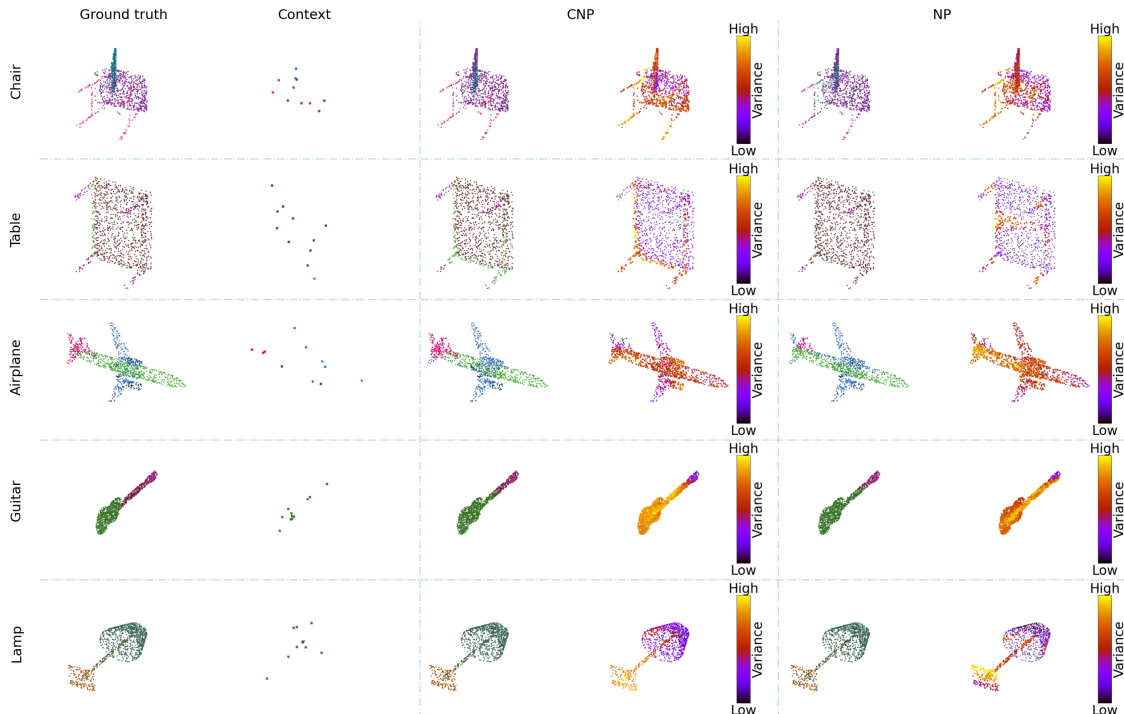


Figure 12: Visualization of part labeling on the ShapeNet part dataset. Each shape depicts 1024 sampled points which form (from left to right): ground truth part labels, 1% context labels, and mean and variance of the DGCNN-based CNP and NP predictions. For better visibility: (i) the size and color of the points have been used to denote uncertainties, (ii) the context label points have been magnified and might differ in spatial alignment with the rest of the shapes.

12. Both the CNP and the NP output more uncertain predictions for points lying at the junctions and boundaries within the shapes. Overall, the CNP can be seen to produce more accurate overall predictions than the NP. The superior prediction results of the CNP is further highlighted in Table 6(a) where we compare it against NP in terms of three evaluation metrics: the standard overall accuracy (OA), the mean class accuracy (MCA) computed as the ratio of sum of accuracy for each part predicted to the number of parts, and the mean-Intersection-over-Union (mIoU) score computed as the average of the ratio of overlap, *i.e.*, the true positive score to the union, *i.e.*, the sum of true positive, false positive and false negative scores for each part. The superior predictive performance of the CNP is in line with the previous works (Garnelo et al., 2018a;b) as its latent variant was originally introduced to allow the sampling of different coherent predictions that align with the provided context. However, in the context of classification, such sampling does not carry any intuition.

Given that the DGCNN-based architecture could endow NPs with strong inductive biases to discover the neighborhood structure of points, it could be the case that the predictive performance of NPs have little to do with the observations. In order to study the importance of the provided context, we ablate the performance of the CNP model by varying the context sizes. In particular, we allow the CNP to take into account a subtotal of 0.1%, 0.5%, 1%, 5%, 10%, 30%, and 50% of the sampled points amounting to 1, 5, 10, 51, 102, 307, and 512 context points, respectively. The number of nearest neighbors k for the former three settings are fixed at 1, 4, and 8, respectively while keeping $k = 40$ for the others. The ablation results are shown in table 6 (b). We observe that the amount of observation provided greatly affects the performance of the model across all three metrics. For instance, on the mIoU metric that is commonly used to evaluate segmentation performances, varying context sizes from 0.1% to 50% can help achieve a gain of roughly 32 points.

The visualizations corresponding to the CNP’s uncertainties with varying amount of context are shown in Figure 13. As the proportion of the context provided increases from 1% to 10%, the model can be seen to

Model	MCA	OA	mIoU	Metric	0.1%	0.5%	1%	5%	10%	30%	50%
CNP	42.103	68.705	46.388	MCA	42.103	45.437	47.647	61.899	63.883	64.624	64.678
NP	38.823	63.247	37.645	OA	68.705	73.445	76.061	88.140	90.040	90.987	90.762
				mIoU	46.388	48.541	51.589	71.894	75.907	78.195	78.348

(a)

(b)

Table 6: Mean class accuracy (MCA), overall accuracy (OA), and mean-Intersection-over-Union (mIoU) scores of part labeling on the ShapeNet test set based on 1024 sampled points: Table (a) compares the metrics for the CNP and the NP by fixing the context size to 1% of the total points, Table (b) compares the performance of the CNP by varying the context sizes.

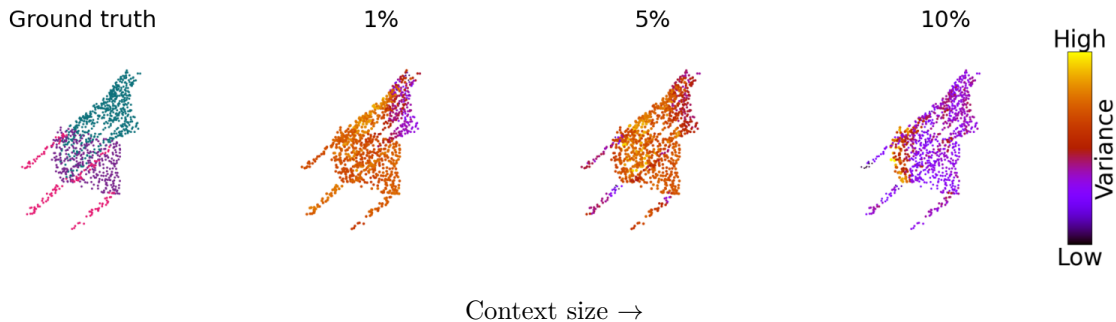


Figure 13: Visualization of the predictive uncertainties of the CNP for part labeling of the point cloud of a chair with varying context sizes. The sizes and colors of the points correspond to uncertainties: larger sizes towards yellow end of the spectrum denote a higher predictive variance.

be more certain about its predictions of parts such as rails, seat, stiles, and legs of the chair. As the number of context points provided reached 10% of the total cloud size, only the predictions for the boundary points lying along the rear apron suffer from higher uncertainties. On the other hand, a context size of 1% of the total points makes the model uncertain in its predictions for all but the top rail part. As with 1d and 2d cases, we refer the reader to Table 3 for more applications of Neural Processes to 3d function modeling.

7 Future Research Directions

The domain of uncertainty-aware deep modeling of stochastic processes carries a huge potential for improvement despite the effectiveness of the current Neural Process variants over static kernel-based Gaussian processes. In this section, we outline some of the major issues faced by the contemporary NPF branches and highlight the directions for further research.

Cost-efficient generalization. The balance between resource efficiency and generalizability has been among the most studied trade-offs for improving the scalability and ubiquity of deep learning models. In terms of Neural Processes, the identification of underfitting due to the mean aggregation step Kim et al. (2019) led to a number of follow-up works adding up the computational costs by considering mechanisms such as self-attention as a get around – for instance, Yoon et al. (2020) improving upon sequential NPs (Singh et al., 2019). Self-attention, in turn, can result in the memory and time complexity grow quadratically with the number of input points hence deeming the application of these to be unsuitable for high dimensional inputs (Gordon et al., 2020).

One efficient solution to attention-based generalizability could be applying restricted attention mechanisms (Beltagy et al., 2020) or inducing points methods (Wu et al., 2021) that scale linearly with sequence length. Using locality-sensitive hashing (Zandieh et al., 2020) and KD-trees (Shen et al., 2005) can further help bringing the cost down to the order of logarithmic scales of the sequence length. Moreover, as a low cost

alternative to avoiding underfitting, it can be plausible to leverage the recent findings in data-efficient meta-learning to the NP family. For instance, we expect to see the amount of supervision required by NPs to attain a desired level of generalization in the samples of the learned predictive distribution (Sun et al., 2021; Al-Shedivat et al., 2021).

Another promising direction for scalable generalization in NPs could be enhancing the latent variable representation using more flexible equivariant transformations (Holderrieth et al., 2021; Kawano et al., 2021) over the context for instance. Such group equivariances can in turn be efficiently scaled to higher dimensions by opting for techniques such as group equivariant subsampling operations Xu et al. (2021). On a similar note, scalability and accuracy can be jointly achieved by making the traditional gaussian processes fast enough to be incorporated in NPs for more accurate predictions on higher dimensional data. Motivation for this can be borrowed from flexible GP inference techniques such as stochastic inference networks (Shi et al., 2019).

Improved set representations. Current state-of-the-art NP variants rely either on 1 or 2-order permutation instantiations of the Janossy pooling mechanism (see Section 2.2). As such, efficient inducing of higher degree input relational reasoning into the models remains an active area of research. For example, NPs could be applied to encode all $N!$ permutations of the context set and average only over randomly sampled subset $k \ll N!$ of encodings to get a more fair estimate of the exact permutation invariant representation (Murphy et al., 2019). Alternately, an adversary could be used to find out permutations with maximum loss values such that the resulting NP training objective will amount to computing permutation-invariant representation that minimizes the adversarial impact (Pabbaraju & Jain, 2019). An advanced step along this direction will be to consider applications modeling the distribution of sets where each element is associated with its own symmetry, for example, sets of 3-d point clouds, graphs, etc. (Maron et al., 2020). Similarly, alternate choices for aggregation functions could be explored given that the performance of Deep Set networks remain highly sensitive to these (Soelch et al., 2019).

Better function priors. Given that NPs posit a prior directly over the functional space occupied by the neural networks and that such priors might not always hold for deeper architectures, improving the function priors can serve as a key enabler for a full Bayesian treatment of Neural Processes. To this end, potential directions remain imposing manifold structure on the latent distribution (Falorsi et al., 2019), using the interpretable priors of GPs as a reference to match with (Tran et al., 2021), and meta-learning of the priors (Harrison et al., 2018).

Likelihood-free density estimation. Modeling the conditional predictive distribution $p(f(T)|T, C)$ requires NPs (and GPs) to rely on an explicit likelihood assumption for p . While the assumption works fine for low dimensional target points, modeling complex higher dimensional predictive distributions using explicit likelihoods require learning magnitudes of greater parameters. This in turn leads to posterior beliefs being biased (Havasi et al., 2018).⁴⁵ Avoiding such biased posterior belief can require the sampling procedure to be sequential which adds computational costs. Using the sampling of high-dimensional images as an example, avoiding biased posterior means switching to the computationally challenging task of conditional image generation (Chrysos & Panagakis, 2021).

In order to efficiently recover the unbiased posterior belief, recent works have studied alternatives in the context of both GPs and NPs. In case of deep GPs, Yu et al. (2019) formulate performing implicit posterior variational inference by searching for a Nash equilibrium while in case of CNPs, Mathieu et al. (2021) consider doing away with pixel-perfect reconstruction and instead use self-supervised contrastive learning of the context samples. However, there still remains a large room for improving the cost/data efficiency of such techniques.

Distribution-free uncertainty quantification. Given their ability to produce confidence sets guaranteeing the user-specified probability of marginal coverage of ground truth labels, distribution-free uncertainty quantification (UQ) Angelopoulos & Bates (2021) techniques have been seeing a gain in popularity over the

⁴⁵Most common choice for p posits a Gaussian likelihood assumption. Modeling the higher dimensional predictive distributions using such p then leads to *biased* non-Gaussian posterior beliefs.

recent years. In addition to the minimal overhead of conformal prediction based on a small amount of calibration data, obtaining such UQ remains independent of the model and the underlying data distribution. Coupling distribution-free UQ with Neural Processes can thus provide a more promising approach to uncertainty estimation and hypothesis testing in the light of noisy observations by minimizing the reliance upon assumptions of the true underlying function (Csáji & Kis, 2019).

Implementation-specific advances. For tasks involving long-tail distributions of the ground truth data generating processes (such as imbalanced classification), the selection of context points during training can greatly affect the performance of the NPs. While a better measure to further evaluate the robustness of NPs can be to train these on different context and target set sizes (Le et al., 2018), such a criteria seems computationally demanding. The NP research community should therefore prioritize evaluating the robustness of their models to the quality of the training context points besides the context and target distributions. A feasible motivation for such an objective can be drawn from other order-sensitive deep learning domains such as exemplar-based continual learning (Jha et al., 2021) wherein the performance of a model is often reported in terms of: (i) different exemplar-selection criteria such as random and herding (Rebuffi et al., 2017), (ii) an average over multiple runs to mitigate the bias arising from the selection of exemplars pertaining to specific task orders.

Application-specific advances. While Neural Processes are often presented in the context of regression (and classification formulated as regression), they can also be adapted for different purposes like model-peeling (Fang et al., 2021) and hypothesis testing. Modeling the processes underlying robust real-world applications such as hand-eye calibration in robot learning tasks could be a challenging yet promising domain where Neural Processes can enable long-term research.

8 Conclusion

In this survey, we provided a comprehensive overview of the recent advances in the Neural Process family for modeling ground truth data generating stochastic processes. We first laid the foundations of Neural Processes and related it to a number of contemporary advances in other deep learning domains – with a special focus on the Janossy pooling operations that govern how the Neural Processes represent the input sets. We introduced a classification scheme that encompasses the up-to-date fundamental research in the domain. We then followed up by summarizing a number of key domains that Neural Processes have been actively applied to. To the end goal of depicting a clearer picture of the empirical frameworks under which Neural Processes can be employed, we carried out a number of representative experiments for 1-d, 2-d and 3-d data generating functions using some established Neural Process architectures. Specifically, we developed a novel NP-based 3-d point cloud segmentation model for the cases with a partially labeled context set to validate the feasibility and effectiveness of NPs in modeling the 3-d data. Lastly, we pointed a few promising research directions that could help overcome the existing limitations of Neural Processes. With a systematic listing of the progress in the family, we hope this survey serves as an introductory material for readers from the academia and the industry, and accelerates the pace of research in the field.

References

- Neil Abcouwer, Shreyansh Daftry, Tyler del Sesto, Olivier Toupet, Masahiro Ono, Siddarth Venkatraman, Ravi Lanka, Jialin Song, and Yisong Yue. Machine learning based path planning for improved rover navigation. In *2021 IEEE Aerospace Conference (50100)*, pp. 1–9. IEEE, 2021. 1
- Idris Ahmed, Goni Umar Modu, Abdullahi Yusuf, Poom Kumam, and Ibrahim Yusuf. A mathematical model of coronavirus disease (covid-19) containing asymptomatic and symptomatic classes. *Results in physics*, 21:103776, 2021. 43
- Maruan Al-Shedivat, Liam Li, Eric Xing, and Ameet Talwalkar. On data efficiency of meta-learning. In *International Conference on Artificial Intelligence and Statistics*, pp. 1369–1377. PMLR, 2021. 53

-
- Tarek Allam Jr, Anita Bahmanyar, Rahul Biswas, Mi Dai, Lluís Galbany, Renée Hložek, Emille EO Ishida, Saurabh W Jha, David O Jones, Richard Kessler, et al. The photometric lsst astronomical time-series classification challenge (plasticc): Data set. *arXiv preprint arXiv:1810.00001*, 2018. 46
- Anastasios N Angelopoulos and Stephen Bates. A gentle introduction to conformal prediction and distribution-free uncertainty quantification. *arXiv preprint arXiv:2107.07511*, 2021. 53
- Antreas Antoniou, Harrison Edwards, and Amos Storkey. How to train your MAML. In *International Conference on Learning Representations*, 2019. URL <https://openreview.net/forum?id=HJGven05Y7>. 11
- Martín Arjovsky, Soumith Chintala, and Léon Bottou. Wasserstein gan. *ArXiv*, abs/1701.07875, 2017. 15
- Dzmitry Bahdanau, Kyung Hyun Cho, and Yoshua Bengio. Neural machine translation by jointly learning to align and translate. In *3rd International Conference on Learning Representations, ICLR 2015*, 2015. 16
- Iz Beltagy, Matthew E Peters, and Arman Cohan. Longformer: The long-document transformer. *arXiv preprint arXiv:2004.05150*, 2020. 52
- Rianne van den Berg, Thomas N Kipf, and Max Welling. Graph convolutional matrix completion. *arXiv preprint arXiv:1706.02263*, 2017. 20
- YK Bharath. Ieee 14 bus system simulink model. *MATLAB Central File Exchange*, 2020. URL <https://www.mathworks.com/matlabcentral/fileexchange/46067-ieee-14-bus-system-simulink-model>. 41
- Mickael Binois and Nathan Wycoff. A survey on high-dimensional gaussian process modeling with application to bayesian optimization. *arXiv preprint arXiv:2111.05040*, 2021. 70
- Benjamin Bloem-Reddy and Yee Whye Teh. Probabilistic symmetries and invariant neural networks. *J. Mach. Learn. Res.*, 21:90–1, 2020. 11
- Martin Bock, Amit Kumar Tyagi, Jan-Ulrich Kreft, and Wolfgang Alt. Generalized voronoi tessellation as a model of two-dimensional cell tissue dynamics. *Bulletin of mathematical biology*, 72(7):1696–1731, 2010. 23
- Samuel Bowman, Luke Vilnis, Oriol Vinyals, Andrew Dai, Rafal Jozefowicz, and Samy Bengio. Generating sentences from a continuous space. In *Proceedings of The 20th SIGNLL Conference on Computational Natural Language Learning*, pp. 10–21, 2016. 33
- Eric Brochu, Vlad M Cora, and Nando De Freitas. A tutorial on bayesian optimization of expensive cost functions, with application to active user modeling and hierarchical reinforcement learning. *arXiv preprint arXiv:1012.2599*, 2010. 32
- Wessel Bruinsma, James Requeima, Andrew Y. K. Foong, Jonathan Gordon, and Richard E Turner. The gaussian neural process. In *Third Symposium on Advances in Approximate Bayesian Inference*, 2021. URL <https://openreview.net/forum?id=rzsDn7Vzxf>. 13, 14, 29, 30
- Carlo Buontempo, Jean-Noël Thépaut, and Cédric Bergeron. Copernicus climate change service. In *IOP Conference Series: Earth and Environmental Science*, volume 509, pp. 012005. IOP Publishing, 2020. 28
- Ronald S Burt. A note on missing network data in the general social survey. *Social Networks*, 9(1):63–73, 1987. 24
- Andrew Carr and David Wingate. Graph neural processes: Towards bayesian graph neural networks. *arXiv preprint arXiv:1902.10042*, 2019. 14, 25, 46
- Andrew Carr, Jared Nielsen, and David Wingate. Wasserstein Neural Processes. In *Optimal Transport and Machine Learning Workshop at the Conference on Neural Information Processing Systems*, 2019. 14, 15

-
- Francesco Paolo Casale, Adrian Dalca, Luca Saglietti, Jennifer Listgarten, and Nicolo Fusi. Gaussian process prior variational autoencoders. *Advances in neural information processing systems*, 31, 2018. 46
- Sergio Casas, Cole Gulino, Simon Suo, Katie Luo, Renjie Liao, and Raquel Urtasun. Implicit latent variable model for scene-consistent motion forecasting. In *European Conference on Computer Vision*, pp. 624–641. Springer, 2020. 1
- Ankush Chakrabarty, Gordon Wichern, and Christopher Laughman. Attentive neural processes and batch bayesian optimization for scalable calibration of physics-informed digital twins. In *ICML workshop on Tackling Climate Change with Machine Learning*, 2021. 43
- Angel X Chang, Thomas Funkhouser, Leonidas Guibas, Pat Hanrahan, Qixing Huang, Zimo Li, Silvio Savarese, Manolis Savva, Shuran Song, Hao Su, et al. Shapenet: An information-rich 3d model repository. *arXiv preprint arXiv:1512.03012*, 2015. 44, 46, 49
- Arslan Chaudhry, Puneet K Dokania, Thalaiyasingam Ajanthan, and Philip HS Torr. Riemannian walk for incremental learning: Understanding forgetting and intransigence. In *Proceedings of the European Conference on Computer Vision (ECCV)*, pp. 532–547, 2018. 37, 46
- Mingyang Chen, Wen Zhang, Wei Zhang, Qiang Chen, and Huajun Chen. Meta relational learning for few-shot link prediction in knowledge graphs. In *Proceedings of the 2019 Conference on Empirical Methods in Natural Language Processing and the 9th International Joint Conference on Natural Language Processing (EMNLP-IJCNLP)*, pp. 4217–4226, 2019. 25
- Ricky TQ Chen, Yulia Rubanova, Jesse Bettencourt, and David K Duvenaud. Neural ordinary differential equations. *Advances in neural information processing systems*, 31, 2018. 35, 43, 44
- Ruijie Chen, Ning Gao, Ngo Anh Vien, Hanna Ziesche, and Gerhard Neumann. Meta-learning regrasping strategies for physical-agnostic objects. *arXiv preprint arXiv:2205.11110*, 2022. 44
- Ting Chen, Simon Kornblith, Mohammad Norouzi, and Geoffrey Hinton. A simple framework for contrastive learning of visual representations. In *International conference on machine learning*, pp. 1597–1607. PMLR, 2020. 39, 40
- Xi Chen, Diederik P. Kingma, Tim Salimans, Yan Duan, Prafulla Dhariwal, John Schulman, Ilya Sutskever, and Pieter Abbeel. Variational lossy autoencoder. In *International Conference on Learning Representations*, 2017. URL <https://openreview.net/forum?id=BysvGP5ee>. 21
- Eunjoon Cho, Seth A Myers, and Jure Leskovec. Friendship and mobility: friendship and mobility: user movement in location-based social networks. In *User Movement in Location-Based Social Networks ACM SIGKDD International Conference on Knowledge Discovery and Data Mining (KDD)*, 2011. 46
- Sumit Chopra, Raia Hadsell, and Yann LeCun. Learning a similarity metric discriminatively, with application to face verification. In *2005 IEEE Computer Society Conference on Computer Vision and Pattern Recognition (CVPR'05)*, volume 1, pp. 539–546. IEEE, 2005. 38
- Grigorios G. Chrysos and Yannis Panagakis. Cope: Conditional image generation using polynomial expansions. *CoRR*, abs/2104.05077, 2021. URL <https://arxiv.org/abs/2104.05077>. 53
- Dan Claudiu Cireşan, Ueli Meier, Luca Maria Gambardella, and Jürgen Schmidhuber. Deep, big, simple neural nets for handwritten digit recognition. *Neural computation*, 22(12):3207–3220, 2010. 1
- Gregory Cohen, Saeed Afshar, Jonathan Tapson, and Andre Van Schaik. Emnist: Extending mnist to handwritten letters. In *2017 international joint conference on neural networks (IJCNN)*, pp. 2921–2926. IEEE, 2017. 46
- Taco S Cohen, Mario Geiger, and Maurice Weiler. A general theory of equivariant cnns on homogeneous spaces. *Advances in neural information processing systems*, 32, 2019. 23

-
- David A Cohn, Zoubin Ghahramani, and Michael I Jordan. Active learning with statistical models. *Journal of artificial intelligence research*, 4:129–145, 1996. 37
- Dorin Comaniciu and Peter Meer. Mean shift: A robust approach toward feature space analysis. *IEEE Transactions on pattern analysis and machine intelligence*, 24(5):603–619, 2002. 44
- John Conway et al. The game of life. *Scientific American*, 223(4):4, 1970. 23
- Ronald James Cotton, Fabian Sinz, and Andreas Tolias. Factorized neural processes for neural processes: K-shot prediction of neural responses. *Advances in Neural Information Processing Systems*, 33:11368–11379, 2020. 42
- Balázs Cs Csáji and Krisztián B Kis. Distribution-free uncertainty quantification for kernel methods by gradient perturbations. *Machine Learning*, 108(8):1677–1699, 2019. 54
- Iva Čvorović-Hajdinjak, Andjelka B Kovačević, Dragana Ilić, Luka Č Popović, Xinyu Dai, Isidora Jankov, Viktor Radović, Paula Sánchez-Sáez, and Robert Nikutta. Conditional neural process for nonparametric modeling of active galactic nuclei light curves. *Astronomische Nachrichten*, 343(1-2):e210103, 2022. 42
- Ben Day, Catalina Cangea, Arian R. Jamasb, and Pietro Liò. Message passing neural processes. *CoRR*, abs/2009.13895, 2020. URL <https://arxiv.org/abs/2009.13895>. 14, 25, 46
- Jia Deng, Wei Dong, Richard Socher, Li-Jia Li, Kai Li, and Li Fei-Fei. Imagenet: A large-scale hierarchical image database. In *2009 IEEE conference on computer vision and pattern recognition*, pp. 248–255. Ieee, 2009. 20
- Li Deng. The mnist database of handwritten digit images for machine learning research. *IEEE Signal Processing Magazine*, 29(6):141–142, 2012. 29
- Carl Doersch, Ankush Gupta, and Andrew Zisserman. Crosstransformers: spatially-aware few-shot transfer. *Advances in Neural Information Processing Systems*, 33:21981–21993, 2020. 39
- William Dolan, Chris Quirk, Chris Brockett, and Bill Dolan. Unsupervised construction of large paraphrase corpora: Exploiting massively parallel news sources. 2004. 46
- Alexey Dosovitskiy, Lucas Beyer, Alexander Kolesnikov, Dirk Weissenborn, Xiaohua Zhai, Thomas Unterthiner, Mostafa Dehghani, Matthias Minderer, Georg Heigold, Sylvain Gelly, Jakob Uszkoreit, and Neil Houlsby. An image is worth 16x16 words: Transformers for image recognition at scale. In *International Conference on Learning Representations*, 2021. URL <https://openreview.net/forum?id=YicbFdNTTy>. 20
- Yann Dubois, Jonathan Gordon, and Andrew YK Foong. Neural process family. <http://yanndubs.github.io/Neural-Process-Family/>, September 2020. 48
- Krishnamurthy Dvijotham, Marta Garnelo, Alhussein Fawzi, and Pushmeet Kohli. Verification of deep probabilistic models. In *Advances in Neural Information Processing Systems, SecML workshop*, 2018. 12
- Harrison Edwards and Amos Storkey. Towards a neural statistician. In *International Conference on Learning Representations*, 2017. URL <https://openreview.net/forum?id=HJDBUF51e>. 12
- Bradley Efron. Bootstrap methods: another look at the jackknife. In *Breakthroughs in statistics*, pp. 569–593. Springer, 1992. 31
- SM Ali Eslami, Danilo Jimenez Rezende, Frederic Besse, Fabio Viola, Ari S Morcos, Marta Garnelo, Avraham Ruderman, Andrei A Rusu, Ivo Danihelka, Karol Gregor, et al. Neural scene representation and rendering. *Science*, 360(6394):1204–1210, 2018. 9, 12
- Luca Falorsi, Pim de Haan, Tim R Davidson, and Patrick Forré. Reparameterizing distributions on lie groups. In *The 22nd International Conference on Artificial Intelligence and Statistics*, pp. 3244–3253. PMLR, 2019. 53

-
- Xinjie Fan, Shujian Zhang, Bo Chen, and Mingyuan Zhou. Bayesian attention modules. *Advances in Neural Information Processing Systems*, 33:16362–16376, 2020. 20
- Cong Fang, Hangfeng He, Qi Long, and Weijie J. Su. Exploring deep neural networks via layer-peeled model: Minority collapse in imbalanced training. *Proceedings of the National Academy of Sciences*, 118(43):e2103091118, 2021. doi: 10.1073/pnas.2103091118. URL <https://www.pnas.org/doi/abs/10.1073/pnas.2103091118>. 54
- Matthias Feurer, Jost Springenberg, and Frank Hutter. Initializing bayesian hyperparameter optimization via meta-learning. In *Proceedings of the AAAI Conference on Artificial Intelligence*, volume 29, 2015. 41
- Chelsea Finn, Pieter Abbeel, and Sergey Levine. Model-agnostic meta-learning for fast adaptation of deep networks. In *International conference on machine learning*, pp. 1126–1135. PMLR, 2017. 10, 11, 41, 42
- Marc Finzi, Samuel Stanton, Pavel Izmailov, and Andrew Gordon Wilson. Generalizing convolutional neural networks for equivariance to lie groups on arbitrary continuous data. In *International Conference on Machine Learning*, pp. 3165–3176. PMLR, 2020. 22, 23
- Edwin Fong and Chris C Holmes. On the marginal likelihood and cross-validation. *Biometrika*, 107(2): 489–496, 2020. 12
- Andrew Foong, Wessel Bruinsma, Jonathan Gordon, Yann Dubois, James Requeima, and Richard Turner. Meta-learning stationary stochastic process prediction with convolutional neural processes. *Advances in Neural Information Processing Systems*, 33:8284–8295, 2020. 10, 14, 15, 28, 30, 43, 46
- Yarin Gal, Rowan McAllister, and Carl Edward Rasmussen. Improving pilco with bayesian neural network dynamics models. In *Data-Efficient Machine Learning workshop, ICML*, volume 4, pp. 25, 2016. 46
- Constantino A Garcia, Abraham Otero, Paulo Felix, Jesus Presedo, and David G Marquez. Nonparametric estimation of stochastic differential equations with sparse gaussian processes. *Physical Review E*, 96(2): 022104, 2017. 43
- Marta Garnelo, Dan Rosenbaum, Christopher Maddison, Tiago Ramalho, David Saxton, Murray Shanahan, Yee Whye Teh, Danilo Rezende, and SM Ali Eslami. Conditional neural processes. In *International Conference on Machine Learning*, pp. 1704–1713. PMLR, 2018a. 2, 3, 4, 6, 7, 9, 10, 11, 13, 14, 15, 20, 30, 32, 40, 41, 43, 44, 46, 47, 48, 51
- Marta Garnelo, Jonathan Schwarz, Dan Rosenbaum, Fabio Viola, Danilo J Rezende, SM Eslami, and Yee Whye Teh. Neural processes. *arXiv preprint arXiv:1807.01622*, 2018b. 9, 13, 14, 16, 20, 27, 28, 32, 35, 47, 51
- Carles Gelada and Jacob Buckman. Bayesian neural networks need not concentrate. <https://jacobbuckman.com/2020-01-22-bayesian-neural-networks-need-not-concentrate/>, 2020. 2
- C Lee Giles, Kurt D Bollacker, and Steve Lawrence. Citeseer: An automatic citation indexing system. In *Proceedings of the third ACM conference on Digital libraries*, pp. 89–98, 1998. 46
- Narendra S Goel, Samaresh C Maitra, and Elliott W Montroll. On the volterra and other nonlinear models of interacting populations. *Reviews of modern physics*, 43(2):231, 1971. 46
- Muhammad Waleed Gondal, Shruti Joshi, Nasim Rahaman, Stefan Bauer, Manuel Wuthrich, and Bernhard Schölkopf. Function contrastive learning of transferable representations, 2021. URL <https://openreview.net/forum?id=IqZpoAAAt2oQ>. 14, 38, 40
- Ian Goodfellow, Jean Pouget-Abadie, Mehdi Mirza, Bing Xu, David Warde-Farley, Sherjil Ozair, Aaron Courville, and Yoshua Bengio. Generative adversarial nets. *Advances in neural information processing systems*, 27, 2014. 42

-
- Jonathan Gordon, Wessel P. Bruinsma, Andrew Y. K. Foong, James Requeima, Yann Dubois, and Richard E. Turner. Convolutional conditional neural processes. In *International Conference on Learning Representations*, 2020. URL <https://openreview.net/forum?id=Skey4eBYPS>. 11, 13, 14, 20, 22, 28, 29, 30, 32, 40, 43, 46, 47, 48, 52
- Erin Grant, Chelsea Finn, Sergey Levine, Trevor Darrell, and Thomas Griffiths. Recasting gradient-based meta-learning as hierarchical bayes. In *International Conference on Learning Representations*, 2018. URL https://openreview.net/forum?id=BJ_UL-k0b. 12
- Samuel Greydanus, Misko Dzamba, and Jason Yosinski. Hamiltonian neural networks. *Advances in Neural Information Processing Systems*, 32, 2019. 1
- Danijar Hafner, Timothy Lillicrap, Ian Fischer, Ruben Villegas, David Ha, Honglak Lee, and James Davidson. Learning latent dynamics for planning from pixels. In *International conference on machine learning*, pp. 2555–2565. PMLR, 2019. 32
- Heidi B Hammel. Lessons learned from (and since) the voyager 2 flybys of uranus and neptune. *Philosophical Transactions of the Royal Society A*, 378(2187):20190485, 2020. 42
- James Harrison, Apoorva Sharma, and Marco Pavone. Meta-learning priors for efficient online bayesian regression. In *International Workshop on the Algorithmic Foundations of Robotics*, pp. 318–337. Springer, 2018. 53
- Marton Havasi, José Miguel Hernández-Lobato, and Juan José Murillo-Fuentes. Inference in deep gaussian processes using stochastic gradient hamiltonian monte carlo. *Advances in neural information processing systems*, 31, 2018. 53
- Kaiming He, Xiangyu Zhang, Shaoqing Ren, and Jian Sun. Deep residual learning for image recognition. In *Proceedings of the IEEE conference on computer vision and pattern recognition*, pp. 770–778, 2016. 37
- Tong He, Dong Gong, Zhi Tian, and Chunhua Shen. Learning and memorizing representative prototypes for 3d point cloud semantic and instance segmentation. In *European Conference on Computer Vision*, pp. 564–580. Springer, 2020. 50
- Yisheng He, Haibin Huang, Haoqiang Fan, Qifeng Chen, and Jian Sun. Ffb6d: A full flow bidirectional fusion network for 6d pose estimation. In *Proceedings of the IEEE/CVF Conference on Computer Vision and Pattern Recognition*, pp. 3003–3013, 2021. 44
- Jay Heo, Junhyeon Park, Hyewon Jeong, Kwang Joon Kim, Juho Lee, Eunho Yang, and Sung Ju Hwang. Cost-effective interactive attention learning with neural attention processes. In *International Conference on Machine Learning*, pp. 4228–4238. PMLR, 2020. 45
- Luke Hewitt, Andrea Gane, Tommi Jaakkola, and Joshua B. Tenenbaum. The variational homoencoder: Learning to infer high-capacity generative models from few examples, 2018. URL <https://openreview.net/forum?id=HJ5AUm-CZ>. 9, 12
- Peter Holderrieth, Michael J Hutchinson, and Yee Whye Teh. Equivariant learning of stochastic fields: Gaussian processes and steerable conditional neural processes. In *International Conference on Machine Learning*, pp. 4297–4307. PMLR, 2021. 13, 14, 23, 53
- Tsung-Yu Hsieh, Yiwei Sun, Xianfeng Tang, Suhang Wang, and Vasant G Honavar. Srvarm: state regularized vector autoregressive model for joint learning of hidden state transitions and state-dependent inter-variable dependencies from multi-variate time series. In *Proceedings of the Web Conference 2021*, pp. 2270–2280, 2021a. 11
- Tsung-Yu Hsieh, Yiwei Sun, Suhang Wang, and Vasant Honavar. Functional autoencoders for functional data representation learning. In *Proceedings of the 2021 SIAM International Conference on Data Mining (SDM)*, pp. 666–674. SIAM, 2021b. 11

-
- JONATHAN H Huggins and Jeffrey W Miller. Using bagged posteriors for robust inference and model criticism. *arXiv preprint arXiv:1912.07104*, 18, 2019. 31
- Mark Huisman. Imputation of missing network data: Some simple procedures. *Journal of Social Structure*, 10(1):1–29, 2009. 25
- Mike Huisman, Jan N. van Rijn, and Aske Plaat. *Metalearning for Deep Neural Networks*, pp. 237–267. Springer International Publishing, Cham, 2022. ISBN 978-3-030-67024-5. doi: 10.1007/978-3-030-67024-5_13. URL https://doi.org/10.1007/978-3-030-67024-5_13. 11
- Robert Hunt, Engin Mendi, and Coskun Bayrak. Using cellular automata to model social networking behavior. In *2011 IEEE 12th International Symposium on Computational Intelligence and Informatics (CINTI)*, pp. 287–290. IEEE, 2011. 23
- Mohammad Rasool Izadi, Yihao Fang, Robert Stevenson, and Lizhen Lin. Optimization of graph neural networks with natural gradient descent. In *2020 IEEE International Conference on Big Data (Big Data)*, pp. 171–179. IEEE, 2020. 27
- Hosagrahar V Jagadish, Johannes Gehrke, Alexandros Labrinidis, Yannis Papakonstantinou, Jignesh M Patel, Raghu Ramakrishnan, and Cyrus Shahabi. Big data and its technical challenges. *Communications of the ACM*, 57(7):86–94, 2014. 46
- Eric Jang, Shixiang Gu, and Ben Poole. Categorical reparameterization with gumbel-softmax. In *International Conference on Learning Representations*, 2017. URL <https://openreview.net/pdf?id=rkE3y85ee>. 45
- Saurav Jha, Martin Schiemer, Franco Zambonelli, and Juan Ye. Continual learning in sensor-based human activity recognition: An empirical benchmark analysis. *Information Sciences*, 575:1–21, 2021. 54
- Martinez Jorge and Iglewicz Boris. Some properties of the tukey g and h family of distributions. *Communications in Statistics-Theory and Methods*, 13(3):353–369, 1984. 15
- Konstantinos Kallidromitis, Denis Gudovskiy, Kozuka Kazuki, Ohama Iku, and Luca Rigazio. Contrastive neural processes for self-supervised learning. In *Asian Conference on Machine Learning*, pp. 594–609. PMLR, 2021. 13, 14, 38, 40, 46
- George Em Karniadakis, Ioannis G Kevrekidis, Lu Lu, Paris Perdikaris, Sifan Wang, and Liu Yang. Physics-informed machine learning. *Nature Reviews Physics*, 3(6):422–440, 2021. 43
- Makoto Kawano, Wataru Kumagai, Akiyoshi Sannai, Yusuke Iwasawa, and Yutaka Matsuo. Group equivariant conditional neural processes. In *International Conference on Learning Representations*, 2021. URL https://openreview.net/forum?id=e8W-hsu_q5. 11, 13, 14, 22, 23, 53
- Kristian Kersting, Nils M. Kriege, Christopher Morris, Petra Mutzel, and Marion Neumann. Benchmark data sets for graph kernels, 2016. URL <http://graphkernels.cs.tu-dortmund.de>. 46
- Seyed Mostafa Kia and Andre F. Marquand. Neural processes mixed-effect models for deep normative modeling of clinical neuroimaging data. In M. Jorge Cardoso, Aasa Feragen, Ben Glocker, Ender Konukoglu, Ipek Oguz, Gozde Unal, and Tom Vercauteren (eds.), *Proceedings of The 2nd International Conference on Medical Imaging with Deep Learning*, volume 102 of *Proceedings of Machine Learning Research*, pp. 297–314. PMLR, 08–10 Jul 2019. URL <https://proceedings.mlr.press/v102/kia19a.html>. 45
- Seyed Mostafa Kia, Christian F Beckmann, and Andre F Marquand. Scalable multi-task gaussian process tensor regression for normative modeling of structured variation in neuroimaging data. *arXiv preprint arXiv:1808.00036*, 2018. 45
- Donggyun Kim, Seongwoong Cho, Wonkwang Lee, and Seunghoon Hong. Multi-task processes. In *International Conference on Learning Representations*, 2022a. URL <https://openreview.net/forum?id=9otKVlgrpZG>. 14, 37, 38

-
- Hyunjik Kim, Andriy Mnih, Jonathan Schwarz, Marta Garnelo, Ali Eslami, Dan Rosenbaum, Oriol Vinyals, and Yee Whye Teh. Attentive neural processes. In *International Conference on Learning Representations*, 2019. URL <https://openreview.net/forum?id=SkE6PjC9KX>. 10, 11, 13, 14, 15, 16, 17, 18, 19, 20, 21, 27, 28, 30, 32, 34, 37, 40, 42, 47, 52
- Mingyu Kim, Kyeong Ryeol Go, and Se-Young Yun. Neural processes with stochastic attention: Paying more attention to the context dataset. In *Fifth Workshop on Meta-Learning at the Conference on Neural Information Processing Systems*, 2021. URL <https://openreview.net/forum?id=URep0STGewu>. 20
- Mingyu Kim, Kyeong Ryeol Go, and Se-Young Yun. Neural processes with stochastic attention: Paying more attention to the context dataset. In *International Conference on Learning Representations*, 2022b. URL <https://openreview.net/forum?id=JPkQwEdYn8>. 14, 20
- Diederik P. Kingma and Max Welling. Auto-Encoding Variational Bayes. In *2nd International Conference on Learning Representations, ICLR 2014, Banff, AB, Canada, April 14-16, 2014, Conference Track Proceedings*, 2014. 8, 26, 33
- Durk P Kingma, Tim Salimans, and Max Welling. Variational dropout and the local reparameterization trick. *Advances in neural information processing systems*, 28, 2015. 50
- Thomas Kipf and Max Welling. Semi-supervised classification with graph convolutional networks. In *International Conference on Learning Representations*, 2019. URL <https://openreview.net/pdf?id=SJU4ayYgl>. 24, 26
- Thomas Kipf, Elise van der Pol, and Max Welling. Contrastive learning of structured world models. In *International Conference on Learning Representations*, 2019. 39
- Thomas N Kipf and Max Welling. Variational graph auto-encoders. *arXiv preprint arXiv:1611.07308*, 2016. 26
- David Klindt, Alexander S Ecker, Thomas Euler, and Matthias Bethge. Neural system identification for large populations separating “what” and “where”. *Advances in Neural Information Processing Systems*, 30, 2017. 42
- Soheil Kolouri, Yang Zou, and Gustavo K. Rohde. Sliced wasserstein kernels for probability distributions. In *2016 IEEE Conference on Computer Vision and Pattern Recognition (CVPR)*, pp. 5258–5267, 2016. doi: 10.1109/CVPR.2016.568. 15
- Soheil Kolouri, Phillip E. Pope, Charles E. Martin, and Gustavo K. Rohde. Sliced wasserstein auto-encoders. In *International Conference on Learning Representations*, 2019. URL <https://openreview.net/forum?id=H1xaJn05FQ>. 15
- Lingkai Kong, Jimeng Sun, and Chao Zhang. Sde-net: Equipping deep neural networks with uncertainty estimates. In *International Conference on Machine Learning*, pp. 5405–5415. PMLR, 2020. 43
- Vivek Kothari, Edgar Liberis, and Nicholas D Lane. The final frontier: Deep learning in space. In *Proceedings of the 21st international workshop on mobile computing systems and applications*, pp. 45–49, 2020. 1
- Alex Krizhevsky, Ilya Sutskever, and Geoffrey E Hinton. Imagenet classification with deep convolutional neural networks. *Advances in neural information processing systems*, 25, 2012. 1
- Brenden M Lake, Ruslan Salakhutdinov, and Joshua B Tenenbaum. Human-level concept learning through probabilistic program induction. *Science*, 350(6266):1332–1338, 2015. 44, 46
- Balaji Lakshminarayanan, Alexander Pritzel, and Charles Blundell. Simple and scalable predictive uncertainty estimation using deep ensembles. *Advances in neural information processing systems*, 30, 2017. 32

-
- Tuan Anh Le, Hyunjik Kim, Marta Garnelo, Dan Rosenbaum, Jonathan Schwarz, and Yee Whye Teh. Empirical evaluation of neural process objectives. In *NeurIPS workshop on Bayesian Deep Learning*, pp. 71, 2018. 4, 5, 54
- Henri Lebesgue. Intégrale, longueur, aire. *Annali di Matematica Pura ed Applicata (1898-1922)*, 7(1): 231–359, 1902. 70
- Yann LeCun. A path towards autonomous machine intelligence. 2022. URL <https://openreview.net/pdf?id=BZ5a1r-kVsf>. 1
- Yann LeCun, Léon Bottou, Yoshua Bengio, and Patrick Haffner. Gradient-based learning applied to document recognition. *Proceedings of the IEEE*, 86(11):2278–2324, 1998. 44, 46, 48
- Byung-Jun Lee, Seunghoon Hong, and Kee-Eung Kim. Residual neural processes. In *Proceedings of the AAAI Conference on Artificial Intelligence*, volume 34, pp. 4545–4552, 2020a. 14, 17, 18
- Juho Lee, Yoonho Lee, Jungtaek Kim, Adam Kosioerek, Seungjin Choi, and Yee Whye Teh. Set transformer: A framework for attention-based permutation-invariant neural networks. In *International Conference on Machine Learning*, pp. 3744–3753. PMLR, 2019. 10
- Juho Lee, Yoonho Lee, Jungtaek Kim, Eunho Yang, Sung Ju Hwang, and Yee Whye Teh. Bootstrapping neural processes. *Advances in neural information processing systems*, 33:6606–6615, 2020b. 14, 21, 30, 31, 32, 46
- Yumeng Li, Ning Gao, Hanna Ziesche, and Gerhard Neumann. Category-agnostic 6d pose estimation with conditional neural processes. *arXiv preprint arXiv:2206.07162*, 2022. 44
- Huidong Liang and Junbin Gao. How neural processes improve graph link prediction. *arXiv preprint arXiv:2109.14894*, 2021. 14, 25, 26, 46
- Xixun Lin, Jia Wu, Chuan Zhou, Shirui Pan, Yanan Cao, and Bin Wang. Task-adaptive neural process for user cold-start recommendation. In *Proceedings of the Web Conference 2021*, pp. 1306–1316, 2021. 41, 46
- Zhenhua Lin and Hongtu Zhu. Mfzca: multiscale functional principal component analysis. In *Proceedings of the AAAI Conference on Artificial Intelligence*, volume 33, pp. 4320–4327, 2019. 11
- Ziwei Liu, Ping Luo, Xiaogang Wang, and Xiaoou Tang. Deep learning face attributes in the wild. In *Proceedings of International Conference on Computer Vision (ICCV)*, December 2015. 29, 46, 48
- Cosme Louart and Romain Couillet. A random matrix and concentration inequalities framework for neural networks analysis. In *2018 IEEE International Conference on Acoustics, Speech and Signal Processing (ICASSP)*, pp. 4214–4218. IEEE, 2018. 2
- Christos Louizos, Xiahao Shi, Klamer Schutte, and Max Welling. The functional neural process. In *Advances in Neural Information Processing Systems*, 2019. 13, 14, 26, 27, 30, 31
- Thomas Lukasiewicz and Jianfeng Wang. Np-match: When neural processes meet semi-supervised learning. In *International Conference on Machine Learning*. PMLR, 2022. 50
- Jianping Luo, Liang Chen, Xia Li, and Qingfu Zhang. Novel multitask conditional neural-network surrogate models for expensive optimization. *IEEE Transactions on Cybernetics*, pp. 1–14, 2020. doi: 10.1109/TCYB.2020.3014126. 41
- Chao Ma, Yingzhen Li, and Jose Miguel Hernandez-Lobato. Variational implicit processes. In Kamalika Chaudhuri and Ruslan Salakhutdinov (eds.), *Proceedings of the 36th International Conference on Machine Learning*, volume 97 of *Proceedings of Machine Learning Research*, pp. 4222–4233. PMLR, 09–15 Jun 2019a. URL <https://proceedings.mlr.press/v97/ma19b.html>. 12
- Chao Ma, Sebastian Tschiatschek, Konstantina Palla, Jose Miguel Hernandez-Lobato, Sebastian Nowozin, and Cheng Zhang. Eddi: Efficient dynamic discovery of high-value information with partial vae. In *International Conference on Machine Learning*, pp. 4234–4243. PMLR, 2019b. 12

-
- David JC MacKay. Probable networks and plausible predictions—a review of practical bayesian methods for supervised neural networks. *Network: computation in neural systems*, 6(3):469, 1995. 2
- Jeffrey Mahler, Jacky Liang, Sherdil Niyaz, Michael Laskey, Richard Doan, Xinyu Liu, Juan Aparicio Ojea, and Ken Goldberg. Dex-net 2.0: Deep learning to plan robust grasps with synthetic point clouds and analytic grasp metrics. *arXiv preprint arXiv:1703.09312*, 2017. 44
- Krzysztof Maleski. Graph cellular automata with relation-based neighbourhoods of cells for complex systems modelling: A case of traffic simulation. *Symmetry*, 9(12):322, 2017. 23
- Stratis Markou, James Requeima, Wessel Bruinsma, and Richard Turner. Efficient gaussian neural processes for regression. In *Workshop on Uncertainty and Robustness in Deep Learning at the International Conference on Machine Learning*, 2021. 30
- Stratis Markou, James Requeima, Wessel Bruinsma, Anna Vaughan, and Richard E Turner. Practical conditional neural process via tractable dependent predictions. In *International Conference on Learning Representations*, 2022. URL <https://openreview.net/forum?id=3pugbNqOh5m>. 14, 30
- Haggai Maron, Or Litany, Gal Chechik, and Ethan Fetaya. On learning sets of symmetric elements. In *International Conference on Machine Learning*, pp. 6734–6744. PMLR, 2020. 53
- Andre F Marquand, Iead Rezek, Jan Buitelaar, and Christian F Beckmann. Understanding heterogeneity in clinical cohorts using normative models: beyond case-control studies. *Biological psychiatry*, 80(7):552–561, 2016. 45
- Jonathan Masci, Ueli Meier, Dan Ciresan, Jürgen Schmidhuber, and Gabriel Fricout. Steel defect classification with max-pooling convolutional neural networks. In *The 2012 international joint conference on neural networks (IJCNN)*, pp. 1–6. IEEE, 2012. 1
- Emile Mathieu, Adam Foster, and Yee Teh. On contrastive representations of stochastic processes. *Advances in Neural Information Processing Systems*, 34, 2021. 14, 38, 53
- Alexander G de G Matthews, James Hensman, Richard Turner, and Zoubin Ghahramani. On sparse variational methods and the kullback-leibler divergence between stochastic processes. In *Artificial Intelligence and Statistics*, pp. 231–239. PMLR, 2016. 29
- Morgan P McBee, Omer A Awan, Andrew T Colucci, Comeron W Ghobadi, Nadja Kadom, Akash P Kansagra, Srinu Tridandapani, and William F Auffermann. Deep learning in radiology. *Academic radiology*, 25(11):1472–1480, 2018. 1
- Andrew Kachites McCallum, Kamal Nigam, Jason Rennie, and Kristie Seymore. Automating the construction of internet portals with machine learning. *Information Retrieval*, 3(2):127–163, 2000. 25, 46
- Nick McGreivy and Ammar Hakim. Convolutional layers are not translation equivariant. 2022. 21
- Igor Molybog and Javad Lavaei. When does maml objective have benign landscape? In *2021 IEEE Conference on Control Technology and Applications (CCTA)*, pp. 220–227. IEEE, 2021. 11
- George Moody. A new method for detecting atrial fibrillation using rr intervals. *Computers in Cardiology*, pp. 227–230, 1983. 46
- Joaquín Muñoz-Sabater, Emanuel Dutra, Anna Agustí-Panareda, Clément Albergel, Gabriele Arduini, Gianpaolo Balsamo, Souhail Boussetta, Margarita Choulga, Shaun Harrigan, Hans Hersbach, et al. Era5-land: A state-of-the-art global reanalysis dataset for land applications. *Earth System Science Data*, 13(9): 4349–4383, 2021. 46
- Ryan L. Murphy, Balasubramaniam Srinivasan, Vinayak Rao, and Bruno Ribeiro. Janossy pooling: Learning deep permutation-invariant functions for variable-size inputs. In *International Conference on Learning Representations*, 2019. URL <https://openreview.net/forum?id=BJluy2RcFm>. 9, 53

-
- Marcel Nassar. Hierarchical bipartite graph convolution networks. In *Workshop on Relational Representation Learning at the Conference on Neural Information Processing Systems*, 2018. 24
- Marcel Nassar, Xin Wang, and Evren Tumer. Conditional graph neural processes: A functional autoencoder approach. In *Third workshop on Bayesian Deep Learning at the Conference on Neural Information Processing Systems*, 2018. 13, 14, 24
- Yuval Netzer, Tao Wang, Adam Coates, Alessandro Bissacco, Bo Wu, and Andrew Y Ng. Reading digits in natural images with unsupervised feature learning. *NIPS Workshop on Deep Learning and Unsupervised Feature Learning*, 2011. 29, 46
- Tung Nguyen and Aditya Grover. Transformer neural processes: Uncertainty-aware meta learning via sequence modeling. In *International Conference on Machine Learning*, pp. 16569–16594. PMLR, 2022. 7, 12, 14, 21
- Alex Nichol and John Schulman. Reptile: a scalable metalearning algorithm. *arXiv preprint arXiv:1803.02999*, 2(3):4, 2018. 11
- M-E. Nilsback and A. Zisserman. Automated flower classification over a large number of classes. In *Proceedings of the Indian Conference on Computer Vision, Graphics and Image Processing*, Dec 2008. 46
- Alexander Norcliffe, Cristian Bodnar, Ben Day, Jacob Moss, and Pietro Liò. Neural {ode} processes. In *International Conference on Learning Representations*, 2021. URL <https://openreview.net/forum?id=27acGyyI1BY>. 14, 35, 43, 46
- Bernt Øksendal. Stochastic differential equations. In *Stochastic differential equations*, pp. 65–84. Springer, 2003. 43, 70
- Chris Olah, Nick Cammarata, Chelsea Voss, Ludwig Schubert, and Gabriel Goh. Naturally occurring equivariance in neural networks. *Distill*, 2020. doi: 10.23915/distill.00024.004. <https://distill.pub/2020/circuits/equivariance>. 22
- Aaron van den Oord, Yazhe Li, and Oriol Vinyals. Representation learning with contrastive predictive coding. *arXiv preprint arXiv:1807.03748*, 2018. 38, 39
- Chirag Pabbaraju and Prateek Jain. Learning functions over sets via permutation adversarial networks. *arXiv preprint arXiv:1907.05638*, 2019. 53
- Ari Pakman, Yueqi Wang, Catalin Mitelut, Jinhyung Lee, and Liam Paninski. Neural clustering processes. In Hal Daumé III and Aarti Singh (eds.), *Proceedings of the 37th International Conference on Machine Learning*, volume 119 of *Proceedings of Machine Learning Research*, pp. 7455–7465. PMLR, 13–18 Jul 2020. URL <https://proceedings.mlr.press/v119/pakman20a.html>. 11, 42
- Young-Jin Park and Han-Lim Choi. A neural process approach for probabilistic reconstruction of no-data gaps in lunar digital elevation maps. *Aerospace Science and Technology*, 113:106672, 2021. 42
- Francesco Pelosin, Saurav Jha, Andrea Torsello, Bogdan Raducanu, and Joost van de Weijer. Towards exemplar-free continual learning in vision transformers: An account of attention, functional and weight regularization. In *Proceedings of the IEEE/CVF Conference on Computer Vision and Pattern Recognition (CVPR) Workshops*, pp. 3820–3829, June 2022. 37
- Ana Pereira and Carsten Thomas. Challenges of machine learning applied to safety-critical cyber-physical systems. *Machine Learning and Knowledge Extraction*, 2(4):579–602, 2020. 2
- Ethan Perez, Florian Strub, Harm De Vries, Vincent Dumoulin, and Aaron Courville. Film: Visual reasoning with a general conditioning layer. In *Proceedings of the AAAI Conference on Artificial Intelligence*, volume 32, 2018. 37, 41

-
- Bryan Perozzi, Rami Al-Rfou, and Steven Skiena. Deepwalk: Online learning of social representations. In *Proceedings of the 20th ACM SIGKDD international conference on Knowledge discovery and data mining*, pp. 701–710, 2014. 26
- Jens Petersen, Gregor Köhler, David Zimmerer, Fabian Isensee, Paul F. Jäger, and Klaus H. Maier-Hein. Gpconvnp: Better generalization for conditional convolutional neural processes on time series data. In Cassio de Campos and Marloes H. Maathuis (eds.), *Proceedings of the Thirty-Seventh Conference on Uncertainty in Artificial Intelligence*, volume 161 of *Proceedings of Machine Learning Research*, pp. 939–949. PMLR, 27–30 Jul 2021. URL <https://proceedings.mlr.press/v161/petersen21a.html>. 14, 35, 36
- Alexander Pondaven, Märt Bakler, Donghu Guo, Hamzah Hashim, Martin Ignatov, and Harrison Zhu. Convolutional neural processes for inpainting satellite images. *arXiv preprint arXiv:2205.12407*, 2022. 43
- Shenghao Qin, Jiacheng Zhu, Jimmy Qin, Wenshuo Wang, and Ding Zhao. Recurrent attentive neural process for sequential data. *CoRR*, abs/1910.09323, 2019. URL <http://arxiv.org/abs/1910.09323>. 14, 34
- Hai Qiu, Jay Lee, Jing Lin, and Gang Yu. Wavelet filter-based weak signature detection method and its application on rolling element bearing prognostics. *Journal of sound and vibration*, 289(4-5):1066–1090, 2006. 46
- Meng Qu, Yoshua Bengio, and Jian Tang. Gmn: Graph markov neural networks. In *International conference on machine learning*, pp. 5241–5250. PMLR, 2019. 27
- Joaquin Quinonero-Candela and Carl Edward Rasmussen. A unifying view of sparse approximate gaussian process regression. *The Journal of Machine Learning Research*, 6:1939–1959, 2005. 71
- Julian F Quinting and Christian M Grams. Eulerian identification of ascending airstreams (elias 2.0) in numerical weather prediction and climate models—part 1: Development of deep learning model. *Geoscientific Model Development*, 15(2):715–730, 2022. 1
- Ahmed Rashed, Josif Grabocka, and Lars Schmidt-Thieme. Attribute-aware non-linear co-embeddings of graph features. In *Proceedings of the 13th ACM conference on recommender systems*, pp. 314–321, 2019. 20
- Sylvestre-Alvise Rebuffi, Alexander Kolesnikov, Georg Sperl, and Christoph H Lampert. icarl: Incremental classifier and representation learning. In *Proceedings of the IEEE conference on Computer Vision and Pattern Recognition*, pp. 2001–2010, 2017. 54
- James Requeima, Jonathan Gordon, John Bronskill, Sebastian Nowozin, and Richard E Turner. Fast and flexible multi-task classification using conditional neural adaptive processes. *Advances in Neural Information Processing Systems*, 32, 2019. 13, 14, 36, 37, 46
- Hannes Isaak Reuter, Andy Nelson, and Andrew Jarvis. An evaluation of void-filling interpolation methods for srtm data. *International Journal of Geographical Information Science*, 21(9):983–1008, 2007. 42
- Carlos Riquelme, George Tucker, and Jasper Snoek. Deep bayesian bandits showdown: An empirical comparison of bayesian deep networks for thompson sampling. In *International Conference on Learning Representations*, 2018. URL <https://openreview.net/forum?id=SyYe6k-CW>. 21
- Olaf Ronneberger, Philipp Fischer, and Thomas Brox. U-net: Convolutional networks for biomedical image segmentation. In *International Conference on Medical image computing and computer-assisted intervention*, pp. 234–241. Springer, 2015. 38
- Fabrice Rossi, Nicolas Delannay, Briec Conan-Guez, and Michel Verleysen. Representation of functional data in neural networks. *Neurocomputing*, 64:183–210, 2005. 11
- Tim GJ Rudner, Vincent Fortuin, Yee Whye Teh, and Yarin Gal. On the connection between neural processes and gaussian processes with deep kernels. In *Workshop on Bayesian Deep Learning, NeurIPS*, pp. 14, 2018. 11

-
- Lars Ruthotto and Eldad Haber. An introduction to deep generative modeling. *GAMM-Mitteilungen*, 44(2): e202100008, 2021. 12
- Justin Salamon, Christopher Jacoby, and Juan Pablo Bello. A dataset and taxonomy for urban sound research. In *Proceedings of the 22nd ACM international conference on Multimedia*, pp. 1041–1044, 2014. 46
- Adam Santoro, David Raposo, David G Barrett, Mateusz Malinowski, Razvan Pascanu, Peter Battaglia, and Timothy Lillicrap. A simple neural network module for relational reasoning. *Advances in neural information processing systems*, 30, 2017. 16
- Franco Scarselli, Marco Gori, Ah Chung Tsoi, Markus Hagenbuchner, and Gabriele Monfardini. The graph neural network model. *IEEE transactions on neural networks*, 20(1):61–80, 2008. 24
- Prithviraj Sen, Galileo Namata, Mustafa Bilgic, Lise Getoor, Brian Galligher, and Tina Eliassi-Rad. Collective classification in network data. *AI magazine*, 29(3):93–93, 2008. 46
- Zhongkai Shangguan, Lei Lin, Wencheng Wu, and Beilei Xu. Neural process for black-box model optimization under bayesian framework. In *Proceedings of the AAAI Spring Symposium on Combining Artificial Intelligence and Machine Learning with Physical Sciences*, 2021. URL http://ceur-ws.org/Vol1-2964/article_66.pdf. 41
- Yirong Shen, Matthias Seeger, and Andrew Ng. Fast gaussian process regression using kd-trees. *Advances in neural information processing systems*, 18, 2005. 52
- Jiaxin Shi, Mohammad Emtiyaz Khan, and Jun Zhu. Scalable training of inference networks for gaussian-process models. In *International Conference on Machine Learning*, pp. 5758–5768. PMLR, 2019. 53
- Gautam Singh, Jaesik Yoon, Youngsung Son, and Sungjin Ahn. Sequential neural processes. *Advances in Neural Information Processing Systems*, 32, 2019. 13, 14, 18, 19, 28, 32, 33, 52
- Anton Sinitin, Vsevolod Plokhotnyuk, Dmitry Pyrkin, Sergei Popov, and Artem Babenko. Editable neural networks. In *International Conference on Learning Representations*, 2020. URL <https://openreview.net/forum?id=HJedXaEtvS>. 45
- Jake Snell, Kevin Swersky, and Richard Zemel. Prototypical networks for few-shot learning. *Advances in neural information processing systems*, 30, 2017. 6, 7, 37
- Jasper Snoek, Oren Rippel, Kevin Swersky, Ryan Kiros, Nadathur Satish, Narayanan Sundaram, Mostofa Patwary, Mr Prabhat, and Ryan Adams. Scalable bayesian optimization using deep neural networks. In *International conference on machine learning*, pp. 2171–2180. PMLR, 2015. 41
- Maximilian Soelch, Adnan Akhundov, Patrick van der Smagt, and Justin Bayer. On deep set learning and the choice of aggregations. In *International Conference on Artificial Neural Networks*, pp. 444–457. Springer, 2019. 53
- Kihyuk Sohn, Honglak Lee, and Xinchun Yan. Learning structured output representation using deep conditional generative models. *Advances in neural information processing systems*, 28, 2015. 18
- Kaori Suefusa, Tomoya Nishida, Harsh Purohit, Ryo Tanabe, Takashi Endo, and Yohei Kawaguchi. Anomalous sound detection based on interpolation deep neural network. In *ICASSP 2020-2020 IEEE International Conference on Acoustics, Speech and Signal Processing (ICASSP)*, pp. 271–275. IEEE, 2020. 45
- Yue Sun, Adhyyan Narang, Ibrahim Gulluk, Samet Oymak, and Maryam Fazel. Towards sample-efficient overparameterized meta-learning. *Advances in Neural Information Processing Systems*, 34, 2021. 53
- Anirudh Suresh and Srivatsan Srinivasan. Improved attentive neural processes. In *Fourth Workshop on Bayesian Deep Learning at the Conference on Neural Information Processing Systems*, 2019. 14, 17

-
- Ilya Sutskever, Geoffrey E Hinton, and Graham W Taylor. The recurrent temporal restricted boltzmann machine. *Advances in neural information processing systems*, 21, 2008. 46
- Kevin Swersky, Jasper Snoek, and Ryan P Adams. Multi-task bayesian optimization. *Advances in neural information processing systems*, 26, 2013. 41
- Binh Tang and David S. Matteson. Graph-based continual learning. In *International Conference on Learning Representations*, 2021. URL <https://openreview.net/forum?id=HHSEK0nPva0>. 27
- Lei Tang and Huan Liu. Leveraging social media networks for classification. *Data Mining and Knowledge Discovery*, 23(3):447–478, 2011. 26
- Jean-Francois Ton, Lucian CHAN, Yee Whye Teh, and Dino Sejdinovic. Noise contrastive meta-learning for conditional density estimation using kernel mean embeddings. In Arindam Banerjee and Kenji Fukumizu (eds.), *Proceedings of The 24th International Conference on Artificial Intelligence and Statistics*, volume 130 of *Proceedings of Machine Learning Research*, pp. 1099–1107. PMLR, 13–15 Apr 2021. URL <https://proceedings.mlr.press/v130/ton21a.html>. 9, 11
- Ba-Hien Tran, Dimitrios Milios, Simone Rossi, and Maurizio Filippone. Sensible priors for bayesian neural networks through wasserstein distance minimization to gaussian processes. In *Third Symposium on Advances in Approximate Bayesian Inference*, 2021. URL <https://openreview.net/forum?id=GshivsoVTb2>. 53
- Eleni Triantafillou, Tyler Zhu, Vincent Dumoulin, Pascal Lamblin, Utku Evci, Kelvin Xu, Ross Goroshin, Carles Gelada, Kevin Swersky, Pierre-Antoine Manzagol, and Hugo Larochelle. Meta-dataset: A dataset of datasets for learning to learn from few examples. In *International Conference on Learning Representations*, 2020. URL <https://openreview.net/forum?id=rkgAGAVKPr>. 37
- Evgenii Tsymbalov, Sergei Makarychev, Alexander Shapeev, and Maxim Panov. Deeper connections between neural networks and gaussian processes speed-up active learning. In *Proceedings of the 28th International Joint Conference on Artificial Intelligence*, pp. 3599–3605, 2019. 12
- J Tueller, RF Mushotzky, S Barthelmy, JKd Cannizzo, N Gehrels, CB Markwardt, GK Skinner, and LM Winter. Swift bat survey of agns. *The Astrophysical Journal*, 681(1):113, 2008. 43
- Aaron Van den Oord, Nal Kalchbrenner, Lasse Espeholt, Oriol Vinyals, Alex Graves, et al. Conditional image generation with pixelcnn decoders. *Advances in neural information processing systems*, 29, 2016. 7
- Ashish Vaswani, Noam Shazeer, Niki Parmar, Jakob Uszkoreit, Llion Jones, Aidan N Gomez, Łukasz Kaiser, and Illia Polosukhin. Attention is all you need. *Advances in neural information processing systems*, 30, 2017. 15, 16, 17, 40
- Anna Vaughan, Will Tebbutt, J Scott Hosking, and Richard E Turner. Convolutional conditional neural processes for local climate downscaling. *arXiv preprint arXiv:2101.07950*, 2021. 45
- Oriol Vinyals, Charles Blundell, Timothy Lillicrap, Daan Wierstra, et al. Matching networks for one shot learning. *Advances in neural information processing systems*, 29, 2016. 29
- Edward Wagstaff, Fabian Fuchs, Martin Engelcke, Ingmar Posner, and Michael A Osborne. On the limitations of representing functions on sets. In *International Conference on Machine Learning*, pp. 6487–6494. PMLR, 2019. 16
- Edward Wagstaff, Fabian B Fuchs, Martin Engelcke, Michael A Osborne, and Ingmar Posner. Universal approximation of functions on sets. *arXiv preprint arXiv:2107.01959*, 2021. 9, 10
- Guanyu Wang, Xovee Xu, Ting Zhong, and Fan Zhou. Conditional collaborative filtering process for top-k recommender system (student abstract). *AAAI Conference on Artificial Intelligence*, 2022a. 41

-
- Jianfeng Wang, Thomas Lukasiewicz, Daniela Massiceti, Xiaolin Hu, Vladimir Pavlovic, and Alexandros Neophytou. Np-match: When neural processes meet semi-supervised learning. In *International Conference on Machine Learning*, pp. 22919–22934. PMLR, 2022b. 45
- Mingzhu Wang, P Wong, Han Luo, Sudip Kumar, V Delhi, and J Cheng. Predicting safety hazards among construction workers and equipment using computer vision and deep learning techniques. In *ISARC. Proceedings of the International Symposium on Automation and Robotics in Construction*, volume 36, pp. 399–406. IAARC Publications, 2019a. 1
- Qi Wang and Herke Van Hoof. Doubly stochastic variational inference for neural processes with hierarchical latent variables. In *International Conference on Machine Learning*, pp. 10018–10028. PMLR, 2020. 14, 18, 46
- Xuesong Wang, Lina Yao, Xianzhi Wang, Feiping Nie, and Boualem Benatallah. Np-prov: Neural processes with position-relevant-only variances. In *International Conference on Web Information Systems Engineering*, pp. 129–142. Springer, 2021a. 14, 28
- Xuesong Wang, Lina Yao, Xianzhi Wang, Hye-young Paik, and Sen Wang. Global convolutional neural processes. In *2021 IEEE International Conference on Data Mining (ICDM)*, pp. 699–708. IEEE, 2021b. 14, 32, 48
- Yaqing Wang, Fenglong Ma, Haoyu Wang, Kishlay Jha, and Jing Gao. Multimodal emergent fake news detection via meta neural process networks. In *Proceedings of the 27th ACM SIGKDD Conference on Knowledge Discovery & Data Mining*, pp. 3708–3716, 2021c. 45
- Yinan Wang, Kaiwen Wang, Wenjun Cai, and Xiaowei Yue. Np-ode: Neural process aided ordinary differential equations for uncertainty quantification of finite element analysis. *IISE Transactions*, 54(3):211–226, 2022c. 43
- Yongguang Wang and Shuzhen Yao. Neural stochastic differential equations with neural processes family members for uncertainty estimation in deep learning. *Sensors*, 21(11):3708, 2021. 43
- Yue Wang, Yongbin Sun, Ziwei Liu, Sanjay E Sarma, Michael M Bronstein, and Justin M Solomon. Dynamic graph cnn for learning on point clouds. *Acm Transactions On Graphics (tog)*, 38(5):1–12, 2019b. 49, 50
- Zhou Wang, Eero P Simoncelli, and Alan C Bovik. Multiscale structural similarity for image quality assessment. In *The Thrity-Seventh Asilomar Conference on Signals, Systems & Computers, 2003*, volume 2, pp. 1398–1402. Ieee, 2003. 43
- James Weber. Description of machine models genrou, gensal, gentpf and gentpj. *PowerWorld Corporation*, 2015. 41
- Noah Weber, Janez Starc, Arpit Mittal, Roi Blanco, and Lluís Màrquez. Optimizing over a bayesian last layer. In *NeurIPS workshop on Bayesian Deep Learning*, 2018. 17, 46
- Ying Wei, Peilin Zhao, and Junzhou Huang. Meta-learning hyperparameter performance prediction with neural processes. In *International Conference on Machine Learning*, pp. 11058–11067. PMLR, 2021. 41
- Maurice Weiler and Gabriele Cesa. General e (2)-equivariant steerable cnns. *Advances in Neural Information Processing Systems*, 32, 2019. 23
- Gordon Wichern, Ankush Chakrabarty, Zhong-Qiu Wang, and Jonathan Le Roux. Anomalous sound detection using attentive neural processes. In *2021 IEEE Workshop on Applications of Signal Processing to Audio and Acoustics (WASPAA)*, pp. 186–190. IEEE, 2021. 45
- Timon Willi, Jonathan Masci, Jürgen Schmidhuber, and Christian Osendorfer. Recurrent neural processes. In *Fourth Workshop on Bayesian Deep Learning at the Conference on Neural Information Processing Systems*,, 2019. 14, 34

-
- Christopher K Williams and Carl Edward Rasmussen. *Gaussian processes for machine learning*, volume 2. MIT press Cambridge, MA, 2006. 2, 29, 70
- Andrew Gordon Wilson, Zhiting Hu, Ruslan Salakhutdinov, and Eric P Xing. Deep kernel learning. In *Artificial intelligence and statistics*, pp. 370–378. PMLR, 2016. 11
- David H Wolpert. The lack of a priori distinctions between learning algorithms. *Neural computation*, 8(7): 1341–1390, 1996. 13
- Dong Mei Wu, Matteo Chinazzi, Alessandro Vespignani, Yi-An Ma, and Rose Yu. Multi-fidelity hierarchical neural processes. 2022. 45
- Luhuan Wu, Andrew Miller, Lauren Anderson, Geoff Pleiss, David Blei, and John Cunningham. Hierarchical inducing point gaussian process for inter-domain observations. In *International Conference on Artificial Intelligence and Statistics*, pp. 2926–2934. PMLR, 2021. 52
- Zonghan Wu, Shirui Pan, Guodong Long, Jing Jiang, and Chengqi Zhang. Graph wavenet for deep spatial-temporal graph modeling. In *Proceedings of the 28th International Joint Conference on Artificial Intelligence*, pp. 1907–1913, 2019. 46
- Jin Xu, Jean-Francois Ton, Hyunjik Kim, Adam Kosior, and Yee Whye Teh. Metafun: Meta-learning with iterative functional updates. In *International Conference on Machine Learning*, pp. 10617–10627. PMLR, 2020. 11
- Jin Xu, Hyunjik Kim, Thomas Rainforth, and Yee Teh. Group equivariant subsampling. *Advances in Neural Information Processing Systems*, 34, 2021. 53
- Keyulu Xu, Weihua Hu, Jure Leskovec, and Stefanie Jegelka. How powerful are graph neural networks? In *International Conference on Learning Representations*, 2019. URL <https://openreview.net/forum?id=ryGs6iA5Km>. 24
- Siqiao Xue, Chao Qu, Xiaoming Shi, Cong Liao, Shiyi Zhu, Xiaoyu Tan, Lintao Ma, Shiyu Wang, Shijun Wang, Yun Hu, et al. A meta reinforcement learning approach for predictive autoscaling in the cloud. *arXiv preprint arXiv:2205.15795*, 2022. 44, 45
- Zesheng Ye and Lina Yao. Contrastive conditional neural processes. In *Proceedings of the IEEE/CVF Conference on Computer Vision and Pattern Recognition (CVPR)*, June 2022. 14, 39, 40, 46
- Li Yi, Vladimir G Kim, Duygu Ceylan, I-Chao Shen, Mengyan Yan, Hao Su, Cewu Lu, Qixing Huang, Alla Sheffer, and Leonidas Guibas. A scalable active framework for region annotation in 3d shape collections. *ACM Transactions on Graphics (ToG)*, 35(6):1–12, 2016. 49
- Boseon Yoo, Jiwoo Lee, Janghoon Ju, Seijun Chung, Soyeon Kim, and Jaesik Choi. Conditional temporal neural processes with covariance loss. In *International Conference on Machine Learning*, pp. 12051–12061. PMLR, 2021. 7, 14, 27, 46
- Jaesik Yoon, Gautam Singh, and Sungjin Ahn. Robustifying sequential neural processes. In *International Conference on Machine Learning*, pp. 10861–10870. PMLR, 2020. 14, 18, 52
- Bing Yu, Haoteng Yin, and Zhanxing Zhu. Spatio-temporal graph convolutional networks: a deep learning framework for traffic forecasting. In *Proceedings of the 27th International Joint Conference on Artificial Intelligence*, pp. 3634–3640, 2018. 27
- Haibin Yu, Yizhou Chen, Bryan Kian Hsiang Low, Patrick Jaillet, and Zhongxiang Dai. Implicit posterior variational inference for deep gaussian processes. *Advances in Neural Information Processing Systems*, 32, 2019. 53
- Xiaohan Yu and Shaochen Mao. Research on patch attentive neural process. *arXiv preprint arXiv:2202.01884*, 2022. 14, 20

-
- Manzil Zaheer, Satwik Kottur, Siamak Ravanbakhsh, Barnabas Poczos, Russ R Salakhutdinov, and Alexander J Smola. Deep sets. *Advances in neural information processing systems*, 30, 2017. 5, 9, 11
- Amir Zandieh, Navid Nouri, Ameya Velingker, Michael Kapralov, and Ilya Razenshteyn. Scaling up kernel ridge regression via locality sensitive hashing. In *International Conference on Artificial Intelligence and Statistics*, pp. 4088–4097. PMLR, 2020. 52
- Friedemann Zenke, Ben Poole, and Surya Ganguli. Continual learning through synaptic intelligence. In *International Conference on Machine Learning*, pp. 3987–3995. PMLR, 2017. 46
- Olek C Zienkiewicz, Robert L Taylor, and Jian Z Zhu. *The finite element method: its basis and fundamentals*. Elsevier, 2005. 44

A Appendix

Stochastic processes. Non-parametric stochastic processes have served as traditional alternatives to presuming a prior distribution over the parameters of a function such as the weight priors in Bayesian neural networks (BNNs). A non-parametric process can be thought of capturing the data generating behavior and hence, presumes a prior over a family of functions that together summarize this behavior. However, unlike the case of BNNs with priors over a finite-dimensional Banach space (of parameters), assigning a distribution over infinite-dimensional Banach space (of functions) is not straightforward due to the lack of a Lebesgue measure (Lebesgue, 1902) on the latter. To achieve the latter goal, the Kolmogorov extension theorem (Øksendal, 2003) provides two necessary conditions for any collection of bounded distributions to mimic a stochastic process over functions. Assuming our dataset to be defined by a target set T containing M features $\{x_1, \dots, x_M\}$ and their values $\{y_1, \dots, y_M\}$ such that T follows a well-defined continuous probability distribution. Then, for the joint (posterior) probability distribution of the values of a context set $C \subset T$ comprising $N < M$ points to define a stochastic process modeled by a smooth, continuous bounded function f , the following two conditions must hold:

1. Exchangeability: it must remain unaffected by the output of the ordering function π of its elements, *i.e.*, $p_{x_{1:N}}(y_{1:N}) = p_{\pi(x_{1:N})}(\pi(y_{1:N}))$,
2. Consistency: it must remain unaffected upon marginalizing arbitrary number of entries of the predictions, *i.e.*, $p_{x_{1:N}}(y_{1:N}) = \int p_{x_{1:M}}(y_{1:M}) dy_{N+1:M}$ where, $1 \leq N \leq M$.

Gaussian processes. One widely used instance of stochastic processes that adhere to the aforementioned criteria are the Gaussian processes (GPs) (Williams & Rasmussen, 2006). GPs restrict T to follow a multivariate Gaussian distribution through the use of a kernel function k that captures the covariance structure among the locations. In the limited data regime, GPs thus offer two major benefits over BNNs as a framework for predictive uncertainty measurement: 1) specifying the prior knowledge analytically in the form of a kernel function that exploits the covariance structure among the datapoints helps them encode any inductive bias into the model, and 2) inference in GPs for a query point $x^* \in T$ involves computing the posterior mean $\mathbb{E}(f(x^*)|f(C))$ as a linear combination of the kernel function values $k(x^*, x); x \in C$ and is thus much simpler than dealing with the intractability of priors as in BNNs. Moreover, unlike BNNs, the GP approach is non-parametric (more intuitively, *infinitely parameterized*) in that it finds a distribution over the possible infinite dimensional function spaces that are consistent with the observed data.

Limitations of GPs. The conventional GPs use the entire sample information in computing the posterior mean and thus lack sparsity. Such dense information leaves standard GPs with a number of setbacks (Binois & Wycoff, 2021): (a) costly training and inference procedures due to the posterior mean function scaling cubically in the number of observations N , (b) difficulty in covariance computation when exposed to high dimensional feature spaces due to the distance between uniformly sampled points concentrating increasingly further away, and (c) data inefficiency due to the challenging notion of encoding prior knowledge for kernel specification. Moreover, designing appropriate analytical priors can be a hard task on its own. While a

range of works address these issues by trading one or more metric(s) (for example, correlation in Quinero-Candela & Rasmussen (2005)) for computation, constructing scalable GP kernels still remains a domain of active research. On the other hand, deep neural networks ensure such scalability of predictive quality with the number of data points. The latter thus make a good alternative to overcome the challenges of GPs.